

EUROPEAN ORGANISATION FOR NUCLEAR RESEARCH (CERN)



JHEP 10 (2017) 112
DOI: [10.1007/JHEP10\(2017\)112](https://doi.org/10.1007/JHEP10(2017)112)



CERN-EP-2017-095
31st October 2017

Searches for the $Z\gamma$ decay mode of the Higgs boson and for new high-mass resonances in pp collisions at $\sqrt{s} = 13$ TeV with the ATLAS detector

The ATLAS Collaboration

This article presents searches for the $Z\gamma$ decay of the Higgs boson and for narrow high-mass resonances decaying to $Z\gamma$, exploiting Z boson decays to pairs of electrons or muons. The data analysis uses 36.1 fb^{-1} of pp collisions at $\sqrt{s} = 13$ TeV recorded by the ATLAS detector at the CERN Large Hadron Collider. The data are found to be consistent with the expected Standard Model background. The observed (expected – assuming Standard Model $pp \rightarrow H \rightarrow Z\gamma$ production and decay) upper limit on the production cross section times the branching ratio for $pp \rightarrow H \rightarrow Z\gamma$ is 6.6 (5.2) times the Standard Model prediction at the 95% confidence level for a Higgs boson mass of 125.09 GeV. In addition, upper limits are set on the production cross section times the branching ratio as a function of the mass of a narrow resonance between 250 GeV and 2.4 TeV, assuming spin-0 resonances produced via gluon–gluon fusion, and spin-2 resonances produced via gluon–gluon or quark–antiquark initial states. For high-mass spin-0 resonances, the observed (expected) limits vary between 88 fb (61 fb) and 2.8 fb (2.7 fb) for the mass range from 250 GeV to 2.4 TeV at the 95% confidence level.

Contents

1	Introduction	2
2	ATLAS detector and data sample	3
3	Simulation samples	5
4	Event selection and categorisation	7
4.1	Event preselection	7
4.2	Reconstruction of Z candidates and H/X candidates and final selection	9
4.3	Categorisation	10
5	Signal and background modelling	13
5.1	Signal modelling	13
5.2	Background modelling	15
6	Systematic uncertainties	17
6.1	Uncertainties from signal and background modelling	19
6.2	Experimental uncertainties affecting the signal efficiency and acceptance	19
6.3	Theoretical and modelling uncertainties	20
7	Statistical procedure	22
8	Results	23
9	Conclusion	27

1 Introduction

Since the observation of a Higgs boson (H) by the ATLAS and CMS collaborations [1, 2], its properties have been measured and presented in subsequent publications. Its mass was determined to be $m_H = 125.09 \pm 0.21(\text{stat}) \pm 0.11(\text{syst})$ GeV [3]. The couplings to Standard Model (SM) elementary particles were measured and confirmed to be consistent with the predictions for a SM Higgs boson within the present uncertainties [4–6], and alternative spin and CP hypotheses were rejected in favour of the SM hypothesis [7–10].

In the SM, the $Z\gamma$ decay proceeds through loop diagrams similar to the $H \rightarrow \gamma\gamma$ decay. The branching ratio for the Higgs boson decay to $Z\gamma$ is predicted by the SM to be $B(H \rightarrow Z\gamma) = (1.54 \pm 0.09) \times 10^{-3}$ at $m_H = 125.09$ GeV, which is comparable with the branching ratio of the Higgs boson decay to a photon pair, $B(H \rightarrow \gamma\gamma) = (2.27 \pm 0.05) \times 10^{-3}$. However, the number of reconstructed events is significantly smaller if Z boson decays into electron or muon pairs are considered ($B(Z \rightarrow ee) = (3.363 \pm 0.004)\%$ and $B(Z \rightarrow \mu\mu) = (3.366 \pm 0.007)\%$ [11]). A $H \rightarrow Z\gamma$ branching ratio different from the SM prediction would be expected if H were a neutral scalar of different origin [12, 13], or a composite state [14], or in models with additional colourless charged scalars, leptons or vector bosons coupled to the Higgs boson and exchanged in the $H \rightarrow Z\gamma$ loop [15–17].

The $H \rightarrow Z(\rightarrow \ell\ell)\gamma$ decay ($\ell = e$ or μ) has been searched for by the ATLAS and CMS collaborations using the full data sets collected at $\sqrt{s} = 7$ and 8 TeV [18, 19]. No significant excess over the expected background was observed. The ATLAS Collaboration reported an observed (expected) upper limit at the 95% confidence level (CL) of 11 (9) times the SM prediction for a Higgs boson mass of $m_H = 125.5$ GeV. The observed (expected) limit from the CMS Collaboration is 9.5 (10) times the SM prediction for a 125 GeV Higgs boson.

Many models of physics beyond the SM introduce new heavy bosons (X) through extensions of the Higgs sector or as additional gauge fields. Searches for heavy $Z\gamma$ resonances were carried out by the D0 Collaboration at the Tevatron and by the ATLAS and CMS collaborations. The D0 Collaboration set upper limits on $\sigma(p\bar{p} \rightarrow X) \cdot B(X \rightarrow Z\gamma)$ ranging from 2.5 (3.1) pb for a scalar (vector) X mass of 140 GeV to 0.19 (0.20) pb for a mass of 600 GeV [20] using about 1 fb^{-1} of $p\bar{p}$ collision data recorded at $\sqrt{s} = 1.96$ TeV. The ATLAS Collaboration excluded technimesons decaying to $Z\gamma$ for technimeson masses between 200 and 700 GeV and between 750 and 890 GeV, and composite spin-0 resonances decaying to $Z\gamma$ for most of the resonance mass range between 200 GeV and 1.18 TeV for certain model parameters using pp collision data recorded at $\sqrt{s} = 8$ TeV [21]. Using 3.2 fb^{-1} of pp collision data recorded at $\sqrt{s} = 13$ TeV, the ATLAS Collaboration set limits on $\sigma(pp \rightarrow X) \cdot B(X \rightarrow Z\gamma)$ between 295 fb and 8.2 fb for spin-0 resonances produced in gluon–gluon fusion for a X mass range from 250 GeV to 2.75 TeV using leptonic and hadronic Z boson decays [22]. The CMS Collaboration set upper limits on $\sigma(pp \rightarrow X) \cdot B(X \rightarrow Z\gamma)$ between about 300 fb and about 2.5 fb for spin-0 resonances produced in gluon–gluon fusion for a mass range of 200 GeV to 3 TeV using leptonic and hadronic Z decays and pp collision data taken at $\sqrt{s} = 8$ and 13 TeV [23].

This article presents improved searches for decays of the Higgs boson to $Z\gamma$ as well as for narrow high-mass resonances decaying to $Z\gamma$ using Z boson decays to electron or muon pairs. The $Z(\rightarrow \ell\ell)\gamma$ final state can be reconstructed completely and with high efficiency, good invariant mass resolution, and relatively small backgrounds. It is therefore a powerful experimental signature. The main background is the non-resonant production of Z bosons in conjunction with photons, which is modelled using samples of simulated events. A smaller contribution arises from Z boson production together with hadronic jets when a jet is misidentified as a photon. This background is studied with a dedicated selection of the photon candidate. Both searches are based on pp collision data recorded at $\sqrt{s} = 13$ TeV with the ATLAS detector at the LHC during 2015 and 2016, corresponding to a total integrated luminosity of 36.1 fb^{-1} . The search for decays of the Higgs boson to $Z\gamma$ benefits from the increased Higgs production cross section due to the increased centre-of-mass energy and also from the larger data set compared to the previous search [18]. In addition, the event categorisation now includes a category sensitive to Higgs boson production via vector-boson fusion. The search is optimised based on the expected production processes and kinematics for a SM Higgs boson. The search for high-mass resonances uses a significantly larger data set than the previous search [22] and is extended to spin-2 resonance production.

2 ATLAS detector and data sample

The ATLAS detector [24] at the LHC is a multipurpose particle detector with a forward-backward symmetric cylindrical geometry and a near 4π coverage in solid angle.¹ It consists of an inner tracking

¹ The ATLAS experiment uses a right-handed coordinate system with its origin at the nominal interaction point (IP) in the centre of the detector and the z -axis along the beam pipe. The x -axis points from the IP to the centre of the LHC ring, and the y -axis points upward. Cylindrical coordinates (r, ϕ) are used in the transverse plane, ϕ being the azimuthal angle around the

detector, electromagnetic and hadronic calorimeters, and a muon spectrometer. The inner detector (ID), immersed in a 2 T axial magnetic field provided by a thin superconducting solenoid, includes silicon pixel and microstrip detectors, which provide precision tracking in the pseudorapidity range $|\eta| < 2.5$, and a transition-radiation tracker (TRT) providing additional tracking and information for electron identification for $|\eta| < 2.0$. For the $\sqrt{s} = 13$ TeV data-taking period, the ID was upgraded with a silicon-pixel insertable B-layer [25], providing additional tracking information from a new layer closest to the interaction point. The solenoid is surrounded by sampling calorimeters: a lead/liquid-argon (LAr) electromagnetic calorimeter covering the region $|\eta| < 3.2$, a hadronic calorimeter with a steel/scintillator-tile barrel section for $|\eta| < 1.7$ and two copper/LAr endcaps for $1.5 < |\eta| < 3.2$. The forward region is covered by additional coarser-granularity LAr calorimeters up to $|\eta| = 4.9$. The calorimeter is surrounded by the muon spectrometer (MS) consisting of three large superconducting toroids each containing eight coils. Precise momentum measurements for muons with pseudorapidity up to $|\eta| = 2.7$ are provided by three layers of tracking chambers. The muon spectrometer also includes separate trigger chambers covering $|\eta|$ up to 2.4.

A two-level trigger system [26] was used during the $\sqrt{s} = 13$ TeV data-taking period. The first-level trigger (L1) is implemented in hardware and uses a subset of the detector information. This is followed by a software-based level which runs algorithms similar to the offline reconstruction software, reducing the event rate to approximately 1 kHz from the maximum L1 rate of 100 kHz.

The pp data collected by ATLAS in 2015 and 2016 were taken at a centre-of-mass energy of $\sqrt{s} = 13$ TeV and with a bunch spacing of 25 ns. After requiring that the full detector was operational during data-taking and application of requirements on the data quality, the integrated luminosity corresponds to 36.1 fb^{-1} , of which 3.2 and 32.9 fb^{-1} were taken during 2015 and 2016, respectively. The average number of pp interactions per bunch crossing (pile-up) ranged from about 13 in 2015 to about 25 in 2016, with a peak instantaneous luminosity of $1.37 \times 10^{34} \text{ cm}^{-2}\text{s}^{-1}$ achieved in 2016.

The events were collected with triggers requiring either one or two electrons or muons in the event. The single-muon trigger has a transverse momentum (p_T) threshold of 26 GeV and applies a requirement on the muon track isolation. The track isolation is defined as the scalar sum of the transverse momenta of the ID tracks in a cone of $\Delta R = \sqrt{(\Delta\eta)^2 + (\Delta\phi)^2} = 0.3$ around the muon. For the trigger used during 2016, the cone size was modified to be $\Delta R = 10/(p_T/\text{GeV})$ for muons with $p_T > 33.3$ GeV. The track isolation is computed from ID tracks with $p_T > 1$ GeV and with a longitudinal impact parameter z_0 within 6 mm of the z_0 of the muon track, excluding the muon track itself. The track isolation is required to be less than 6% (7%) of the muon's transverse momentum in the 2015 (2016) data set. A second single-muon trigger with a p_T threshold of 50 GeV has no requirement on the track isolation. The dimuon trigger has p_T thresholds of 22 GeV and 8 GeV and does not apply track isolation criteria. Single-electron triggers with p_T thresholds at 24 GeV (26 GeV), 60 GeV, and 120 GeV (140 GeV) are used, as well as a dielectron trigger with a p_T threshold of 12 GeV (17 GeV) during the 2015 (2016) data taking. In the 2016 data-taking period, the lowest-threshold single-electron trigger required the track isolation in a cone of $\Delta R = 0.2$ for $p_T < 50$ GeV and $\Delta R = 10/(p_T/\text{GeV})$ for $p_T > 50$ GeV to be less than 10% of the electron's transverse energy. For all electron triggers, electron candidates must satisfy identification criteria based on the properties of the energy cluster in the electromagnetic calorimeter and its associated track. The single-electron triggers with lower thresholds use tighter criteria for the electron identification. For $H \rightarrow Z\gamma$ events that pass the analysis preselection (see Section 4), the efficiency to pass the trigger selection is

z -axis. The pseudorapidity is defined in terms of the polar angle θ as $\eta = -\ln \tan(\theta/2)$. The transverse energy is defined as $E_T = E \sin(\theta)$.

92.9% (96.9%) for Z boson decays to muon (electron) pairs. For a high-mass resonance at 1 TeV, the corresponding efficiencies are 94.3% and 99.8% for muon and electron final states, respectively.

3 Simulation samples

Samples of simulated Monte Carlo (MC) events are used to optimise the search strategy, evaluate the selection efficiency and to study the different background contributions. The generated event samples were processed with the detailed ATLAS detector simulation [27] based on GEANT4 [28] (one exception is noted below).

For the $H \rightarrow Z\gamma$ search, the mass of the Higgs boson is chosen to be $m_H = 125$ GeV and the corresponding width is $\Gamma_H = 4.1$ MeV [29]. The SM Higgs boson production was simulated with PowHEG Box v2 [30–32] using the combined parton distribution function (PDF) set PDF4LHC following the recommendations [33] based on the CT14 [34], MMHT14 [35] and NNPDF3.0 [36] PDF sets and the Hessian reduction method [37–39]. The techniques used for the simulation of gluon–gluon fusion (ggF) production, vector-boson fusion (VBF) production, and production in association with a vector boson (WH and ZH , together referred to as VH) and the perturbative order achieved are summarised in Table 1 and detailed below. Higgs boson production in association with a $t\bar{t}$ pair and other production processes are not considered as their contributions to the total Higgs production cross section are of the order of 0.1% or less.

Table 1: Higgs boson production processes produced with PowHEG Box with the techniques used and their precision in α_s for the event generation (gen.). The total cross section is known with higher precision in QCD and electroweak (norm.) than available in the event generation. The events were reweighted to reproduce the more precise total cross section.

Process	Technique	QCD (gen.)	QCD (norm.)	EW (norm.)
ggF	MiNLO & NNLOPS	NNLO (incl.), NLO ($H + 1\text{-jet}$)	NNNLO	NLO
VBF	PowHEG	NLO	approx. NNLO	NLO
VH	MiNLO	NLO (incl. and $H + 1\text{-jet}$)	NNLO	NLO

Higgs boson production via ggF was simulated with PowHEG Box, using the MiNLO approach [40], which achieves next-to-leading-order (NLO) precision for both the inclusive and the $H+1\text{-jet}$ process in quantum chromodynamics (QCD). In addition, the NNLOPS approach [41] was used to improve the precision for inclusive observables to next-to-next-to-leading-order (NNLO) in QCD: the Higgs transverse momentum spectrum achieved by this technique was found to be in agreement with the result obtained using QCD resummation with next-to-next-to-leading logarithmic (NNLL)+NNLO precision from the HqT calculation [42, 43]. Top and bottom quark mass effects are included up to NLO precision in QCD. The central scale choice for the nominal factorisation (μ_F) and renormalisation scales (μ_R) is $\mu_F = \mu_R = m_H/2$. The events were reweighted to reproduce the inclusive cross section at next-to-next-to-next-to-leading-order (NNNNLO) precision in QCD and NLO precision in electroweak corrections [29, 33, 44–47].

Higgs boson production via VBF was simulated with PowHEG Box at NLO precision in QCD [48]. The events were reweighted to reproduce the inclusive cross section with approximate-NNLO precision in QCD and NLO precision in electroweak corrections [29, 33, 49–51].

Higgs boson production in association with a vector boson via quark–antiquark initial states was simulated at NLO precision in QCD for inclusive events and $H + 1$ -jet events using the MiNLO technique [52]. The events were reweighted to reproduce the total VH production cross section, including also production via gluon–gluon initial states, at NNLO precision in QCD with NLO electroweak corrections [29, 33, 53–55].

The effects of parton showering, hadronisation and multiple parton interactions (MPI) were simulated using PYTHIA 8.186 [56] configured with the AZNLO set of parameters [57] and the CTEQ6L1 [58] PDF set. The events were reweighted to reproduce the $H \rightarrow Z\gamma$ branching ratio calculated with HDECAY [29, 59, 60].

Three additional event samples of gluon–gluon fusion production are used for the studies of theoretical uncertainties. The first is an event sample generated with MADGRAPH5_AMC@NLO version 5.2.3.3 with FxFx multijet merging [61, 62] of $H + 0$ -jet and $H + 1$ -jet at NLO precision in QCD, using the NNPDF 3.0 PDF set. The decay of the Higgs boson and the parton showering, hadronisation and MPI were provided by PYTHIA 8.186 using the A14 set of parameters [63] and the NNPDF2.3 PDF set [64]. Two more samples were simulated with PowHEG Box v1 [30–32, 65] with the CT10 PDF set [66] and PYTHIA 8.186 for parton showering and hadronisation using the AZNLO set of parameters and the CTEQ6L1 PDF set. The two samples were produced with and without MPI to study the uncertainties in the signal acceptance related to the modelling of non-perturbative effects.

Production of CP -even, high-mass spin-0 resonances X in the mass range $m_X \in [300–2500]$ GeV was simulated for the gluon–gluon fusion and vector-boson fusion production processes and for an intrinsic resonance width of 4 MeV, which is much smaller than the experimental resolution (see Section 5) and referred to as narrow width assumption (NWA). Due to the assumed narrow width of the resonance, the interference between the resonant signal and the non-resonant background is neglected. The ggF (VBF) process was simulated for $m_X = 300, 500, 700, 750, 800, 1000, 1500, 2000$ and 2500 GeV ($m_X = 300, 500, 1000$ and 2500 GeV). Both the ggF and VBF processes were produced with PowHEG Box v1 with the CT10 PDF set.

Production of CP -even, high-mass spin-2 resonances X with mass $m_X = 250, 300, 500, 750, 1000, 1500, 2000$ and 2500 GeV for an intrinsic resonance width of 4 MeV via gluon–gluon and quark–antiquark initial states was simulated at LO in QCD in the Higgs Characterisation Model [67] with MADGRAPH5_AMC@NLO 2.3.3 [61].

For the high-mass spin-0 (spin-2) resonances, the parton showering, hadronisation and MPI were simulated with PYTHIA 8.186 using the AZNLO (A14) set of parameters and the CTEQ6L1 (NNPDF2.3) PDF set.

The signal shape and the reconstruction and selection efficiency of the studied high-mass resonances are parameterised as a function of m_X . The parameterisation allows the extraction of the signal shape and efficiency for any mass point at which no simulation sample is available.

The background mainly originates from non-resonant production of a Z boson and a prompt photon ($Z+\gamma$), with a smaller contribution from production of Z bosons in association with jets ($Z+jets$), with one jet misidentified as a photon. $Z+\gamma$ production within the SM is primarily due to radiation of photons from final-state leptons (FSR) or initial-state quarks (ISR). Both SM processes were simulated using the SHERPA generator [68] (version 2.1.1 for $Z+\gamma$ and version 2.2.0 for $Z+jets$), and the matrix elements were calculated using the COMIX [69] and OPENLOOPS [70] generators, where $Z+\gamma$ production was calculated for real emission of up to two partons at leading order (LO) in QCD and merged with the SHERPA parton

shower [71] using the ME+PS@LO prescription [72]. The process of Z +jets was calculated for up to two partons at next-to-leading-order (NLO) and four partons at LO and merged with the parton shower using the ME+PS@NLO prescription [73]. For the $Z+\gamma$ (Z +jets) samples, the CT10 (NNPDF3.0) PDF set was used in conjunction with dedicated parton shower tuning developed by the SHERPA authors. To study the background model in detail, a large sample of $Z+\gamma$ events was simulated using fast simulation of the calorimeter response [74].

For all event samples, the additional inelastic pp collisions per bunch crossing were simulated with PYTHIA 8.186 using the A2 set of tuned parameters [75] and the MRSTW2008LO PDF set [76]. The MC events were reweighted to reproduce the distribution of the average number of interactions per bunch crossing observed in the data.

Corrections derived from trigger, identification, reconstruction, and isolation efficiency measurements for electrons and muons, from identification and isolation efficiency measurements for photons, and from selection efficiency measurements for jets are applied to the simulated events to improve the description of the data. Similarly, energy scale and resolution corrections for all simulated objects are also taken into account.

4 Event selection and categorisation

4.1 Event preselection

Events are required to have at least one primary vertex candidate, determined using the tracks with transverse momentum $p_T > 400$ MeV reconstructed in the ID. The primary vertex candidate with the largest sum of the squared transverse momenta of the associated tracks ($\sum p_T^2$) is considered to be the primary vertex of the interaction of interest. For $H/X \rightarrow Z\gamma$ signal events, the selected primary vertex is within 0.3 mm of the true primary interaction vertex for more than 99% of the events.

The $H/X \rightarrow Z(\rightarrow \ell\ell)\gamma$ candidate events are selected by requiring two same-flavour opposite-charge leptons ($\ell = e, \mu$) to form a Z boson candidate and at least one photon candidate.

Muon candidates with $|\eta| < 2.5$ are reconstructed by combining tracks in the ID with tracks in the MS. To extend the acceptance beyond that of the ID, muon candidates are reconstructed from tracks reconstructed only in the MS up to $|\eta| = 2.7$ [77]. Muon candidates are required to satisfy the *medium* criterion and have $p_T > 10$ GeV. In order to ensure good track quality, the ID tracks associated with muons in $|\eta| < 2.5$ are required to have at least one hit in the silicon pixel detector and at least five hits in the silicon microstrip detector, as well as to extend into the TRT for $0.1 < |\eta| < 1.9$. The muon candidates in $2.5 < |\eta| < 2.7$ are required to have hits in each of the three layers of MS tracking chambers.

Electron candidates are reconstructed from a cluster of energy deposits in neighbouring cells of the EM calorimeter and a track, matched to the cluster, in the ID. They are required to have $p_T > 10$ GeV and be within the fiducial region $|\eta| < 2.47$ excluding the candidates in the transition region between the barrel and endcap EM calorimeters, $1.37 < |\eta| < 1.52$. The electrons are identified with the *medium* likelihood-based criterion [78] built from the shower shapes of the clusters, the number of hits associated with the track in the ID and the quality of the track-cluster matching.

Both the muon and electron candidates are required to be associated with the primary vertex by requiring the longitudinal impact parameter, Δz_0 , computed with respect to the primary vertex position along the

beam-line, to satisfy $|\Delta z_0 \cdot \sin \theta| < 0.5$ mm, where θ is the polar angle of the track. In addition the significance of the transverse impact parameter d_0 calculated with respect to the measured beam-line position must satisfy $|d_0|/\sigma_{d_0} < 3$ (5) for muons (electrons) where σ_{d_0} is the uncertainty in d_0 .

The efficiency of the muon identification is higher than 99% (60%) for $p_T > 10$ GeV muons with $|\eta| > 0.1$ ($|\eta| < 0.1$) (similar to Ref. [77]), while the efficiency of the electron identification ranges from about 80% for electrons with $p_T = 10$ GeV to higher than 90% for electrons with $p_T > 50$ GeV (similar to Ref. [78]). The efficiency is typically about 5% higher in the barrel region of the detector than in the endcaps.

The lepton candidates are further required to satisfy additional criteria for track isolation, which is defined similarly to the track isolation used in the trigger (see Section 2), but uses a different track selection and a different cone size in some cases. The track isolation is computed as the scalar sum of the transverse momenta of all tracks in a cone around the lepton candidate with $p_T > 1$ GeV which satisfy loose track-quality criteria and originate from the selected primary vertex, excluding the track associated with the lepton candidate. For muon candidates, the cone size is chosen to be $\Delta R = 0.3$ for $p_T < 33.3$ GeV and $\Delta R = 10/(p_T/\text{GeV})$ for $p_T > 33.3$ GeV. For electron candidates, the cone size is chosen to be $\Delta R = 0.2$ for $p_T < 50$ GeV and $\Delta R = 10/(p_T/\text{GeV})$ for $p_T > 50$ GeV. The requirement on the track isolation is chosen such that it is 99% efficient over the full lepton p_T range.

An overlap removal procedure is applied to the selected lepton candidates. If two electrons share the same track, or the two electron clusters satisfy $|\Delta\eta| < 0.075$ and $|\Delta\phi| < 0.125$, then only the highest- p_T electron is retained. Electron candidates that are within $\Delta R = 0.02$ of a selected muon candidate are also discarded.

Photon candidates are reconstructed from energy clusters in the electromagnetic calorimeter. Clusters matched to a conversion vertex, reconstructed from either two tracks consistent with a vertex originating from a photon conversion or one track that does not have any hits in the innermost pixel layer and has an electron-like response in the TRT, are reconstructed as converted photon candidates. Clusters without any matching track (clusters with a matching track are reconstructed as electrons as described above) or conversion vertex are reconstructed as unconverted photon candidates [79]. Photon candidates are required to have $p_T > 10$ GeV and $|\eta| < 1.37$ or $1.52 < |\eta| < 2.37$. The identification of photon candidates is based on the lateral and longitudinal shape of the electromagnetic shower [79, 80]. A *loose* identification is used for preselection and for background studies.

In order to suppress the events arising from FSR processes and $H \rightarrow \ell\ell^* \rightarrow \ell\ell\gamma$ decays, photon candidates within a $\Delta R = 0.3$ cone around a selected electron or muon candidate are rejected.

The selection criteria described in the preceding paragraphs define the event preselection for the leptons and photons included in the reconstruction of the invariant mass of the $\ell\ell$ and $\ell\ell\gamma$ systems.

The event categorisation described in Section 4.3 used in the search for decays of the Higgs boson to $Z\gamma$ makes use of hadronic jets produced in association with the Higgs boson candidate. Jets are reconstructed using the anti- k_t algorithm [81] with a radius parameter of 0.4 with three-dimensional topological clusters as input [82]. Jets are corrected on an event-by-event basis for soft energy deposits originating from pile-up interactions [83] and calibrated using a combination of simulation- and data-driven correction factors accounting for the non-compensating response of the calorimeter and energy loss in inactive regions [84]. Jets are required to have a transverse momentum larger than 25 GeV and $|\eta| < 4.4$. To reduce the contamination from jets produced in pile-up interactions, jets with transverse momentum smaller than 60 GeV and contained within the inner detector's acceptance ($|\eta| < 2.4$) are required to pass a selection based on the jet vertex tagging algorithm [85], which is 92% efficient for jets originating from the hard interaction.

The jet vertex tagging algorithm is based on the tracks associated with the jet which are consistent with originating from the selected primary vertex. Jet–lepton and jet–photon overlap removal is performed where the jet is removed if the lepton or photon is within a cone of size $\Delta R = 0.2$.

4.2 Reconstruction of Z candidates and H/X candidates and final selection

The Z boson candidates are reconstructed from two same-flavour opposite-sign leptons satisfying the preselection criteria and with an invariant mass $m_{\ell\ell}$ larger than 45 GeV. Leptons are required to be consistent with the objects that triggered the event. Trigger efficiency turn-on effects are mitigated by transverse momentum requirements on the leptons that fired the single-lepton or dilepton trigger. If the event was triggered by a single-lepton trigger, the transverse momentum is required to be at least 27 GeV for the leading lepton, and at least 1 GeV higher than the respective trigger threshold in cases where the event was triggered by one of the higher-threshold triggers. If the event was triggered by a dilepton trigger, the transverse momentum is required to be at least 24 GeV (18 GeV) for the leading muon (electron) and 10 GeV (18 GeV) for the subleading muon (electron). For $Z \rightarrow \mu\mu$ candidates with an invariant mass between 66 and 89 GeV, the invariant mass resolution of the Z boson candidate is improved by correcting the muon momenta for collinear FSR by including any reconstructed electromagnetic cluster with p_T above 1.5 GeV lying close to a muon track (with $\Delta R < 0.15$) if the corrected invariant mass is below 100 GeV [86]. A constrained kinematic fit is applied to recompute the four-momenta of the dilepton pair [87] for $Z \rightarrow \mu\mu$ and $Z \rightarrow ee$ candidates. The fit models the lepton energy and momentum response as a Gaussian distribution for each lepton, and the Gaussian width is given by the expected resolution. The Z lineshape is used as a constraint with the approximation of the leptons being massless. The lineshape is modelled by a Breit–Wigner distribution. After the application of the FSR corrections and the kinematic fit, Z boson candidates are required to have an invariant mass within 15 GeV of the Z boson mass, $m_Z = 91.2$ GeV [11]. If multiple Z boson candidates pass all requirements, the candidate with the mass closest to the Z boson mass is chosen. About 0.2% (0.5%) of events that pass the final $H \rightarrow Z\gamma$ ($X \rightarrow Z\gamma$) selection have more than one Z boson candidate within the 15 GeV mass window.

Higgs boson and X candidates are reconstructed from the Z boson candidate and the highest- p_T photon candidate after the preselection.

For the main analyses with the exception of the background studies, the photon candidate used for the reconstruction of the H/X candidate is required to pass the *tight* identification [79]. The efficiency of the tight identification ranges from 67% (60%) to 90% (95%) for unconverted (converted) isolated photons from p_T of 15 GeV to 50 GeV and larger.

Photon candidates are furthermore required to be isolated from additional activity in the detector. A combined requirement on the isolation energy in the calorimeter and the inner detector is used. The calorimeter isolation is computed as the sum of transverse energies of positive-energy topological clusters [82] in the calorimeter within a cone of $\Delta R = 0.2$ centred around the photon shower barycentre. The transverse energy of the photon candidate is removed and the contributions of the underlying event and pile-up are subtracted based on the method suggested in Ref. [88]. The track isolation for a cone size of $\Delta R = 0.2$ is used and for converted photons the tracks associated with the conversion are removed. The calorimeter (track) isolation is required to be less than 6.5% (5%) of the photon p_T . The efficiency of the isolation requirement for photons satisfying the tight identification criteria ranges from approximately 60% for p_T of 15 GeV to more than 90% for p_T of 40 GeV and larger.

For the $H \rightarrow Z\gamma$ ($X \rightarrow Z\gamma$) search, the photon transverse momentum requirement is tightened to 15 GeV ($p_T/m_{Z\gamma} > 0.3$).

The invariant mass of the final-state particles, $m_{Z\gamma}$, is required to satisfy $115 \text{ GeV} < m_{Z\gamma} < 170 \text{ GeV}$ for the $H \rightarrow Z\gamma$ search and $200 \text{ GeV} < m_{Z\gamma} < 2500 \text{ GeV}$ for the high-mass resonance search. Figure 1 shows the invariant mass distribution for simulated $H \rightarrow Z\gamma$ candidates after the final selection with and without the lepton momentum corrections from the FSR recovery and the kinematic fit. Improvements of the $m_{\mu\mu\gamma}$ resolution of 3% are observed for $m_H = 125 \text{ GeV}$ from the FSR recovery. The kinematic fit improves the $m_{\mu\mu\gamma}$ ($m_{ee\gamma}$) resolution by 7% (13%) at the same mass. For high invariant masses, the $m_{\mu\mu\gamma}$ resolution improvement varies from 10% at $m_X = 300 \text{ GeV}$ to about 50% for $m_X > 1.5 \text{ TeV}$, while the $m_{ee\gamma}$ resolution is improved by 9% at $m_X = 300 \text{ GeV}$ and by 3% or less above $m_X = 500 \text{ GeV}$. The constrained kinematic fit is particularly effective at large m_X for the $Z \rightarrow \mu\mu$ final state due to the decreasing precision of the momentum measurement for increasing muon p_T .

4.3 Categorisation

Events are split into mutually exclusive event categories that are optimised to improve the sensitivity of both the $H \rightarrow Z\gamma$ and $X \rightarrow Z\gamma$ searches. The event categories separate events on the basis of the expected signal-to-background ratio and of the expected three-body invariant mass resolution. Different categories are used in the search for decays of the Higgs boson to $Z\gamma$ and the search for high-mass resonances.

The $H \rightarrow Z\gamma$ search uses six exclusive event categories and events are assigned to the categories in the following order:

- **VBF-enriched** : Events are required to have at least two jets. A boosted decision tree (BDT) that was trained to separate VBF events from other Higgs boson production modes and non-Higgs back-

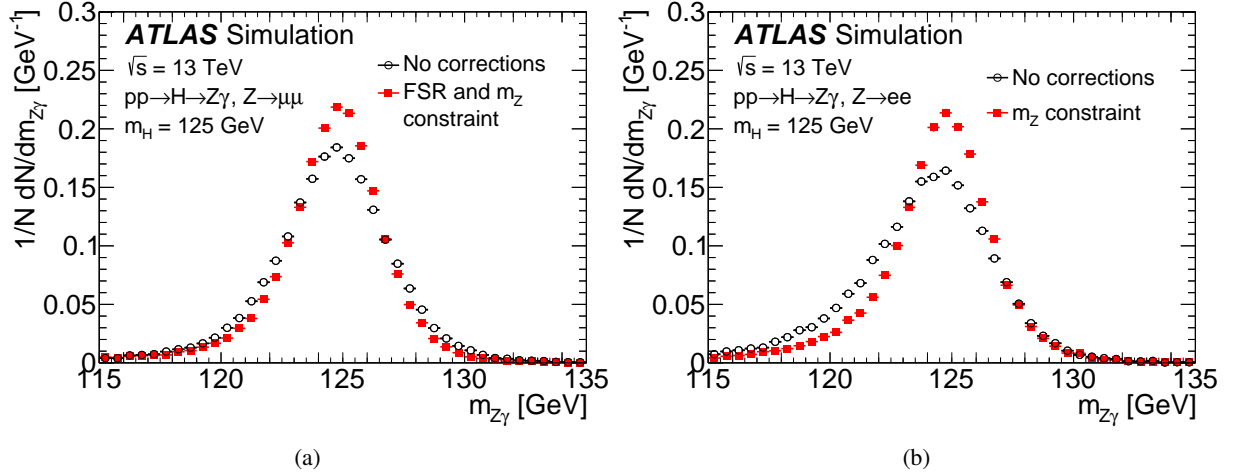


Figure 1: Invariant mass distribution, $m_{Z\gamma}$, for the final selection before and after application of the final-state radiation corrections ($Z \rightarrow \mu\mu$ only) and the Z boson mass constrained kinematic fit for simulated $H \rightarrow Z\gamma$ events with $m_H = 125 \text{ GeV}$ in the gluon–gluon fusion production mode. Events are separated by lepton type, (a) $Z \rightarrow \mu\mu$ and (b) $Z \rightarrow ee$.

grounds is applied. It uses six kinematic variables as input, computed from the Z boson candidate, the photon candidate and the two jets with the largest transverse momenta:

- The invariant mass of the two jets (m_{jj}),
- The separation of the jets in pseudorapidity ($\Delta\eta_{jj}$),
- The azimuthal separation of the $Z\gamma$ and the dijet systems ($\Delta\phi_{Z\gamma,jj}$),
- The component of the transverse momentum of the $Z\gamma$ system that is perpendicular to the difference of the 3-momenta of the Z boson and the photon candidate ($p_{Tt} = 2|p_x^Z p_y^\gamma - p_x^\gamma p_y^Z|/p_T^{Z\gamma}$),
- The smallest ΔR separation between the Z boson or photon candidate and the two jets ($\Delta R_{Z/\gamma,j}^{\min}$),
- The difference between the pseudorapidity of the $Z\gamma$ system and the average pseudorapidity of the two jets ($|\eta_{Z\gamma} - (\eta_{j1} + \eta_{j2})/2|$).

The variable p_{Tt} is strongly correlated with the transverse momentum of the $Z\gamma$ system, but has better experimental resolution [89, 90]. Any requirement on $\Delta\phi_{Z\gamma,jj}$ effectively vetoes additional jets in the event by restricting the phase space for additional emissions and, to avoid uncontrolled theoretical uncertainties, the BDT does not use shape information for events with $\Delta\phi_{Z\gamma,jj} > 2.94$ by merging these events into one bin. A minimum value of the BDT output ($\text{BDT} > 0.82$) is required. The expected and observed distributions for two input variables, m_{jj} as a typical variable to select events with VBF topology and $\Delta\phi_{Z\gamma,jj}$, which serves as an implicit third-jet veto, are shown in Figure 2 for selected events with at least two jets.

- **High relative p_T** : Events are required to have a high p_T photon, $p_T^\gamma/m_{Z\gamma} > 0.4$.
- **ee high p_{Tt}** : Events are required to have high p_{Tt} ($p_{Tt} > 40$ GeV) and a Z boson candidate decay to electrons.
- **ee low p_{Tt}** : Events are required to have low p_{Tt} ($p_{Tt} < 40$ GeV) and a Z boson candidate decay to electrons.
- **$\mu\mu$ high p_{Tt}** : Events are required to have high p_{Tt} ($p_{Tt} > 40$ GeV) and a Z boson candidate decay to muons.
- **$\mu\mu$ low p_{Tt}** : Events are required to have low p_{Tt} ($p_{Tt} < 40$ GeV) and a Z boson candidate decay to muons.

For SM $H \rightarrow Z(\rightarrow \ell\ell)\gamma$ events, the reconstruction and selection efficiency (including kinematic acceptance) is 21.5%. Table 2 shows the expected signal efficiency times acceptance for each of the different SM Higgs boson production processes in each category, as well as the expected relative contribution of a given production process to each category. The VBF-enriched category is expected to be about 68% pure in VBF events. The high relative p_T and high p_{Tt} categories are expected to be slightly enriched in VBF and VH events. Overall, about 40 $H \rightarrow Z\gamma$ events are expected to be selected. Table 3 summarises for each category: the number of selected events from data in the fit range $115 \text{ GeV} < m_{Z\gamma} < 150 \text{ GeV}$ (see Section 5); the expected number of events (S_{90}) in an interval around the $m_{Z\gamma}$ peak position expected to contain 90% of the SM signal events; w_{90} defined to be half of the width of the interval; the expected S_{90}/B_{90} , where B_{90} is the background yield in the same mass window determined from data; and the expected $S_{90}/\sqrt{S_{90} + B_{90}}$. The window is constructed so that it includes 45% of the signal events on either side of the peak position for $m_H = 125.09$ GeV. The largest fraction of the signal is expected in the

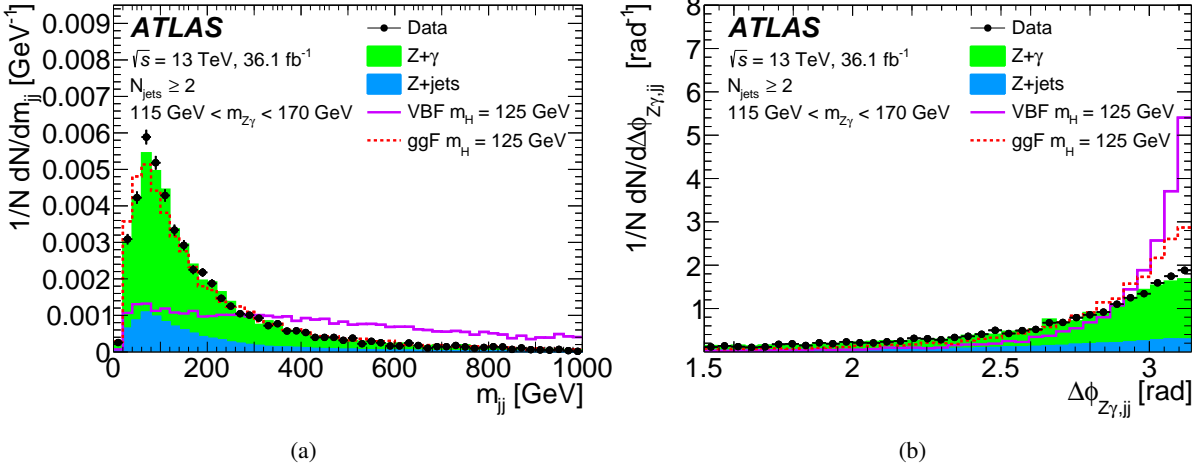


Figure 2: Kinematic variables used in the BDT used to define the VBF-enriched category: (a) the invariant mass of the two jets with the highest transverse momenta, m_{jj} and (b) the azimuthal separation of the $Z\gamma$ and the dijet system, $\Delta\phi_{Z\gamma,jj}$ for events with at least two jets and $115 \text{ GeV} < m_{Z\gamma} < 170 \text{ GeV}$. The observed distribution (normalised to unity) is shown as data points. The contributions from $Z + \gamma$ events (obtained from simulation) and the contribution from $Z + \text{jets}$ (obtained from data control regions described in the text) are shown as stacked histograms. The corresponding expected distributions for Higgs bosons produced via gluon–gluon fusion and vector-boson fusion production for $m_H = 125 \text{ GeV}$ are shown as open histograms. The $\Delta\phi_{Z\gamma,jj}$ distribution is shown before the suppression of the shape information for $\Delta\phi_{Z\gamma,jj} > 2.94$.

Table 2: The expected signal efficiency times acceptance, denoted by ϵ , per production mode for each category after the full event selection, as well as the expected fraction f of each production process relative to the total signal yield, for simulated SM Higgs boson production assuming $m_H = 125 \text{ GeV}$. The expected number of signal events per production process is also given.

Category	ggF		VBF		WH		ZH	
	$\epsilon[\%]$	$f[\%]$	$\epsilon[\%]$	$f[\%]$	$\epsilon[\%]$	$f[\%]$	$\epsilon[\%]$	$f[\%]$
VBF-enriched	0.25	30.5	6.5	67.5	0.34	1.3	0.24	0.6
High relative p_T	1.1	71.5	2.6	14.3	4.0	8.3	4.1	5.3
ee high p_{T_t}	1.7	80.8	2.8	11.0	3.2	4.7	3.6	3.3
ee low p_{T_t}	7.1	93.2	3.6	4.1	3.7	1.5	4.2	1.1
$\mu\mu$ high p_{T_t}	2.2	80.4	3.6	11.3	4.1	4.8	4.2	3.1
$\mu\mu$ low p_{T_t}	9.2	93.4	4.7	4.1	4.6	1.5	4.8	1.0
Total efficiency (%)	21.5		23.8		20.2		21.0	
Expected events		35		3.3		1.0		0.7

low $p_{\text{T}t}$ categories, which have the smallest expected significance. The VBF-enriched category shows the largest contribution to the expected significance.

Table 3: The number of data events selected in the mass range used for the background fit to the $m_{Z\gamma}$ spectrum (115–150 GeV) per category. In addition, the following numbers are given: the expected number of Higgs boson signal events in an interval around the peak position for a signal of $m_H = 125.09$ GeV, expected to contain 90% of the SM signal (S_{90}), the half-width of the S_{90} interval (w_{90}), as well as the expected signal-to-background ratio in the S_{90} window (S_{90}/B_{90}) with B_{90} determined from data, and the expected significance estimate $S_{90}/\sqrt{S_{90} + B_{90}}$.

Category	Events	S_{90}	w_{90} [GeV]	S_{90}/B_{90} [10^{-2}]	$S_{90}/\sqrt{S_{90} + B_{90}}$
VBF-enriched	88	1.2	3.9	9.5	0.32
High relative p_{T}	443	2.3	3.9	3.0	0.26
ee high $p_{\text{T}t}$	1053	3.3	3.9	1.1	0.19
ee low $p_{\text{T}t}$	11707	11.2	4.2	0.3	0.18
$\mu\mu$ high $p_{\text{T}t}$	1413	4.0	3.7	1.2	0.22
$\mu\mu$ low $p_{\text{T}t}$	16529	14.5	3.8	0.3	0.21

The search for high-mass resonances uses two categories, one for each Z boson candidate decay mode, $Z \rightarrow ee$ and $Z \rightarrow \mu\mu$, to benefit from both the better invariant mass resolution in the electron channel at large $m_{Z\gamma}$ and the differences in the systematic uncertainties between electrons and muons. The invariant mass resolution, measured by the Gaussian width of the signal model (see Section 5), ranges from 2.8 GeV (3.1 GeV) at $m_X = 250$ GeV to 16 GeV (36 GeV) at $m_X = 2.4$ TeV for $Z \rightarrow ee$ ($Z \rightarrow \mu\mu$).

5 Signal and background modelling

The signal and background yields are extracted from the data $m_{Z\gamma}$ distribution by assuming analytical models. The parameters that describe the shape of the signal are obtained from simulated signal samples. The analytical models used for the background shape are chosen using simulated background samples and the values of their free parameters are determined from the fit to data.

5.1 Signal modelling

The signal mass distribution in the searches for both the Higgs boson and the high-mass resonance decay to $Z\gamma$ is well modelled with a double-sided Crystal Ball (DSCB) function (a Gaussian function with power-law tails on both sides) [91, 92]. The peak position and width of the Gaussian component are represented by μ_{CB} and σ_{CB} , respectively.

To determine the parameters of the DSCB for the $H \rightarrow Z\gamma$ search, a fit is performed to all the categories (see Section 4.3) from the simulated signal samples produced via ggF, VBF and VH processes at $m_H = 125$ GeV. A shift of 90 MeV is applied to the peak position μ_{CB} to build a signal model for $m_H = 125.09$ GeV. For the high-mass search, a simultaneous fit is performed to all signal samples, $m_X = [300–2500]$ GeV ($m_X = [250–2500]$ GeV) for the spin-0 (spin-2) interpretation. This allows a parameterisation of the signal shape for masses m_X for which no simulation sample is available. The m_X dependence of the signal shape parameters is parameterised by polynomials, and their coefficients are determined during

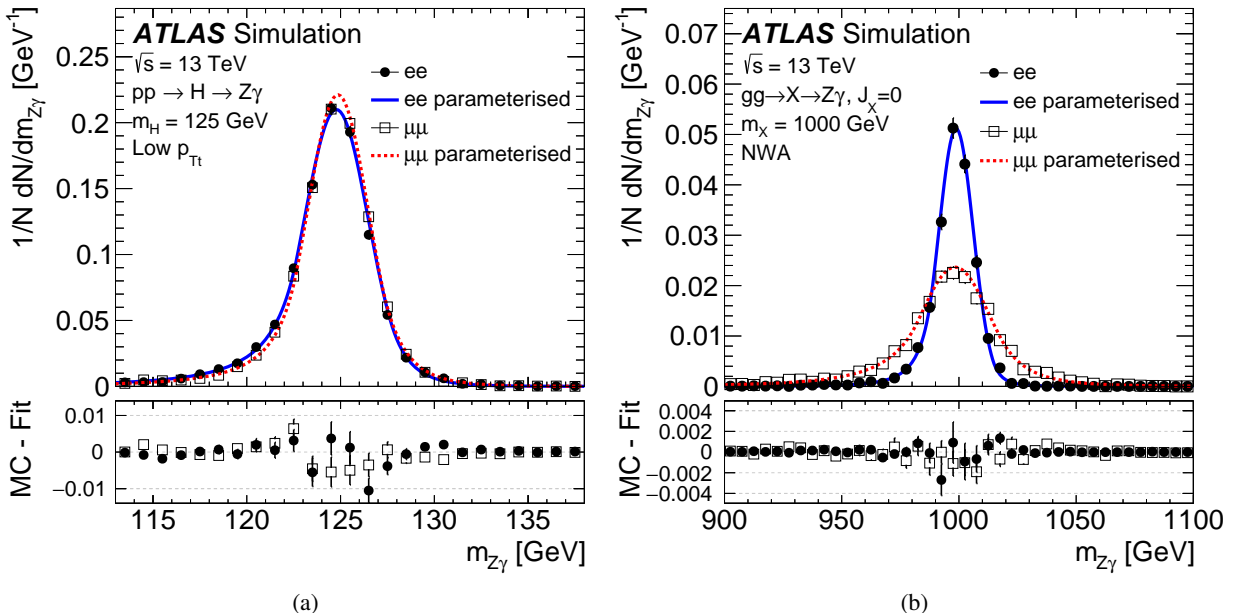


Figure 3: The differential distribution of the invariant $Z\gamma$ mass ($m_{Z\gamma}$) for (a) Higgs bosons with $m_H = 125$ GeV in the low p_{T_ℓ} categories and (b) high-mass spin-0 particles produced via gluon–gluon fusion and with $m_X = 1000$ GeV, using the narrow width assumption (NWA). The markers show the $m_{Z\gamma}$ distributions and the solid and dotted lines the fitted parameterisations used in the searches. The bottom part of the figures shows the residuals between the markers and the parameterisation.

the simultaneous fit. The parameterisation is done separately for each of the three models considered, a spin-0 resonance and a spin-2 resonance produced via either gluon–gluon or quark–antiquark initial states.

Figure 3 shows the MC-simulated $m_{Z\gamma}$ distribution at $m_H = 125$ GeV for the low p_{T_ℓ} categories and at $m_X = 1000$ GeV. Similar fit qualities are obtained for all the categories in both searches.

Additionally, the signal efficiency defined as the number of events satisfying all the selection criteria (as given in Section 4) normalised to the total number of events is needed to extract $\sigma \cdot B(H/X \rightarrow Z\gamma)$ from the measured yield. For the $H \rightarrow Z\gamma$ search, the signal efficiency times the acceptance in each category are shown in Table 2.²

For the search for high-mass resonances, the signal efficiency is parameterised as a function of the resonance mass with an exponentiated second-order polynomial. Figure 4(a) shows the reconstruction and selection efficiency for $X \rightarrow Z(\rightarrow \ell\ell)\gamma$ events for a spin-0 resonance produced in gluon–gluon fusion, separately for $Z \rightarrow ee$ and $Z \rightarrow \mu\mu$. The efficiencies range from about 30% to about 46% in the mass range from 250 GeV to 2.4 TeV. For a spin-0 resonance produced via vector-boson fusion, the efficiency is larger by up to 4% over the full resonance mass range considered. Figure 4(b) shows the reconstruction and selection efficiency for spin-2 resonances produced via gluon–gluon and quark–antiquark initial states as a function of the resonance mass. For spin-2 resonances produced in gluon–gluon (quark–antiquark) initial states, the efficiencies range from about 22% (28%) to about 35% (54%) in the mass range from

² The efficiency difference between $m_H = 125$ GeV and $m_H = 125.09$ GeV is estimated to be smaller than 1%.

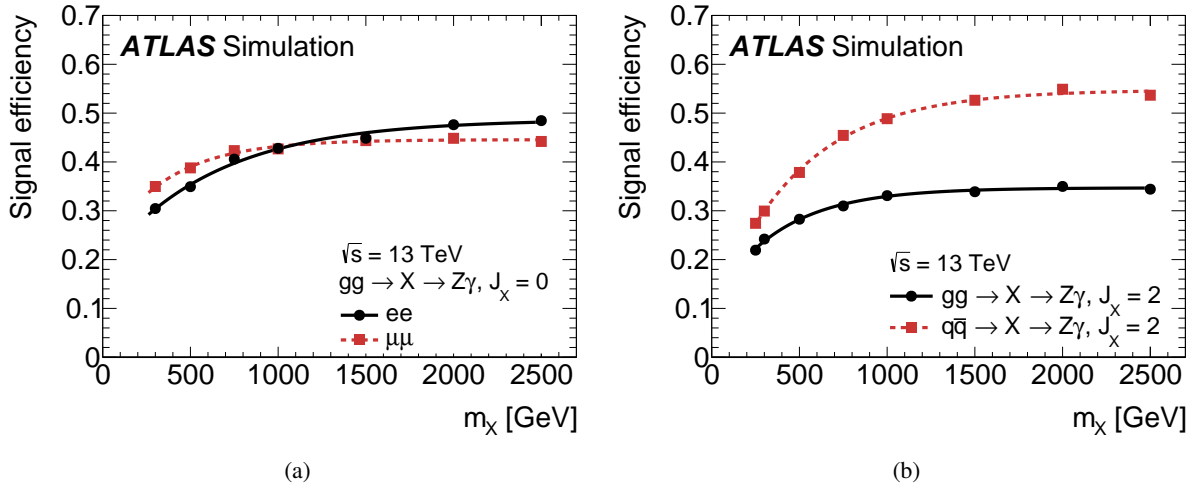


Figure 4: Reconstruction and selection efficiency (including kinematic acceptance) for the $X \rightarrow Z\gamma$ final state as a function of the resonance mass m_X (a) for a spin-0 resonance via gluon–gluon fusion, separately for the ee and the $\mu\mu$ categories, and (b) for a spin-2 resonance produced via either the gluon–gluon or the quark–antiquark initial states. The markers show the efficiencies obtained from simulation, while the curves represent the parameterisation used in the analysis. The efficiencies are given with respect to (a) $X \rightarrow Z(\rightarrow ee)\gamma$ and $X \rightarrow Z(\rightarrow \mu\mu)\gamma$, respectively, and (b) $X \rightarrow Z(\rightarrow \ell\ell)\gamma$ where $\ell = e, \mu$.

250 GeV to 2.4 TeV. The efficiency differences between the spin-0 resonance produced via gluon–gluon fusion, the spin-2 resonance produced via gluon–gluon initial states and the spin-2 resonance produced via quark–antiquark initial states are primarily related to the different photon transverse momentum distributions between the different production mechanisms.

5.2 Background modelling

The background is mainly composed of non-resonant production of a Z boson in association with a photon (irreducible background), and of inclusive Z +jets events where a jet is misidentified as a photon (reducible background), and the relative contributions are determined using data as described below. Contributions from other sources, such as $t\bar{t}$ production, W/Z events, and, for the $H \rightarrow Z\gamma$ search, from other Higgs boson decays are expected to be negligible based on studies of simulated events. The background exhibits a smoothly falling distribution as a function of the invariant mass of the candidate Z boson and photon, $m_{Z\gamma}$.

The estimated background composition is used to construct simulated background samples with the same composition as the data background. These samples are used in the optimisation of the selection criteria, the choice of analytical model of the background shape, and the estimation of the related systematic uncertainties. The searches rely only indirectly on the measured background composition since the background shape parameters are determined from the data.

The composition of the background is estimated using a combined binned fit to the calorimeter isolation distribution of the photon candidate in the signal region and in a control region enriched in Z +jets background. In the control region, photon candidates are required to fail the tight identification, but

to pass a modified loose identification. It differs from the tight identification by removing the requirements on four out of nine shower shape variables which are the least correlated with the calorimeter isolation [93]. The calorimeter isolation distribution for photons and the contribution of true photons to the control region are determined from simulation, while the calorimeter isolation distribution for jets is determined in the fit and assumed to be the same in the signal and control regions. This assumption is supported by extensive studies performed in the context of earlier analyses [93]. The composition is determined in the inclusive selection for the $H \rightarrow Z\gamma$ search and the fraction of $Z+\gamma$ events is found to be 0.838 ± 0.005 (stat.) ± 0.031 (syst.). For the high-mass resonance search, the fraction of $Z+\gamma$ events is found to be 0.916 ± 0.009 (stat.) $^{+0.013}_{-0.019}$ (syst.). The systematic uncertainties are estimated by varying the set of shower shape variables that are removed from the tight identification to define the modified loose identification [93]. The results of the composition estimate are cross-checked with a two-dimensional sideband technique [93] based on the calorimeter isolation of the photon candidate and whether or not the photon candidate satisfies the tight identification criteria (when the photon fails the tight identification it is still required to pass the modified loose identification), which gives consistent results.

The analytical model of the background and the $m_{Z\gamma}$ range used for the final fit are chosen to limit the bias in the extracted signal yield, while at the same time limiting the number of free parameters in the fit to avoid degradation of the sensitivity [1]. For each category used in either analysis, the bias (also referred to as spurious signal) is estimated as a function of the signal invariant mass by performing a signal+background fit to a $m_{Z\gamma}$ background-only distribution with small statistical fluctuations. The background-only distribution is constructed from the fast simulation of $Z+\gamma$ events, and the contribution from $Z+jets$ events is included by reweighting the $Z+\gamma$ simulated distribution as follows: for each category, the shape of the $Z+jets$ contribution is determined in a data control region defined by requiring that the photon candidate fails to satisfy the identification and isolation criteria. To smooth statistical fluctuations in the $Z+jets$ shape, a first-order polynomial is fitted to the ratio of the $Z+jets$ and $Z+\gamma$ shapes, and the smoothed $Z+jets$ shape is constructed from the fit result and the $Z+\gamma$ shape. The reweighting of the $Z+\gamma$ distribution to take into account the $Z+jets$ contribution is determined from the smoothed $Z+jets$ shape. The normalisation of the $Z+jets$ contribution is determined from the number of events obtained when applying the selection and categorisation to the $Z+\gamma$ and $Z+jets$ simulation samples and the purity of the inclusive sample, measured as described above. The spurious signal is required to be less than 40% (20%) of the expected statistical uncertainty in the signal yield, which is dominated by the expected statistical uncertainty of the background, in the search for Higgs boson (high-mass resonance) decays to $Z\gamma$. The looser requirement for the $H \rightarrow Z\gamma$ search is chosen to improve the robustness of the procedure against statistical fluctuations in the simulated $Z+\gamma$ event sample. If two or more considered functions satisfy this requirement, the function with the fewest number of parameters is chosen.

For the $H \rightarrow Z\gamma$ search, the fit range is also optimised on the basis of the spurious signal estimates, taking into account the spurious signal and the number of parameters of the chosen functions in all categories. A fit range from 115 GeV to 150 GeV is selected. A second-order Bernstein polynomial is chosen as the parameterisation for the VBF and high relative p_T categories, and a fourth-order Bernstein polynomial is chosen for the other categories. For the chosen parameterisation, the largest spurious signal obtained in a window of 121–129 GeV is assigned as a systematic uncertainty in each category associated with the choice of background function and ranges from 1.7 events in the VBF category to 25 events in the $\mu\mu$ low p_T category. The choice of background functions is validated by using second- and third-order polynomials for the smoothing of the $Z+jets$ background shape and by varying the $Z+\gamma$ purity by $\pm 15\%$. The large variation of the $Z+\gamma$ purity is chosen to cover the purity differences between the different categories and intended to also account for the additional uncertainty in the estimation of the $Z+jets$ invariant mass distribution.

The high-mass resonance search considers as a background model a class of functions [22] given by

$$f_{\text{bkg}}^k(x; b, a_k) = N(1 - x^{1/3})^b x^{\sum_{j=0}^k a_k \log(x)^j}, \quad (1)$$

where $x = m_{Z\gamma}/\sqrt{s}$, N is a normalisation factor, k determines the number of terms considered in the exponent, and b and a_k are determined by the fit. When testing on the background-only distribution constructed using the simulated $Z+\gamma$ sample taking into account $Z+\text{jets}$ contributions as discussed before, the spurious signal criterion is found to be satisfied for the full mass range for $k = 0$. The spurious signal used as an estimate of the systematic uncertainty is parameterised as a smooth function of the invariant mass. It ranges from 3.6 (6.1) events at 250 GeV to 0.01 (0.005) events at 2.4 TeV for the $Z \rightarrow \mu\mu$ ($Z \rightarrow ee$) channel. The choice of analytic function for the background shape is validated by using second- and third-order polynomials for the smoothing of the $Z+\text{jets}$ background shape, by varying the $Z+\gamma$ purity by $\pm 5\%$ (motivated by the range of purities estimated in the two categories), and by varying the PDFs in the $Z+\gamma$ simulation using the uncertainties associated with the different eigenvectors of the PDF set.

The possibility of needing higher-order functions when fitting the selected analytical function to the data $m_{Z\gamma}$ distribution is further investigated by an F -test. The test statistic F defined as

$$F = \left(\frac{\chi_0^2 - \chi_1^2}{p_1 - p_0} \right) / \left(\frac{\chi_1^2}{n - p_1} \right), \quad (2)$$

compares the fit qualities between less and more complex functions. The χ_0^2 (χ_1^2) is the χ^2 value of a binned fit with the less (more) complex parameterisation, p_k is the number of free parameters of each fit, and n is the number of bins of the invariant mass distribution. Should the probability to find values of F more extreme than the one measured on data be less than 5%, the less complex parameterisation would be rejected in favour of the more complex parameterisation. The binning for the F -test is chosen to guarantee a sufficient number of events in each bin. For the $H \rightarrow Z\gamma$ search, the test is carried out to determine if there is any indication that a higher-order Bernstein polynomial is required. It does not lead to a change in the chosen parameterisation. For the high-mass search, the test is performed to determine whether or not the quality of the fit to data is improved significantly if using $k = 1$. The test confirms that the choice of $k = 0$ is adequate. The χ^2 per degree of freedom is 1.2 for 30 degrees of freedom (1.1 for 17 degrees of freedom) or better for the chosen parameterisations for the $H \rightarrow Z\gamma$ (high-mass resonance) search.

6 Systematic uncertainties

The experimental and theoretical uncertainties that are considered in the searches can be grouped into three classes: uncertainties associated with the parameterisation of the signal and background distributions (see Section 6.1), experimental uncertainties in the efficiency and acceptance affecting the expected event yields (see Section 6.2), and theoretical uncertainties in the modelling of the signal in the simulation (see Section 6.3). The nuisance parameters in the likelihood function (see Section 7) represent the uncertainties which are studied in each category using the simulated signal samples generated at $m_H = 125$ GeV for the $H \rightarrow Z\gamma$ search, and $m_X = [300 - 2500]$ GeV at high-mass. The main experimental sources of uncertainty are summarised in Table 4.

Table 4: The main sources of experimental uncertainty for the $H/X \rightarrow Z\gamma$ searches. The gluon–gluon fusion signal samples produced at $m_H = 125$ GeV and $m_X = [300\text{--}2500]$ GeV are used to estimate the systematic uncertainty. The ranges for the uncertainties span the variations among different categories and different m_X resonance masses. The uncertainty values are given as fractions of the total predictions, except for the spurious signal uncertainty, which is reported as the absolute number of events. Values are not listed if systematic sources are negligible or not applicable.

Sources	$H \rightarrow Z\gamma$	$X \rightarrow Z\gamma$
<i>Luminosity [%]</i>		
Luminosity	3.2	3.2
<i>Signal efficiency [%]</i>		
Modelling of pile-up interactions	0.02–0.03	< 0.01–0.2
Photon identification efficiency	0.7–1.7	2.0–2.6
Photon isolation efficiency	0.07–0.4	0.6–0.6
Electron identification efficiency	0.0–1.6	0.0–2.6
Electron isolation efficiency	0.0–0.2	0.0–3.5
Electron reconstruction efficiency	0.0–0.4	0.0–1.0
Electron trigger efficiency	0.0–0.1	0.0–0.2
Muon selection efficiency	0.0–1.6	0.0–0.7
Muon trigger efficiency	0.0–3.5	0.0–4.2
MC statistical uncertainty	–	1.2–2.0
Jet energy scale, resolution, and pile-up	0.2–10	–
Total (signal efficiency)	2.1–10	4.0–6.3
<i>Signal modelling on σ_{CB} [%]</i>		
Electron and photon energy scale	0.6–3.5	1.0–4.0
Electron and photon energy resolution	1.1–4.0	4.0–30
Muon momentum scale	0.0–0.5	0.0–3.0
Muon ID resolution	0.0–3.7	0.0–2.0
Muon MS resolution	0.0–1.7	0.0–4.0
<i>Signal modelling on μ_{CB} [%]</i>		
Electron and photon energy scale	0.1–0.2	0.2–0.6
Muon momentum scale	0.0–0.03	0.0–0.03
Higgs mass	0.2	–
<i>Background modelling [Events]</i>		
Spurious signal	1.7–25	0.005–6.1

6.1 Uncertainties from signal and background modelling

The uncertainties in the lepton and photon momentum and energy scale and resolution impact the modelling of the signal. Their impact is assessed by comparing the nominal $m_{Z\gamma}$ shape parameters with the $m_{Z\gamma}$ shape parameters after varying the lepton and photon momentum and energy scale and resolution by their uncertainties. Uncertainties in both the position (μ_{CB}) and width (σ_{CB}) of the signal $m_{Z\gamma}$ distribution are considered.

The systematic uncertainties in the muon momentum scale and resolution were determined from $Z \rightarrow \mu\mu$ and $J/\psi \rightarrow \mu\mu$ events using the techniques described in Ref. [77]. At $m_H = 125$ GeV, the uncertainty in the muon momentum scale (resolution) varies σ_{CB} by up to 0.5% (4.0%). In the high-mass search, the effect of the muon momentum scale (resolution) uncertainty is to change σ_{CB} by up to 3.0% (4.0%). The typical effect of the muon momentum scale uncertainty is to change μ_{CB} by < 0.1% of its nominal value.

The systematic uncertainties in the electron and photon energy scale and resolution follow those in Refs. [94, 95]. The overall energy scale factors and their uncertainties were determined using $Z \rightarrow ee$ events. Compared to Ref. [95], several systematic uncertainties were re-evaluated with the 13 TeV data, including uncertainties related to the observed LAr cell non-linearity, the material simulation, the intercalibration of the first and second layer of the calorimeter, and the pedestal corrections. At $m_H = 125$ GeV, the uncertainty in the electron and photon energy scale (resolution) results in variation in σ_{CB} between 0.6% and 3.5% (1.1% and 4.0%) depending on the category. For a high-mass resonance, σ_{CB} varies between 1.0% and 4.0% (4.0% and 30%) due to uncertainties in the electron/photon momentum scale (momentum resolution). The variation in μ_{CB} is less than 0.2% (0.6%) at $m_H = 125$ GeV (at high masses).

For the $H \rightarrow Z\gamma$ search, an additional uncertainty in the assumed Higgs mass $m_H = 125.09$ GeV is added in the fit, reflecting the 0.24 GeV [3] uncertainty in the measured Higgs boson mass.

The uncertainty due to the choice of background function is taken to be the signal yield (spurious signal) obtained when fitting the $m_{Z\gamma}$ spectra reconstructed from background-only distributions as discussed in Section 5.

6.2 Experimental uncertainties affecting the signal efficiency and acceptance

Experimental uncertainties affecting the signal efficiency and acceptance can be either correlated between all event categories (yield uncertainties) or anticorrelated between some of the categories (migration uncertainties) when they are related to how the signal populates the event categories.

The uncertainty in the combined 2015+2016 integrated luminosity is 3.2%, correlated between all categories. It is derived, following a methodology similar to that detailed in Ref. [96], from a preliminary calibration of the luminosity scale using $x-y$ beam-separation scans performed in August 2015 and May 2016.

A variation in the pile-up reweighting of the simulation is included to cover the uncertainty in the ratio of the predicted and measured inelastic cross sections in the fiducial volume defined by $m > 13$ GeV where m is the mass of the hadronic system [97]. The uncertainty in the signal efficiency is no more than 0.03% (0.2%) for the $H \rightarrow Z\gamma$ (high-mass resonance) search.

The uncertainties in the reconstruction, identification, isolation, and trigger efficiency measurements for muons, electrons and photons (see Section 4) are treated as fully correlated between all categories. They are determined from control samples of $J/\psi \rightarrow \mu\mu$ and $Z \rightarrow \mu\mu$ for muons, $J/\psi \rightarrow ee$ and $Z \rightarrow ee$ for electrons, and $Z \rightarrow \ell\ell\gamma$, $Z \rightarrow ee$, and inclusive photons for photons, using methods described in Refs. [77, 78, 80].

For the $H \rightarrow Z\gamma$ search, the uncertainties in the signal efficiency from the photon identification and isolation are found to be no more than 1.7% and 0.4%, respectively. The uncertainties in the signal efficiency from the electron reconstruction, identification, isolation, and trigger are found to be no more than 0.4%, 1.6%, 0.2%, and 0.1%, respectively. The uncertainties in the signal efficiency from the muon selection and trigger are determined to be no more than 1.6% and 3.5%, respectively. For the high-mass search, the uncertainties in the signal efficiency from photon identification and isolation are found to be no more than 2.6% and 0.6%, respectively. The uncertainties in the signal efficiency from the electron reconstruction, identification, isolation, and trigger are found to be no more than 1.0%, 2.6%, 3.5%, and 0.2%, respectively. The uncertainties in the efficiency from the muon selection and trigger are determined to be as large as 0.7% and 4.2%, respectively. The uncertainty due to the limited size of the simulated event samples ranges from 1.2% to 2.0% for the search for high-mass resonances.

In the $H \rightarrow Z\gamma$ search, the expected signal yield in the VBF category is affected by the jet energy scale and resolution and the jet vertex tagging efficiency. The corresponding uncertainties are anticorrelated with the other categories. Uncertainties in the jet energy scale and resolution are estimated from the transverse momentum balance in dijet, γ +jet and Z +jet events [84]. Uncertainties in the efficiency of the jet vertex tagging are estimated by shifting the associated corrections applied to the simulation by an amount allowed by the data. The uncertainties in the category acceptances are as large as 4.6%, 6.9%, and 4.8% from the data-driven jet calibration, the impact of the jet flavour composition on the calibration, and the jet vertex tagging.

6.3 Theoretical and modelling uncertainties

For the $H \rightarrow Z\gamma$ search, theoretical and modelling uncertainties in the SM predictions for Higgs boson production and the decay to the $Z\gamma$ final state are taken into account and are summarised in Table 5. They fall into two classes: uncertainties in the total predicted cross sections, the predicted decay branching ratio and the total efficiency, correlated between all categories; and uncertainties in the event fractions per category, anticorrelated between certain categories.

Uncertainties related to the total acceptance and efficiency for $H \rightarrow Z\gamma$ events affect the extraction of the signal strength, the branching ratio of $H \rightarrow Z\gamma$ assuming SM Higgs boson production, as well as the product of the Higgs boson production cross section and the branching ratio of $H \rightarrow Z\gamma$ (see Section 7). The uncertainty in the total efficiency due to the modelling of multiple-parton interactions is estimated from the difference in efficiency with and without multiple-particle interactions for the gluon–gluon fusion simulation sample, and found to be 5.3%.

The uncertainties related to the predicted Higgs boson production cross section affect the extraction of the signal strength as well as the branching ratio of $H \rightarrow Z\gamma$ assuming SM Higgs boson production. The uncertainties in the predicted total cross sections of the different Higgs boson production processes due to the perturbative order of the calculation and the combined uncertainties in the PDFs and α_s are 3.9% and 3.2% for gluon–gluon fusion production, respectively, and range from 0.4% to 3.8% for the other production processes for a Higgs boson mass of 125.09 GeV and a centre-of-mass energy of 13 TeV [29].

Table 5: The main sources of theoretical and modelling uncertainties for the $H \rightarrow Z\gamma$ search. For the uncertainties in the total efficiency and the acceptance of the different categories, the gluon–gluon fusion samples produced with PowHEG Box v1 with and without MPI are used, as well as the nominal PowHEG Box v2 gluon–gluon fusion signal sample along with the sample generated with `MADGRAPH5_AMC@NLO`, as described in the text. The combined uncertainty on the total cross section and efficiency is given assuming the cross sections predicted by the SM. The ranges for the uncertainties cover the variations among different categories. The uncertainty values are given as relative uncertainties.

Sources	
<i>Total cross section and efficiency [%]</i>	
Underlying event	5.3
ggF perturbative order	3.9
ggF PDF and α_s	3.2
VBF perturbative order	0.4
VBF PDF and α_s	2.1
WH (ZH) perturbative order	0.5 (3.8)
WH (ZH) PDF and α_s	1.9 (1.6)
Interference	5.0
$B(H \rightarrow Z\gamma)$	5.9
Total (total cross section and efficiency)	10
<i>Category acceptance [%]</i>	
ggF $H + 2$ -jets in VBF-enriched category	0.5–45
ggF BDT variables	0.2–15
ggF Higgs p_T	8.4–22
PDF and α_s	0.2–2.0
Underlying event	2.9–25
Total (category acceptance)	9.5–49

An additional 5.0% [98] uncertainty accounts for the effect, in the selected phase space of the $\ell\ell\gamma$ final state, of the interfering $H \rightarrow \ell\ell\gamma$ decay amplitudes that are neglected in the calculation of Ref. [29]. They originate from internal photon conversion in Higgs boson decays to diphotons ($H \rightarrow \gamma^*\gamma \rightarrow \ell\ell\gamma$) or from Higgs boson decays to dileptons with an off-shell lepton ($H \rightarrow \ell\ell^* \rightarrow \ell\ell\gamma$) [99, 100].

The uncertainty in the predicted Higgs boson branching ratio to $Z\gamma$ affects the extraction of the signal strength. The relative theoretical uncertainty in the predicted Higgs boson branching ratio is 5.9% [29].

Uncertainties in the modelling of kinematic distributions in the simulation of Higgs boson production processes affect the predicted event fractions in the different categories. The uncertainty in the modelling of the production of jets in gluon–gluon fusion production due to the perturbative order in QCD is estimated by scale variations in MCFM [101]. It accounts for the uncertainty in the overall normalisation of $H + 2$ -jets events as well as the uncertainty due to the use of $\Delta\phi_{Z\gamma,jj}$, which serves to apply an implicit third-jet veto, in the VBF BDT. The estimation of this uncertainty uses an extension of the Stewart–Tackmann method [102, 103]. It corresponds to 45% of the ggF contribution to the VBF category. Additional uncertainties are assigned to account for potential mismodelling of the variables that serve as input to the VBF BDT (see Section 4). They are estimated by reweighting the simulated ggF events to match the distributions in m_{jj} , $\Delta\eta_{jj}$, p_{Tt} , $\Delta R_{Z/\gamma,j}^{\min}$, and $|\eta_{Z\gamma} - (\eta_{j1} + \eta_{j2})/2|$ obtained from `MADGRAPH5_AMC@NLO`. The resulting uncertainty in the ggF contribution to the VBF category is 15%. Uncertainties in the modelling

of the Higgs boson p_T spectrum are taken to be the envelope of the variations of the renormalisation, factorisation, and resummation scales obtained using HRes 2.3 [104] to simulate the p_T spectrum. The resulting uncertainties are evaluated using the Stewart–Tackmann method [102, 103] for the high relative p_T and the p_{Tt} categorisation and found to range from 8.4% to 22%. Uncertainties from the choice of PDF set and α_s are evaluated using the combined error PDF set, which takes into account 30 variations of NNLO PDFs and two variations of α_s , following the PDF4LHC recommendations [33] and are found to range from 0.2% to 2.0%. The uncertainty in the acceptance due to the modelling of multiple-parton interactions is estimated from the difference in acceptance with and without multiple-particle interactions for the gluon–gluon fusion simulation sample and ranges from 2.9% to 25%.

7 Statistical procedure

A profile-likelihood-ratio test statistic [105] is used to search for a localised excess over a smoothly falling background in the $m_{Z\gamma}$ distribution of the data, as well as to quantify its significance and estimate either its production cross section or signal strength.

The extended unbinned likelihood function $\mathcal{L}(\alpha, \theta)$ is given by the product of a Poisson term, constructed from the number of observed events, n , the expected event yield, N , and the probability density function of the invariant mass distribution for each candidate event i , $f_{\text{tot}}(m_{Z\gamma}^i, \alpha, \theta)$ [22]:

$$\mathcal{L}\left((\alpha, \theta) \middle| \{m_{Z\gamma}^i\}_{i=1..n}\right) = \frac{e^{-N(\alpha, \theta)} N^n(\alpha, \theta)}{n!} \prod_{i=1}^n f_{\text{tot}}(m_{Z\gamma}^i, \alpha, \theta) \times G(\theta), \quad (3)$$

where α represents the parameter of interest and θ are the nuisance parameters. The function $G(\theta)$ represents the prior constraints on the nuisance parameters. The expected event yield N is the sum of the expected number of signal (N_{sig}), background (N_{bkg}), and spurious signal ($N_{\text{spur}} \cdot \theta_{\text{spur}}$) events, where θ_{spur} is the nuisance parameter associated with the spurious signal. For the high-mass resonance search, the parameter of interest is $\alpha = \sigma(pp \rightarrow X) \cdot B(X \rightarrow Z\gamma)$. The $H \rightarrow Z\gamma$ search is performed to extract several parameters of interest: the signal strength $\mu = \sigma(pp \rightarrow H) \cdot B(H \rightarrow Z\gamma) / (\sigma(pp \rightarrow H)_{\text{SM}} \cdot B(H \rightarrow Z\gamma)_{\text{SM}})$, $\sigma(pp \rightarrow H) \cdot B(H \rightarrow Z\gamma)$, and $B(H \rightarrow Z\gamma)$ assuming $\sigma(pp \rightarrow H)_{\text{SM}}$. The signal strength μ is related to the number of signal events by $N_{\text{sig}} = L_{\text{tot}} \times \mu \times (\sigma(pp \rightarrow H)_{\text{SM}} \cdot B(H \rightarrow Z\gamma)_{\text{SM}}) \times \varepsilon$, where L_{tot} is the total integrated luminosity, ε is the signal efficiency, and $\sigma(pp \rightarrow H)_{\text{SM}} \cdot B(H \rightarrow Z\gamma)_{\text{SM}}$ is predicted by the SM. The theoretical uncertainties are taken into account as described in Section 6.

The probability density function for the invariant mass ($f_{\text{tot}}(m_{Z\gamma}^i, \alpha, \theta)$) is built from the probability density functions f_{sig} and f_{bkg} describing the signal and background invariant mass distributions, respectively:

$$f_{\text{tot}}(m_{Z\gamma}^i, \alpha, \theta) = \frac{1}{N} \sum_c \left\{ \left[N_{\text{sig}}^{(c)}(\alpha, \theta_{\text{sig}}) + N_{\text{spur}}^{(c)} \cdot \theta_{\text{spur}}^{(c)} \right] \times f_{\text{sig}}^{(c)}(m_{Z\gamma}^i, \theta_{\text{sig}}) + N_{\text{bkg}}^{(c)} \times f_{\text{bkg}}^{(c)}(m_{Z\gamma}^i, \theta_{\text{bkg}}) \right\}. \quad (4)$$

The index c indicates the category. The θ_{bkg} are nuisance parameters that determine the shape of the background. The nuisance parameters associated with the uncertainties in the signal parameterisation, efficiency and acceptance are denoted by θ_{sig} . Nuisance parameters associated with uncertainties in the event yield or the $m_{Z\gamma}$ resolution are assigned log-normal probability density functions, while nuisance

parameters associated with the $m_{Z\gamma}$ signal peak position are assigned Gaussian probability density functions. The nuisance parameters associated with the spurious signal, θ_{spur} , are assigned Gaussian probability density functions.

The probability that the background can produce a fluctuation greater than or equal to an excess observed in data is quantified by the p -value of the $\alpha = 0$ hypothesis, p_0 , which can also be expressed in terms of number of Gaussian standard deviations and provides an estimate of the local significance of a possible deviation from the expected background. The global significance, corrected for the effect that a deviation can occur anywhere in the search region, is estimated taking into account the trial factors [106]. The compatibility between the data and increasing non-zero values of α is used to set upper limits at the 95% CL on $\sigma(pp \rightarrow H/X) \cdot B(H/X \rightarrow Z\gamma)$, $B(H \rightarrow Z\gamma)$, and the signal strength for $pp \rightarrow H \rightarrow Z\gamma$, respectively, using a modified frequentist (CL_s) method [107], by identifying the value α for which the value of CL_s is equal to 0.05.

The results are derived using closed-form asymptotic formulae [105] for masses up to 1.6 TeV. Due to the small number of events at large $m_{Z\gamma}$ in the high-mass resonance search, the results for $m_X > 1.6$ TeV are derived using ensemble tests. The expected cross-section limits obtained from the asymptotic formulae agree to better than 10% with those obtained from the ensemble tests up to m_X of 1.7 TeV. At high m_X , the observed (expected) central values are underestimated by 35% (23%) in the asymptotic approach.

8 Results

No evidence of a localised excess is visible near the anticipated Higgs mass $m_H = 125.09$ GeV, as shown in Figure 5 where the invariant mass distributions $m_{Z\gamma}$ for the individual categories of the $H \rightarrow Z\gamma$ search are displayed with the background-only fit performed in the range of $115 \text{ GeV} < m_{Z\gamma} < 150 \text{ GeV}$. At $m_H = 125.09$ GeV, the observed p -value is 0.16 under the background-only hypothesis, in which the dominant contribution comes from the $\mu\mu$ low $p_{T\ell}$ category. The p -value corresponds to a local significance of 1.0σ . The expected p -value for a SM Higgs boson at $m_H = 125.09$ GeV is 0.33, corresponding to a significance of 0.5σ . The observed 95% CL limit on $\sigma(pp \rightarrow H) \cdot B(H \rightarrow Z\gamma)$ is found to be 6.6 times the SM prediction, corresponding to the limit of 547 fb. Assuming SM Higgs boson production, the upper limit on the branching ratio of the Higgs boson decay to $Z\gamma$ is found to be 1.0%. The expected 95% CL limit on $\sigma(pp \rightarrow H) \cdot B(H \rightarrow Z\gamma)$ assuming no (a SM) Higgs boson decay to $Z\gamma$ is 4.4 (5.2) times the SM prediction.

The invariant mass distributions of events satisfying the high-mass selection are displayed for both categories (ee and $\mu\mu$) in Figure 6 and compared to the background-only fit performed in the fit range $200 \text{ GeV} < m_{Z\gamma} < 2500 \text{ GeV}$. The highest masses measured in the ee and $\mu\mu$ final states are 1.47 TeV and 1.57 TeV, respectively. In the fit range, no significant excess is observed with respect to the background-only hypothesis. The largest deviation is observed around $m_X = 960$ GeV corresponding to a local significance of 2.7σ . The global significance, evaluated using the search region of [250–2400] GeV in mass, is found to be 0.8σ . The observed and expected upper limits on $\sigma(pp \rightarrow X) \cdot B(X \rightarrow Z\gamma)$ as a function of m_X are shown in Figure 7. The observed limits vary between 88 fb and 2.8 fb for the mass range from 250 GeV to 2.4 TeV at the 95% CL for a spin-0 resonance produced via gluon–gluon fusion, while the expected limits range from 61 fb to 2.7 fb in the same mass range. For a spin-0 resonance produced via vector-boson fusion, the limits are up to 4% lower due to the slightly larger efficiency for this production process.

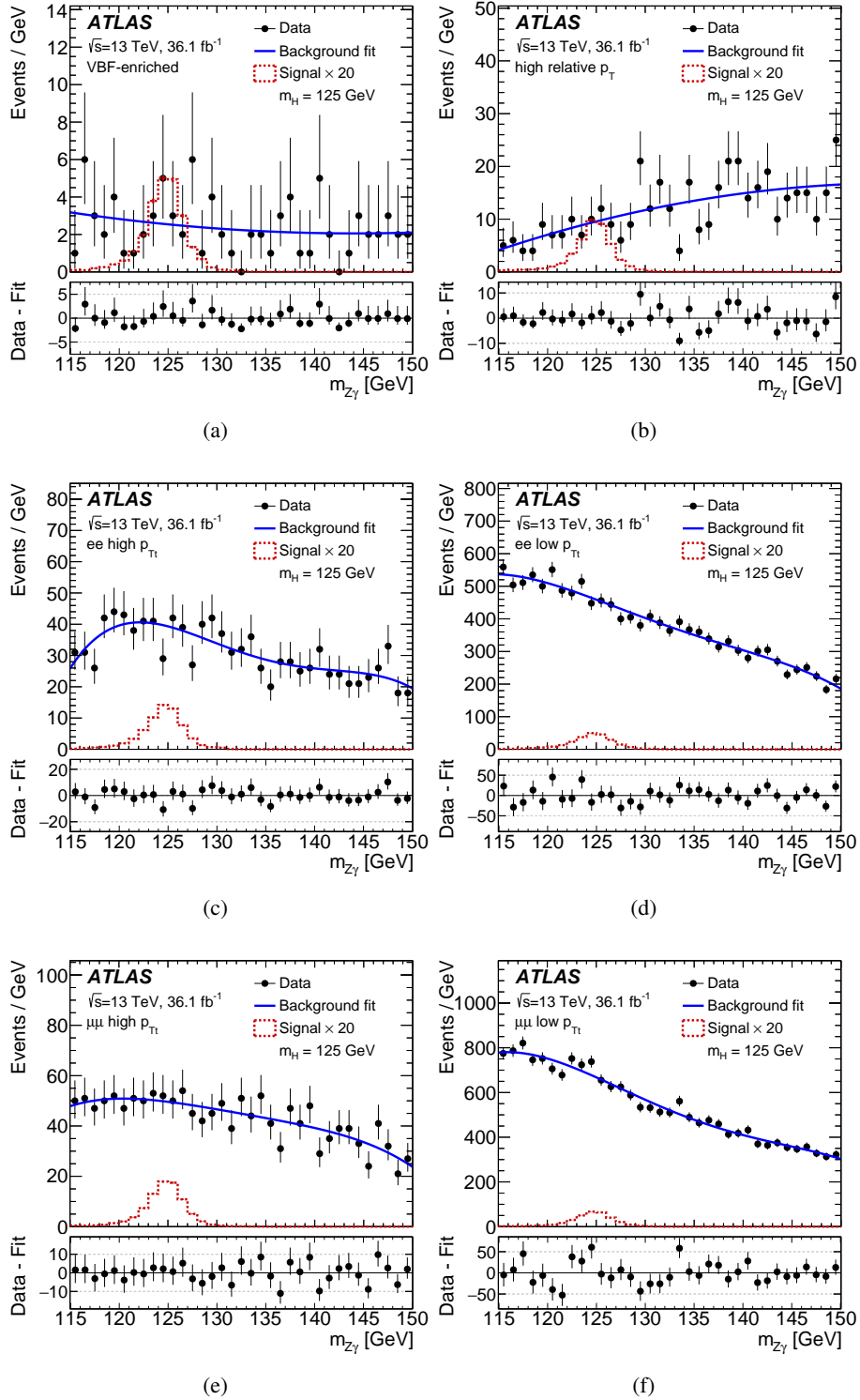


Figure 5: The invariant $Z\gamma$ mass ($m_{Z\gamma}$) distributions of events satisfying the $H \rightarrow Z\gamma$ selection in data for the six event categories: (a) VBF-enriched, (b) high p_T^γ , (c) ee high p_{Tt} , (d) ee low p_{Tt} , (e) $\mu\mu$ high p_{Tt} , and (f) $\mu\mu$ low p_{Tt} . The points represent the data and the statistical uncertainty. The solid lines show the background-only fits to the data, performed independently in each category. The dashed histogram corresponds to the expected signal for a SM Higgs boson with $m_H = 125 \text{ GeV}$ decaying to $Z\gamma$ with a rate 20 times the SM prediction. The bottom part of the figures shows the residuals of the data with respect to the background-only fit.

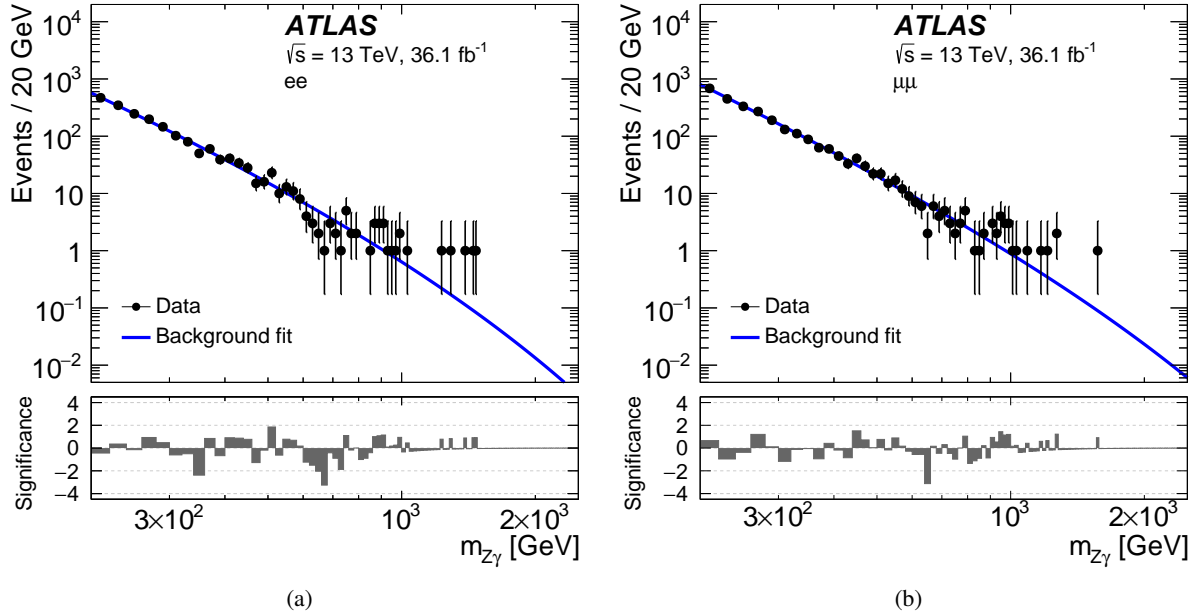


Figure 6: The invariant $Z\gamma$ mass ($m_{Z\gamma}$) distributions of events satisfying the high-mass selection in data for the two event categories: (a) ee and (b) $\mu\mu$. The points represent the data and the statistical uncertainty. The solid lines show the background-only fit to the data, performed independently in each category. The bottom part of the figures shows the significance, here defined as the residual of the data with respect to the background-only fit divided by the statistical uncertainty of the data.

The results are also interpreted in terms of spin-2 resonances. Observed and expected upper limits at the 95% CL on $\sigma(pp \rightarrow X) \cdot B(X \rightarrow Z\gamma)$ are derived and shown in Figure 8 for both the gg and $q\bar{q}$ processes. The observed limits for the gg ($q\bar{q}$) process vary between 117 fb (94 fb) and 3.7 fb (2.3 fb) for the mass range from 250 GeV to 2.4 TeV, while the expected limits range between 82 fb (66 fb) and 3.6 fb (2.2 fb) in the same mass range.

The limits on $\sigma(pp \rightarrow X) \cdot B(X \rightarrow Z\gamma)$ for high-mass resonances are valid for resonances with a natural width that is small compared to the detector resolution.

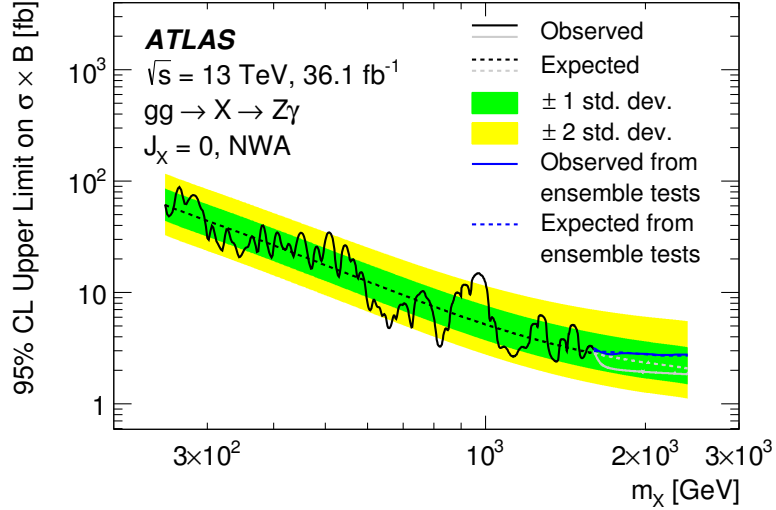


Figure 7: The observed (solid line) and expected (dashed line) upper limit derived at the 95% CL on $\sigma(pp \rightarrow X) \cdot B(X \rightarrow Z\gamma)$ at $\sqrt{s} = 13$ TeV as a function of the high-mass spin-0 resonance's mass, assuming production via gluon–gluon fusion and using the narrow width assumption (NWA). For $m_X > 1.6$ TeV results are derived from ensemble tests in addition to the results obtained using closed-form asymptotic formulae. The shaded regions correspond to the ± 1 and ± 2 standard deviation bands for the expected exclusion limit derived using asymptotic formulae.

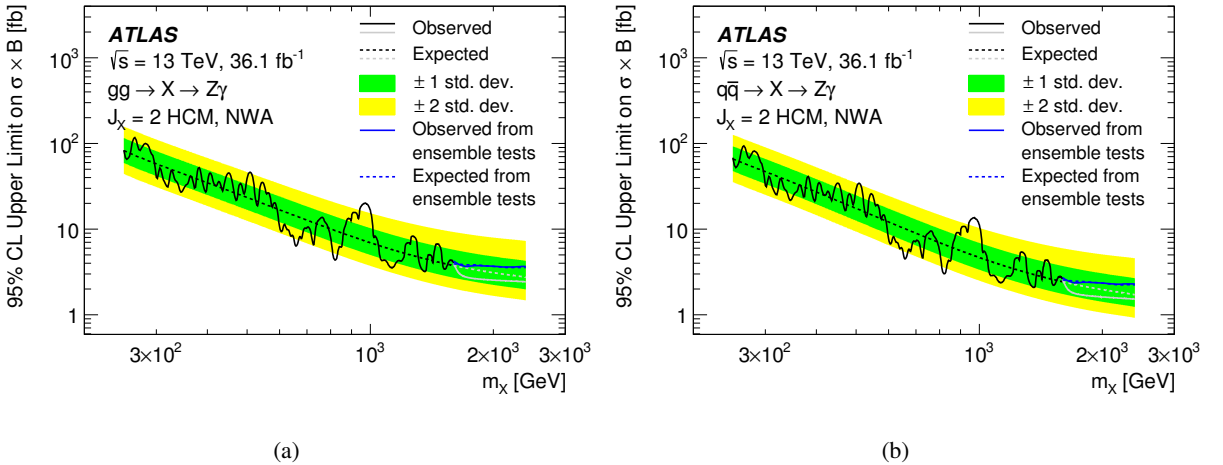


Figure 8: The observed (solid line) and expected (dashed line) upper limit derived at the 95% CL on $\sigma(pp \rightarrow X) \cdot B(X \rightarrow Z\gamma)$ at $\sqrt{s} = 13$ TeV as a function of the spin-2 resonance mass produced via (a) gluon–gluon initial states and (b) $q\bar{q}$ initial states modelled using the Higgs Characterisation Model (HCM), using the narrow width assumption (NWA). For $m_X > 1.6$ TeV results are derived from ensemble tests in addition to the results obtained using closed-form asymptotic formulae. The shaded regions correspond to the ± 1 and ± 2 standard deviation bands for the expected exclusion limit derived using asymptotic formulae.

9 Conclusion

Searches for $Z\gamma$ decays of the SM Higgs boson ($H \rightarrow Z\gamma$) and of a narrow high-mass resonance ($X \rightarrow Z\gamma$) in 36.1 fb^{-1} of pp collisions at $\sqrt{s} = 13 \text{ TeV}$ at the LHC have been performed with the ATLAS experiment. The observed data are consistent with the expected background. No evidence for the $H \rightarrow Z\gamma$ and $X \rightarrow Z\gamma$ decays is observed and upper limits are set on $\sigma(pp \rightarrow H) \cdot B(H \rightarrow Z\gamma)$ at $m_H = 125.09 \text{ GeV}$ and also on $\sigma(pp \rightarrow X) \cdot B(X \rightarrow Z\gamma)$ as a function of m_X . For the Higgs mass of 125.09 GeV , the observed 95% CL upper limit on the $\sigma(pp \rightarrow H) \cdot B(H \rightarrow Z\gamma)$ is 6.6 times the SM prediction. The search for high-mass $Z\gamma$ resonances was studied using both the spin-0 and spin-2 interpretations. The observed limit varies between 88 fb and 2.8 fb for the mass range from 250 GeV to 2.4 TeV for a spin-0 resonance, where a resonance produced in gluon–gluon fusion is used as a benchmark model. For spin-2 resonances, LO predictions from the Higgs Characterisation Model are used as benchmarks. The limits for spin-2 resonances range between 117 fb (94 fb) and 3.7 fb (2.3 fb) for the mass range from 250 GeV to 2.4 TeV for a resonance produced via gluon–gluon (quark–antiquark) initial states. The corresponding expected limits for this mass range vary between 61 fb and 2.7 fb for a spin-0 resonance, and between 82 fb (66 fb) and 3.6 fb (2.2 fb) for a spin-2 resonance produced via gluon–gluon (quark–antiquark) initial states.

Acknowledgements

We thank CERN for the very successful operation of the LHC, as well as the support staff from our institutions without whom ATLAS could not be operated efficiently.

We acknowledge the support of ANPCyT, Argentina; YerPhI, Armenia; ARC, Australia; BMWFW and FWF, Austria; ANAS, Azerbaijan; SSTC, Belarus; CNPq and FAPESP, Brazil; NSERC, NRC and CFI, Canada; CERN; CONICYT, Chile; CAS, MOST and NSFC, China; COLCIENCIAS, Colombia; MSMT CR, MPO CR and VSC CR, Czech Republic; DNRF and DNSRC, Denmark; IN2P3-CNRS, CEA-DSM/IRFU, France; SRNSF, Georgia; BMBF, HGF, and MPG, Germany; GSRT, Greece; RGC, Hong Kong SAR, China; ISF, I-CORE and Benoziyo Center, Israel; INFN, Italy; MEXT and JSPS, Japan; CNRST, Morocco; NWO, Netherlands; RCN, Norway; MNiSW and NCN, Poland; FCT, Portugal; MNE/IFA, Romania; MES of Russia and NRC KI, Russian Federation; JINR; MESTD, Serbia; MSSR, Slovakia; ARRS and MIZŠ, Slovenia; DST/NRF, South Africa; MINECO, Spain; SRC and Wallenberg Foundation, Sweden; SERI, SNSF and Cantons of Bern and Geneva, Switzerland; MOST, Taiwan; TAEK, Turkey; STFC, United Kingdom; DOE and NSF, United States of America. In addition, individual groups and members have received support from BCKDF, the Canada Council, CANARIE, CRC, Compute Canada, FQRNT, and the Ontario Innovation Trust, Canada; EPLANET, ERC, ERDF, FP7, Horizon 2020 and Marie Skłodowska-Curie Actions, European Union; Investissements d’Avenir Labex and Idex, ANR, Région Auvergne and Fondation Partager le Savoir, France; DFG and AvH Foundation, Germany; Herakleitos, Thales and Aristeia programmes co-financed by EU-ESF and the Greek NSRF; BSF, GIF and Minerva, Israel; BRF, Norway; CERCA Programme Generalitat de Catalunya, Generalitat Valenciana, Spain; the Royal Society and Leverhulme Trust, United Kingdom.

The crucial computing support from all WLCG partners is acknowledged gratefully, in particular from CERN, the ATLAS Tier-1 facilities at TRIUMF (Canada), NDGF (Denmark, Norway, Sweden), CC-IN2P3 (France), KIT/GridKA (Germany), INFN-CNAF (Italy), NL-T1 (Netherlands), PIC (Spain), ASGC

(Taiwan), RAL (UK) and BNL (USA), the Tier-2 facilities worldwide and large non-WLCG resource providers. Major contributors of computing resources are listed in Ref. [108].

References

- [1] ATLAS Collaboration, *Observation of a new particle in the search for the Standard Model Higgs boson with the ATLAS detector at the LHC*, *Phys. Lett. B* **716** (2012) 1, arXiv: [1207.7214 \[hep-ex\]](#).
- [2] CMS Collaboration, *Observation of a new boson at a mass of 125 GeV with the CMS experiment at the LHC*, *Phys. Lett. B* **716** (2012) 30, arXiv: [1207.7235 \[hep-ex\]](#).
- [3] ATLAS and CMS Collaborations, *Combined Measurement of the Higgs Boson Mass in pp Collisions at $\sqrt{s} = 7$ and 8 TeV with the ATLAS and CMS Experiments*, *Phys. Rev. Lett.* **114** (2015) 191803, arXiv: [1503.07589 \[hep-ex\]](#).
- [4] ATLAS Collaboration, *Measurements of the Higgs boson production and decay rates and coupling strengths using pp collision data at $\sqrt{s} = 7$ and 8 TeV in the ATLAS experiment*, *Eur. Phys. J. C* **76** (2016) 6, arXiv: [1507.04548 \[hep-ex\]](#).
- [5] CMS Collaboration, *Precise determination of the mass of the Higgs boson and tests of compatibility of its couplings with the standard model predictions using proton collisions at 7 and 8 TeV*, *Eur. Phys. J. C* **75** (2015) 212, arXiv: [1412.8662 \[hep-ex\]](#).
- [6] ATLAS and CMS Collaborations, *Measurements of the Higgs boson production and decay rates and constraints on its couplings from a combined ATLAS and CMS analysis of the LHC pp collision data at $\sqrt{s} = 7$ and 8 TeV*, *JHEP* **08** (2016) 045, arXiv: [1606.02266 \[hep-ex\]](#).
- [7] ATLAS Collaboration, *Evidence for the spin-0 nature of the Higgs boson using ATLAS data*, *Phys. Lett. B* **726** (2013) 120, arXiv: [1307.1432 \[hep-ex\]](#).
- [8] ATLAS Collaboration, *Study of the spin and parity of the Higgs boson in diboson decays with the ATLAS detector*, *Eur. Phys. J. C* **75** (2015) 476, [Erratum: *Eur. Phys. J. C*76 (2016) 152], arXiv: [1506.05669 \[hep-ex\]](#).
- [9] CMS Collaboration, *Study of the mass and spin-parity of the Higgs boson candidate via its decays to Z boson pairs*, *Phys. Rev. Lett.* **110** (2013) 081803, arXiv: [1212.6639 \[hep-ex\]](#).
- [10] CMS Collaboration, *Constraints on the spin-parity and anomalous HVV couplings of the Higgs boson in proton collisions at 7 and 8 TeV*, *Phys. Rev. D* **92** (2015) 012004, arXiv: [1411.3441 \[hep-ex\]](#).
- [11] C. Patrignani et al., *Review of Particle Physics*, *Chin. Phys. C* **40** (2016) 100001.
- [12] I. Low, J. Lykken and G. Shaughnessy, *Singlet scalars as Higgs imposters at the Large Hadron Collider*, *Phys. Rev. D* **84** (2011) 035027, arXiv: [1105.4587 \[hep-ph\]](#).

- [13] I. Low, J. Lykken and G. Shaughnessy, *Have we observed the Higgs (impostor)?*, *Phys. Rev. D* **86** (2012) 093012, arXiv: [1207.1093 \[hep-ph\]](#).
- [14] A. Azatov, R. Contino, A. Di Iura and J. Galloway, *New Prospects for Higgs Compositeness in $h \rightarrow Z\gamma$* , *Phys. Rev. D* **88** (2013) 075019, arXiv: [1308.2676 \[hep-ph\]](#).
- [15] C.-W. Chiang and K. Yagyu, *Higgs boson decays to $\gamma\gamma$ and $Z\gamma$ in models with Higgs extensions*, *Phys. Rev. D* **87** (2013) 033003, arXiv: [1207.1065 \[hep-ph\]](#).
- [16] C.-S. Chen, C.-Q. Geng, D. Huang and L.-H. Tsai, *New Scalar Contributions to $h \rightarrow Z\gamma$* , *Phys. Rev. D* **87** (2013) 075019, arXiv: [1301.4694 \[hep-ph\]](#).
- [17] M. Carena, I. Low and C. E. Wagner, *Implications of a Modified Higgs to Diphoton Decay Width*, *JHEP* **08** (2012) 060, arXiv: [1206.1082 \[hep-ph\]](#).
- [18] ATLAS Collaboration, *Search for Higgs boson decays to a photon and a Z boson in pp collisions at $\sqrt{s} = 7$ and 8 TeV with the ATLAS detector*, *Phys. Lett. B* **732** (2014) 8, arXiv: [1402.3051 \[hep-ex\]](#).
- [19] CMS Collaboration, *Search for a Higgs boson decaying into a Z and a photon in pp collisions at $\sqrt{s} = 7$ and 8 TeV*, *Phys. Lett. B* **726** (2013) 587, arXiv: [1307.5515 \[hep-ex\]](#).
- [20] D0 Collaboration, V. M. Abazov et al., *Search for a scalar or vector particle decaying into $Z\gamma$ in $p\bar{p}$ collisions at $\sqrt{s}=1.96$ TeV*, *Phys. Lett. B* **671** (2009) 349, arXiv: [0806.0611 \[hep-ex\]](#).
- [21] ATLAS Collaboration, *Search for new resonances in $W\gamma$ and $Z\gamma$ final states in pp collisions at $\sqrt{s} = 8$ TeV with the ATLAS detector*, *Phys. Lett. B* **738** (2014) 428, arXiv: [1407.8150 \[hep-ex\]](#).
- [22] ATLAS Collaboration, *Search for heavy resonances decaying to a Z boson and a photon in pp collisions at $\sqrt{s} = 13$ TeV with the ATLAS detector*, *Phys. Lett. B* **764** (2017) 11, arXiv: [1607.06363 \[hep-ex\]](#).
- [23] CMS Collaboration, *Search for high-mass $Z\gamma$ resonances in proton–proton collisions at $\sqrt{s} = 8$ and 13 TeV using jet substructure techniques*, *Phys. Lett. B* **772** (2017) 363, arXiv: [1612.09516 \[hep-ex\]](#).
- [24] ATLAS Collaboration, *The ATLAS experiment at the CERN Large Hadron Collider*, *JINST* **3** (2008) S08003.
- [25] ATLAS Collaboration, *ATLAS Insertable B-Layer Technical Design Report*, ATLAS-TDR-19 (2010), URL: <https://cds.cern.ch/record/1291633>, *ATLAS Insertable B-Layer Technical Design Report Addendum*, ATLAS-TDR-19-ADD-1, 2012, URL: <https://cds.cern.ch/record/1451888>.
- [26] ATLAS Collaboration, *Performance of the ATLAS Trigger System in 2015*, *Eur. Phys. J. C* **77** (2017) 317, arXiv: [1611.09661 \[hep-ex\]](#).
- [27] ATLAS Collaboration, *The ATLAS simulation infrastructure*, *Eur. Phys. J. C* **70** (2010) 823, arXiv: [1005.4568 \[physics.ins-det\]](#).
- [28] S. Agostinelli et al., *GEANT4 - a simulation toolkit*, *Nucl. Instrum. Methods A* **506** (2003) 250.

- [29] D. de Florian et al.,
Handbook of LHC Higgs Cross Sections: 4. Deciphering the Nature of the Higgs Sector, (2016), arXiv: [1610.07922 \[hep-ph\]](#).
- [30] P. Nason, *A new method for combining NLO QCD with shower Monte Carlo algorithms*, *JHEP* **11** (2004) 040, arXiv: [hep-ph/0409146](#).
- [31] S. Frixione, P. Nason and C. Oleari,
Matching NLO QCD computations with Parton Shower simulations: the POWHEG method, *JHEP* **11** (2007) 070, arXiv: [0709.2092 \[hep-ph\]](#).
- [32] S. Alioli, P. Nason, C. Oleari and E. Re, *A general framework for implementing NLO calculations in shower Monte Carlo programs: the POWHEG BOX*, *JHEP* **06** (2010) 043, (using ATLAS svn revisions r2856 for v1, r3080 for v2 ggF, r3052 for v2 VBF, and r3133 for v2 VH), arXiv: [1002.2581 \[hep-ph\]](#).
- [33] J. Butterworth et al., *PDF4LHC recommendations for LHC Run II*, *J. Phys G* **43** (2016) 023001, arXiv: [1510.03865 \[hep-ph\]](#).
- [34] S. Dulat et al.,
New parton distribution functions from a global analysis of quantum chromodynamics, *Phys. Rev. D* **93** (2016) 033006, arXiv: [1506.07443 \[hep-ph\]](#).
- [35] L. A. Harland-Lang, A. D. Martin, P. Motylinski and R. S. Thorne,
Parton distributions in the LHC era: MMHT 2014 PDFs, *Eur. Phys. J. C* **75** (2015) 204, arXiv: [1412.3989 \[hep-ph\]](#).
- [36] R. D. Ball et al., *Parton distributions for the LHC Run II*, *JHEP* **04** (2015) 040, arXiv: [1410.8849 \[hep-ph\]](#).
- [37] J. Gao and P. Nadolsky, *A meta-analysis of parton distribution functions*, *JHEP* **07** (2014) 035, arXiv: [1401.0013 \[hep-ph\]](#).
- [38] S. Carrazza, S. Forte, Z. Kassabov, J. I. Latorre and J. Rojo,
An Unbiased Hessian Representation for Monte Carlo PDFs, *Eur. Phys. J. C* **75** (2015) 369, arXiv: [1505.06736 \[hep-ph\]](#).
- [39] G. Watt and R. S. Thorne, *Study of Monte Carlo approach to experimental uncertainty propagation with MSTW 2008 PDFs*, *JHEP* **08** (2012) 052, arXiv: [1205.4024 \[hep-ph\]](#).
- [40] K. Hamilton, P. Nason and G. Zanderighi,
Finite quark-mass effects in the NNLOPS POWHEG+MiNLO Higgs generator, *JHEP* **05** (2015) 140, arXiv: [1501.04637 \[hep-ph\]](#).
- [41] K. Hamilton, P. Nason, E. Re and G. Zanderighi,
NNLOPS simulation of Higgs boson production, *JHEP* **10** (2013) 222, arXiv: [1309.0017 \[hep-ph\]](#).
- [42] G. Bozzi, S. Catani, D. de Florian and M. Grazzini,
Transverse-momentum resummation and the spectrum of the Higgs boson at the LHC, *Nucl. Phys. B* **737** (2006) 73, arXiv: [hep-ph/0508068](#).
- [43] D. de Florian, G. Ferrera, M. Grazzini and D. Tommasini,
Transverse-momentum resummation: Higgs boson production at the Tevatron and the LHC, *JHEP* **11** (2011) 064, arXiv: [1109.2109 \[hep-ph\]](#).

- [44] C. Anastasiou, C. Duhr, F. Dulat, F. Herzog and B. Mistlberger, *Higgs Boson Gluon-Fusion Production in QCD at Three Loops*, *Phys. Rev. Lett.* **114** (2015) 212001, arXiv: [1503.06056 \[hep-ph\]](#).
- [45] C. Anastasiou et al., *High precision determination of the gluon fusion Higgs boson cross-section at the LHC*, *JHEP* **05** (2016) 058, arXiv: [1602.00695 \[hep-ph\]](#).
- [46] S. Actis, G. Passarino, C. Sturm and S. Uccirati, *NLO electroweak corrections to Higgs boson production at hadron colliders*, *Phys. Lett. B* **670** (2008) 12, arXiv: [0809.1301 \[hep-ph\]](#).
- [47] C. Anastasiou, R. Boughezal and F. Petriello, *Mixed QCD-electroweak corrections to Higgs boson production in gluon fusion*, *JHEP* **04** (2009) 003, arXiv: [0811.3458 \[hep-ph\]](#).
- [48] P. Nason and C. Oleari, *NLO Higgs boson production via vector-boson fusion matched with shower in POWHEG*, *JHEP* **02** (2010) 037, arXiv: [0911.5299 \[hep-ph\]](#).
- [49] M. Ciccolini, A. Denner and S. Dittmaier, *Strong and electroweak corrections to the production of Higgs+2jets via weak interactions at the LHC*, *Phys. Rev. Lett.* **99** (2007) 161803, arXiv: [0707.0381 \[hep-ph\]](#).
- [50] M. Ciccolini, A. Denner and S. Dittmaier, *Electroweak and QCD corrections to Higgs production via vector-boson fusion at the LHC*, *Phys. Rev. D* **77** (2008) 013002, arXiv: [0710.4749 \[hep-ph\]](#).
- [51] P. Bolzoni, F. Maltoni, S.-O. Moch and M. Zaro, *Higgs production via vector-boson fusion at NNLO in QCD*, *Phys. Rev. Lett.* **105** (2010) 011801, arXiv: [1003.4451 \[hep-ph\]](#).
- [52] K. Hamilton, P. Nason, C. Oleari and G. Zanderighi, *Merging H/W/Z + 0 and 1 jet at NLO with no merging scale: a path to parton shower + NNLO matching*, *JHEP* **05** (2013) 082, arXiv: [1212.4504 \[hep-ph\]](#).
- [53] O. Brein, A. Djouadi and R. Harlander, *NNLO QCD corrections to the Higgs-strahlung processes at hadron colliders*, *Phys. Lett. B* **579** (2004) 149, arXiv: [hep-ph/0307206](#).
- [54] L. Altenkamp, S. Dittmaier, R. V. Harlander, H. Rzehak and T. J. E. Zirke, *Gluon-induced Higgs-strahlung at next-to-leading order QCD*, *JHEP* **02** (2013) 078, arXiv: [1211.5015 \[hep-ph\]](#).
- [55] A. Denner, S. Dittmaier, S. Kallweit and A. Mück, *Electroweak corrections to Higgs-strahlung off W/Z bosons at the Tevatron and the LHC with HAWK*, *JHEP* **03** (2012) 075, arXiv: [1112.5142 \[hep-ph\]](#).
- [56] T. Sjöstrand, S. Mrenna, P. Skands, *A brief introduction to PYTHIA 8.1*, *Comput. Phys. Commun.* **178** (2008) 852, arXiv: [0710.3820 \[hep-ph\]](#).
- [57] ATLAS Collaboration, *Measurement of the Z/γ^* boson transverse momentum distribution in pp collisions at $\sqrt{s} = 7$ TeV with the ATLAS detector*, *JHEP* **09** (2014) 145, arXiv: [1406.3660 \[hep-ex\]](#).

- [58] J. Pumplin et al.,
New generation of parton distributions with uncertainties from global QCD analysis, **JHEP 07** (2002) 012, arXiv: [hep-ph/0201195](#).
- [59] A. Djouadi, J. Kalinowski and M. Spira, *HDECAY: A program for Higgs boson decays in the standard model and its supersymmetric extension*, **Comput. Phys. Commun.** **108** (1998) 56, arXiv: [hep-ph/9704448](#).
- [60] A. Djouadi, M. M. Mühlleitner and M. Spira, *Decays of supersymmetric particles: The Program SUSY-HIT (SUspect-SdecaY-Hdecay-Interface)*, **Acta Phys. Polon. B** **38** (2007) 635, arXiv: [hep-ph/0609292](#).
- [61] J. Alwall et al., *The automated computation of tree-level and next-to-leading order differential cross sections, and their matching to parton shower simulations*, **JHEP 07** (2014) 079, arXiv: [1405.0301 \[hep-ph\]](#).
- [62] R. Frederix and S. Frixione, *Merging meets matching in MC@NLO*, **JHEP 12** (2012) 061, arXiv: [1209.6215 \[hep-ph\]](#).
- [63] ATLAS Collaboration, *ATLAS Pythia8 tunes to 7 TeV data*, ATL-PHYS-PUB-2014-021 (2014), URL: <https://cds.cern.ch/record/1966419>.
- [64] R. D. Ball et al., *Parton distributions with LHC data*, **Nucl. Phys. B** **867** (2013) 244, arXiv: [1207.1303 \[hep-ph\]](#).
- [65] E. Bagnaschi, G. Degrassi, P. Slavich and A. Vicini, *Higgs production via gluon fusion in the POWHEG approach in the SM and in the MSSM*, **JHEP 02** (2012) 088, arXiv: [1111.2854 \[hep-ph\]](#).
- [66] H.-L. Lai, M. Guzzi, J. Huston, Z. Li, P. M. Nadolsky et al., *New parton distributions for collider physics*, **Phys. Rev. D** **82** (2010) 074024, arXiv: [1007.2241 \[hep-ph\]](#).
- [67] P. Artoisenet et al., *A framework for Higgs characterisation*, **JHEP 11** (2013) 043, arXiv: [1306.6464 \[hep-ph\]](#).
- [68] T. Gleisberg et al., *Event generation with SHERPA 1.1*, **JHEP 02** (2009) 007, arXiv: [0811.4622 \[hep-ph\]](#).
- [69] T. Gleisberg and S. Höche, *Comix, a new matrix element generator*, **JHEP 12** (2008) 039, arXiv: [0808.3674 \[hep-ph\]](#).
- [70] F. Caccioli, P. Maierhöfer and S. Pozzorini, *Scattering Amplitudes with Open Loops*, **Phys. Rev. Lett.** **108** (2012) 111601, arXiv: [1111.5206 \[hep-ph\]](#).
- [71] S. Schumann and F. Krauss, *A Parton shower algorithm based on Catani-Seymour dipole factorisation*, **JHEP 03** (2008) 038, arXiv: [0709.1027 \[hep-ph\]](#).
- [72] S. Höche, F. Krauss, S. Schumann and F. Siegert, *QCD matrix elements and truncated showers*, **JHEP 05** (2009) 053, arXiv: [0903.1219 \[hep-ph\]](#).
- [73] S. Höche, F. Krauss, M. Schönherr and F. Siegert, *QCD matrix elements + parton showers: The NLO case*, **JHEP 04** (2013) 027, arXiv: [1207.5030 \[hep-ph\]](#).

- [74] ATLAS Collaboration, *The simulation principle and performance of the ATLAS fast calorimeter simulation FastCaloSim*, ATL-PHYS-PUB-2010-013 (2010),
URL: <https://cds.cern.ch/record/1300517>.
- [75] ATLAS Collaboration, *Summary of ATLAS Pythia 8 tunes*, ATL-PHYS-PUB-2012-003 (2012),
URL: <https://cds.cern.ch/record/1474107>.
- [76] A. D. Martin, W. J. Stirling, R. S. Thorne and G. Watt, *Parton distributions for the LHC*, Eur. Phys. J. C **63** (2009) 189, arXiv: [0901.0002 \[hep-ph\]](#).
- [77] ATLAS Collaboration, *Muon reconstruction performance of the ATLAS detector in proton–proton collision data at $\sqrt{s}=13$ TeV*, Eur. Phys. J. C **76** (2016) 292, arXiv: [1603.05598 \[hep-ex\]](#).
- [78] ATLAS Collaboration, *Electron efficiency measurements with the ATLAS detector using the 2015 LHC proton-proton collision data*, ATLAS-CONF-2016-024 (2016),
URL: <https://cds.cern.ch/record/2157687>.
- [79] ATLAS Collaboration, *Measurement of the photon identification efficiencies with the ATLAS detector using LHC Run-1 data*, Eur. Phys. J. C **76** (2016) 666, arXiv: [1606.01813 \[hep-ex\]](#).
- [80] ATLAS Collaboration, *Photon identification in 2015 ATLAS data*, ATLAS-PHYS-PUB-2016-014 (2016), URL: <https://cds.cern.ch/record/2203125>.
- [81] M. Cacciari, G. P. Salam and G. Soyez, *The anti- k_t jet clustering algorithm*, JHEP **04** (2008) 063, arXiv: [0802.1189 \[hep-ph\]](#).
- [82] ATLAS Collaboration,
Topological cell clustering in the ATLAS calorimeters and its performance in LHC Run 1, Eur. Phys. J. C **77** (2017) 490, arXiv: [1603.02934 \[hep-ex\]](#).
- [83] ATLAS Collaboration, *Pile-up subtraction and suppression for jets in ATLAS*, ATLAS-CONF-2013-083 (2013), URL: <https://cds.cern.ch/record/1570994>.
- [84] ATLAS Collaboration, *Jet energy scale measurements and their systematic uncertainties in proton-proton collisions at $\sqrt{s} = 13$ TeV with the ATLAS detector*, (2017), arXiv: [1703.09665 \[hep-ex\]](#).
- [85] ATLAS Collaboration, *Tagging and suppression of pileup jets with the ATLAS detector*, ATLAS-CONF-2014-018 (2014), URL: <https://cds.cern.ch/record/1700870>.
- [86] ATLAS Collaboration, *Measurement of the Higgs boson mass from the $H \rightarrow \gamma\gamma$ and $H \rightarrow ZZ^* \rightarrow 4\ell$ channels with the ATLAS detector using 25 fb^{-1} of pp collision data*, Phys. Rev. D **90** (2014) 052004, arXiv: [1406.3827 \[hep-ex\]](#).
- [87] ATLAS Collaboration,
Measurements of Higgs boson production and couplings in the four-lepton channel in pp collisions at center-of-mass energies of 7 and 8 TeV with the ATLAS detector, Phys. Rev. D **91** (2015) 012006, arXiv: [1408.5191 \[hep-ex\]](#).
- [88] M. Cacciari, G. P. Salam and S. Sapeta, *On the characterisation of the underlying event*, JHEP **04** (2010) 065, arXiv: [0912.4926 \[hep-ph\]](#).
- [89] OPAL collaboration, K. Ackerstaff et al., *Search for anomalous production of dilepton events with missing transverse momentum in e^+e^- collisions at $\sqrt{s} = 161$ GeV and 172 GeV*, Eur. Phys. J. C **4** (1998) 47, arXiv: [hep-ex/9710010](#).

- [90] M. Vesterinen and T. R. Wyatt, *A Novel Technique for Studying the Z Boson Transverse Momentum Distribution at Hadron Colliders*, *Nucl. Instrum. Meth. A* **602** (2009) 432, arXiv: [0807.4956 \[hep-ex\]](#).
- [91] M. Oreglia, *A Study of the Reactions $\psi' \rightarrow \gamma\gamma\psi$* , 1980,
URL: <https://www.slac.stanford.edu/cgi-wrap/getdoc/slac-r-236.pdf>.
- [92] ATLAS Collaboration, *Search for Scalar Diphoton Resonances in the Mass Range 65-600 GeV with the ATLAS Detector in pp Collision Data at $\sqrt{s} = 8$ TeV*,
Phys. Rev. Lett. **113** (2014) 171801, arXiv: [1407.6583 \[hep-ex\]](#).
- [93] ATLAS Collaboration, *Measurement of the inclusive isolated prompt photon cross section in pp collisions at $\sqrt{s} = 7$ TeV with the ATLAS detector*, *Phys. Rev. D* **83** (2011) 052005, arXiv: [1012.4389 \[hep-ex\]](#).
- [94] ATLAS Collaboration,
Electron and photon energy calibration with the ATLAS detector using LHC Run 1 data,
Eur. Phys. J. C **74** (2014) 3071, arXiv: [1407.5063 \[hep-ex\]](#).
- [95] ATLAS Collaboration, *Electron and photon energy calibration with the ATLAS detector using data collected in 2015 at $\sqrt{s} = 13$ TeV*, ATLAS-PHYS-PUB-2016-015 (2016),
URL: <https://cds.cern.ch/record/2203514>.
- [96] ATLAS Collaboration,
Luminosity determination in pp collisions at $\sqrt{s} = 8$ TeV using the ATLAS detector at the LHC,
Eur. Phys. J. C **76** (2016) 653, arXiv: [1608.03953 \[hep-ex\]](#).
- [97] ATLAS Collaboration, *Measurement of the Inelastic Proton-Proton Cross Section at $\sqrt{s} = 13$ TeV with the ATLAS Detector at the LHC*, *Phys. Rev. Lett.* **117** (2016) 182002, arXiv: [1606.02625 \[hep-ex\]](#).
- [98] D. A. Dicus, C. Kao and W. W. Repko,
Comparison of $H \rightarrow \ell\bar{\ell}\gamma$ and $H \rightarrow \gamma Z, Z \rightarrow \ell\bar{\ell}$ including the ATLAS cuts,
Phys. Rev. D **89** (2014) 033013, arXiv: [1310.4380 \[hep-ph\]](#).
- [99] L.-B. Chen, C.-F. Qiao and R.-L. Zhu,
Reconstructing the 125 GeV SM Higgs boson through $\ell\bar{\ell}\gamma$, *Phys. Lett. B* **726** (2013) 306, arXiv: [1211.6058 \[hep-ph\]](#).
- [100] A. Firat and R. Stroynowski, *Internal conversions in Higgs decays to two photons*,
Phys. Rev. D **76** (2007) 057301, arXiv: [0704.3987 \[hep-ph\]](#).
- [101] J. M. Campbell and R. Ellis, *MCFM for the Tevatron and the LHC*,
Nucl. Phys. Proc. Suppl. **205-206** (2010) 10, arXiv: [1007.3492 \[hep-ph\]](#).
- [102] I. W. Stewart and F. J. Tackmann,
Theory Uncertainties for Higgs and Other Searches Using Jet Bins,
Phys. Rev. D **85** (2012) 034011, arXiv: [1107.2117 \[hep-ph\]](#).
- [103] S. Gangal and F. J. Tackmann,
Next-to-leading-order uncertainties in Higgs+2 jets from gluon fusion,
Phys. Rev. D **87** (2013) 093008, arXiv: [1302.5437 \[hep-ph\]](#).
- [104] M. Grazzini and H. Sargsyan, *Heavy-quark mass effects in Higgs boson production at the LHC*,
JHEP **09** (2013) 129, arXiv: [1306.4581 \[hep-ph\]](#).

- [105] G. Cowan, K. Cranmer, E. Gross and O. Vitells,
Asymptotic formulae for likelihood-based tests of new physics, *Eur. Phys. J. C* **71** (2011) 1554,
arXiv: [1007.1727 \[physics.data-an\]](https://arxiv.org/abs/1007.1727), Erratum: *Eur. Phys. J. C* **73** (2013) 2501.
- [106] E. Gross and O. Vitells, *Trial factors or the look elsewhere effect in high energy physics*,
Eur. Phys. J. C **70** (2010) 525, arXiv: [1005.1891 \[physics.data-an\]](https://arxiv.org/abs/1005.1891).
- [107] A. L. Read, *Presentation of search results: The CL_s technique*,
J. Phys. G: Nucl. Part. Phys. **28** (2002) 2693.
- [108] ATLAS Collaboration, *ATLAS Computing Acknowledgements 2016–2017*,
ATL-GEN-PUB-2016-002, url: <https://cds.cern.ch/record/2202407>.

The ATLAS Collaboration

M. Aaboud^{137d}, G. Aad⁸⁸, B. Abbott¹¹⁵, O. Abdinov^{12,*}, B. Abeloos¹¹⁹, S.H. Abidi¹⁶¹,
O.S. AbouZeid¹³⁹, N.L. Abraham¹⁵¹, H. Abramowicz¹⁵⁵, H. Abreu¹⁵⁴, R. Abreu¹¹⁸, Y. Abulaiti^{148a,148b},
B.S. Acharya^{167a,167b,a}, S. Adachi¹⁵⁷, L. Adamczyk^{41a}, J. Adelman¹¹⁰, M. Adersberger¹⁰², T. Adye¹³³,
A.A. Affolder¹³⁹, T. Agatonovic-Jovin¹⁴, C. Agheorghiesei^{28c}, J.A. Aguilar-Saavedra^{128a,128f},
S.P. Ahlen²⁴, F. Ahmadov^{68,b}, G. Aielli^{135a,135b}, S. Akatsuka⁷¹, H. Akerstedt^{148a,148b}, T.P.A. Åkesson⁸⁴,
E. Akilli⁵², A.V. Akimov⁹⁸, G.L. Alberghi^{22a,22b}, J. Albert¹⁷², P. Albicocco⁵⁰, M.J. Alconada Verzini⁷⁴,
S.C. Alderweireldt¹⁰⁸, M. Aleksa³², I.N. Aleksandrov⁶⁸, C. Alexa^{28b}, G. Alexander¹⁵⁵,
T. Alexopoulos¹⁰, M. Alhroob¹¹⁵, B. Ali¹³⁰, M. Aliev^{76a,76b}, G. Alimonti^{94a}, J. Alison³³, S.P. Alkire³⁸,
B.M.M. Allbrooke¹⁵¹, B.W. Allen¹¹⁸, P.P. Allport¹⁹, A. Aloisio^{106a,106b}, A. Alonso³⁹, F. Alonso⁷⁴,
C. Alpigiani¹⁴⁰, A.A. Alshehri⁵⁶, M.I. Alstaty⁸⁸, B. Alvarez Gonzalez³², D. Álvarez Piqueras¹⁷⁰,
M.G. Alvaggi^{106a,106b}, B.T. Amadio¹⁶, Y. Amaral Coutinho^{26a}, C. Amelung²⁵, D. Amidei⁹²,
S.P. Amor Dos Santos^{128a,128c}, S. Amoroso³², G. Amundsen²⁵, C. Anastopoulos¹⁴¹, L.S. Ancu⁵²,
N. Andari¹⁹, T. Andeen¹¹, C.F. Anders^{60b}, J.K. Anders⁷⁷, K.J. Anderson³³, A. Andreazza^{94a,94b},
V. Andrei^{60a}, S. Angelidakis⁹, I. Angelozzi¹⁰⁹, A. Angerami³⁸, A.V. Anisenkov^{111,c}, N. Anjos¹³,
A. Annovi^{126a,126b}, C. Antel^{60a}, M. Antonelli⁵⁰, A. Antonov^{100,*}, D.J. Antrim¹⁶⁶, F. Anulli^{134a},
M. Aoki⁶⁹, L. Aperio Bella³², G. Arabidze⁹³, Y. Arai⁶⁹, J.P. Araque^{128a}, V. Araujo Ferraz^{26a},
A.T.H. Arce⁴⁸, R.E. Ardell⁸⁰, F.A. Arduh⁷⁴, J-F. Arguin⁹⁷, S. Argyropoulos⁶⁶, M. Arik^{20a},
A.J. Armbruster³², L.J. Armitage⁷⁹, O. Arnaez¹⁶¹, H. Arnold⁵¹, M. Arratia³⁰, O. Arslan²³,
A. Artamonov⁹⁹, G. Artoni¹²², S. Artz⁸⁶, S. Asai¹⁵⁷, N. Asbah⁴⁵, A. Ashkenazi¹⁵⁵, L. Asquith¹⁵¹,
K. Assamagan²⁷, R. Astalos^{146a}, M. Atkinson¹⁶⁹, N.B. Atlay¹⁴³, K. Augsten¹³⁰, G. Avolio³², B. Axen¹⁶,
M.K. Ayoub¹¹⁹, G. Azuelos^{97,d}, A.E. Baas^{60a}, M.J. Baca¹⁹, H. Bachacou¹³⁸, K. Bachas^{76a,76b},
M. Backes¹²², M. Backhaus³², P. Bagnaia^{134a,134b}, M. Bahmani⁴², H. Bahrasemani¹⁴⁴, J.T. Baines¹³³,
M. Bajic³⁹, O.K. Baker¹⁷⁹, E.M. Baldin^{111,c}, P. Balek¹⁷⁵, F. Balli¹³⁸, W.K. Balunas¹²⁴, E. Banas⁴²,
A. Bandyopadhyay²³, Sw. Banerjee^{176,e}, A.A.E. Bannoura¹⁷⁸, L. Barak³², E.L. Barberio⁹¹,
D. Barberis^{53a,53b}, M. Barbero⁸⁸, T. Barillari¹⁰³, M-S Barisits³², J.T. Barkeloo¹¹⁸, T. Barklow¹⁴⁵,
N. Barlow³⁰, S.L. Barnes^{36c}, B.M. Barnett¹³³, R.M. Barnett¹⁶, Z. Barnovska-Blenessy^{36a},
A. Baroncelli^{136a}, G. Barone²⁵, A.J. Barr¹²², L. Barranco Navarro¹⁷⁰, F. Barreiro⁸⁵,
J. Barreiro Guimarães da Costa^{35a}, R. Bartoldus¹⁴⁵, A.E. Barton⁷⁵, P. Bartos^{146a}, A. Basalaev¹²⁵,
A. Bassalat^{119,f}, R.L. Bates⁵⁶, S.J. Batista¹⁶¹, J.R. Batley³⁰, M. Battaglia¹³⁹, M. Bauce^{134a,134b},
F. Bauer¹³⁸, H.S. Bawa^{145,g}, J.B. Beacham¹¹³, M.D. Beattie⁷⁵, T. Beau⁸³, P.H. Beauchemin¹⁶⁵,
P. Bechtle²³, H.P. Beck^{18,h}, H.C. Beck⁵⁷, K. Becker¹²², M. Becker⁸⁶, M. Beckingham¹⁷³, C. Becot¹¹²,
A.J. Beddall^{20e}, A. Beddall^{20b}, V.A. Bednyakov⁶⁸, M. Bedognetti¹⁰⁹, C.P. Bee¹⁵⁰, T.A. Beermann³²,
M. Begalli^{26a}, M. Begel²⁷, J.K. Behr⁴⁵, A.S. Bell⁸¹, G. Bella¹⁵⁵, L. Bellagamba^{22a}, A. Bellerive³¹,
M. Bellomo¹⁵⁴, K. Belotskiy¹⁰⁰, O. Beltramo³², N.L. Belyaev¹⁰⁰, O. Benary^{155,*},
D. Benchekroun^{137a}, M. Bender¹⁰², K. Bendtz^{148a,148b}, N. Benekos¹⁰, Y. Benhammou¹⁵⁵,
E. Benhar Noccioli¹⁷⁹, J. Benitez⁶⁶, D.P. Benjamin⁴⁸, M. Benoit⁵², J.R. Bensinger²⁵, S. Bentvelsen¹⁰⁹,
L. Beresford¹²², M. Beretta⁵⁰, D. Berge¹⁰⁹, E. Bergeaas Kuutmann¹⁶⁸, N. Berger⁵, J. Beringer¹⁶,
S. Berlendis⁵⁸, N.R. Bernard⁸⁹, G. Bernardi⁸³, C. Bernius¹⁴⁵, F.U. Bernlochner²³, T. Berry⁸⁰, P. Berta⁸⁶,
C. Bertella^{35a}, G. Bertoli^{148a,148b}, F. Bertolucci^{126a,126b}, I.A. Bertram⁷⁵, C. Bertsche⁴⁵, D. Bertsche¹¹⁵,
G.J. Besjes³⁹, O. Bessidskaia Bylund^{148a,148b}, M. Bessner⁴⁵, N. Besson¹³⁸, C. Betancourt⁵¹,
A. Bethani⁸⁷, S. Bethke¹⁰³, A.J. Bevan⁷⁹, J. Beyer¹⁰³, R.M. Bianchi¹²⁷, O. Biebel¹⁰², D. Biedermann¹⁷,
R. Bielski⁸⁷, K. Bierwagen⁸⁶, N.V. Biesuz^{126a,126b}, M. Biglietti^{136a}, T.R.V. Billoud⁹⁷, H. Bilokon⁵⁰,
M. Bindi⁵⁷, A. Bingul^{20b}, C. Bini^{134a,134b}, S. Biondi^{22a,22b}, T. Bisanz⁵⁷, C. Bittrich⁴⁷, D.M. Bjergaard⁴⁸,
C.W. Black¹⁵², J.E. Black¹⁴⁵, K.M. Black²⁴, R.E. Blair⁶, T. Blazek^{146a}, I. Bloch⁴⁵, C. Blocker²⁵,

A. Blue⁵⁶, W. Blum^{86,*}, U. Blumenschein⁷⁹, S. Blunier^{34a}, G.J. Bobbink¹⁰⁹, V.S. Bobrovnikov^{111,c},
 S.S. Bocchetta⁸⁴, A. Bocci⁴⁸, C. Bock¹⁰², M. Boehler⁵¹, D. Boerner¹⁷⁸, D. Bogavac¹⁰²,
 A.G. Bogdanchikov¹¹¹, C. Bohm^{148a}, V. Boisvert⁸⁰, P. Bokan^{168,i}, T. Bold^{41a}, A.S. Boldyrev¹⁰¹,
 A.E. Bolz^{60b}, M. Bomben⁸³, M. Bona⁷⁹, M. Boonekamp¹³⁸, A. Borisov¹³², G. Borissov⁷⁵, J. Bortfeldt³²,
 D. Bortoletto¹²², V. Bortolotto^{62a}, D. Boscherini^{22a}, M. Bosman¹³, J.D. Bossio Sola²⁹, J. Boudreau¹²⁷,
 J. Bouffard², E.V. Bouhova-Thacker⁷⁵, D. Boumediene³⁷, C. Bourdarios¹¹⁹, S.K. Boutle⁵⁶, A. Boveia¹¹³,
 J. Boyd³², I.R. Boyko⁶⁸, J. Bracinik¹⁹, A. Brandt⁸, G. Brandt⁵⁷, O. Brandt^{60a}, U. Bratzler¹⁵⁸, B. Brau⁸⁹,
 J.E. Brau¹¹⁸, W.D. Breaden Madden⁵⁶, K. Brendlinger⁴⁵, A.J. Brennan⁹¹, L. Brenner¹⁰⁹, R. Brenner¹⁶⁸,
 S. Bressler¹⁷⁵, D.L. Briglin¹⁹, T.M. Bristow⁴⁹, D. Britton⁵⁶, D. Britzger⁴⁵, F.M. Brochu³⁰, I. Brock²³,
 R. Brock⁹³, G. Brooijmans³⁸, T. Brooks⁸⁰, W.K. Brooks^{34b}, J. Brosamer¹⁶, E. Brost¹¹⁰,
 J.H. Broughton¹⁹, P.A. Bruckman de Renstrom⁴², D. Bruncko^{146b}, A. Bruni^{22a}, G. Bruni^{22a},
 L.S. Bruni¹⁰⁹, BH Brunt³⁰, M. Bruschi^{22a}, N. Bruscino²³, P. Bryant³³, L. Bryngemark⁴⁵, T. Buanes¹⁵,
 Q. Buat¹⁴⁴, P. Buchholz¹⁴³, A.G. Buckley⁵⁶, I.A. Budagov⁶⁸, F. Buehrer⁵¹, M.K. Bugge¹²¹,
 O. Bulekov¹⁰⁰, D. Bullock⁸, T.J. Burch¹¹⁰, S. Burdin⁷⁷, C.D. Burgard⁵¹, A.M. Burger⁵,
 B. Burghgrave¹¹⁰, K. Burkhardt⁴², S. Burke¹³³, I. Burmeister⁴⁶, J.T.P. Burr¹²², E. Busato³⁷, D. Büscher⁵¹,
 V. Büscher⁸⁶, P. Bussey⁵⁶, J.M. Butler²⁴, C.M. Buttar⁵⁶, J.M. Butterworth⁸¹, P. Butti³², W. Buttinger²⁷,
 A. Buzatu^{35c}, A.R. Buzykaev^{111,c}, S. Cabrera Urbán¹⁷⁰, D. Caforio¹³⁰, V.M. Cairo^{40a,40b}, O. Cakir^{4a},
 N. Calace⁵², P. Calafuria¹⁶, A. Calandri⁸⁸, G. Calderini⁸³, P. Calfayan⁶⁴, G. Callea^{40a,40b}, L.P. Caloba^{26a},
 S. Calvente Lopez⁸⁵, D. Calvet³⁷, S. Calvet³⁷, T.P. Calvet⁸⁸, R. Camacho Toro³³, S. Camarda³²,
 P. Camarri^{135a,135b}, D. Cameron¹²¹, R. Caminal Armadans¹⁶⁹, C. Camincher⁵⁸, S. Campana³²,
 M. Campanelli⁸¹, A. Camplani^{94a,94b}, A. Campoverde¹⁴³, V. Canale^{106a,106b}, M. Cano Bret^{36c},
 J. Cantero¹¹⁶, T. Cao¹⁵⁵, M.D.M. Capeans Garrido³², I. Caprini^{28b}, M. Caprini^{28b}, M. Capua^{40a,40b},
 R.M. Carbone³⁸, R. Cardarelli^{135a}, F. Cardillo⁵¹, I. Carli¹³¹, T. Carli³², G. Carlino^{106a}, B.T. Carlson¹²⁷,
 L. Carminati^{94a,94b}, R.M.D. Carney^{148a,148b}, S. Caron¹⁰⁸, E. Carquin^{34b}, S. Carrá^{94a,94b},
 G.D. Carrillo-Montoya³², D. Casadei¹⁹, M.P. Casado^{13,j}, M. Casolino¹³, D.W. Casper¹⁶⁶,
 R. Castelijn¹⁰⁹, V. Castillo Gimenez¹⁷⁰, N.F. Castro^{128a,k}, A. Catinaccio³², J.R. Catmore¹²¹, A. Cattai³²,
 J. Caudron²³, V. Cavalieri¹⁶⁹, E. Cavallaro¹³, D. Cavalli^{94a}, M. Cavalli-Sforza¹³, V. Cavasinni^{126a,126b},
 E. Celebi^{20d}, F. Ceradini^{136a,136b}, L. Cerdà Alberich¹⁷⁰, A.S. Cerqueira^{26b}, A. Cerri¹⁵¹,
 L. Cerrito^{135a,135b}, F. Cerutti¹⁶, A. Cervelli¹⁸, S.A. Cetin^{20d}, A. Chafaq^{137a}, D. Chakraborty¹¹⁰,
 S.K. Chan⁵⁹, W.S. Chan¹⁰⁹, Y.L. Chan^{62a}, P. Chang¹⁶⁹, J.D. Chapman³⁰, D.G. Charlton¹⁹, C.C. Chau³¹,
 C.A. Chavez Barajas¹⁵¹, S. Che¹¹³, S. Cheatham^{167a,167c}, A. Chegwidden⁹³, S. Chekanov⁶,
 S.V. Chekulaev^{163a}, G.A. Chelkov^{68,l}, M.A. Chelstowska³², C. Chen⁶⁷, H. Chen²⁷, J. Chen^{36a},
 S. Chen^{35b}, S. Chen¹⁵⁷, X. Chen^{35c,m}, Y. Chen⁷⁰, H.C. Cheng⁹², H.J. Cheng^{35a,35d}, A. Cheplakov⁶⁸,
 E. Cheremushkina¹³², R. Cherkaooui El Moursli^{137e}, E. Cheu⁷, K. Cheung⁶³, L. Chevalier¹³⁸,
 V. Chiarella⁵⁰, G. Chiarelli^{126a,126b}, G. Chiodini^{76a}, A.S. Chisholm³², A. Chitan^{28b}, Y.H. Chiu¹⁷²,
 M.V. Chizhov⁶⁸, K. Choi⁶⁴, A.R. Chomont³⁷, S. Chouridou¹⁵⁶, Y.S. Chow^{62a}, V. Christodoulou⁸¹,
 M.C. Chu^{62a}, J. Chudoba¹²⁹, A.J. Chuinard⁹⁰, J.J. Chwastowski⁴², L. Chytka¹¹⁷, A.K. Ciftci^{4a},
 D. Cinca⁴⁶, V. Cindro⁷⁸, I.A. Cioara²³, C. Ciocca^{22a,22b}, A. Ciocio¹⁶, F. Cirotto^{106a,106b}, Z.H. Citron¹⁷⁵,
 M. Citterio^{94a}, M. Ciubancan^{28b}, A. Clark⁵², B.L. Clark⁵⁹, M.R. Clark³⁸, P.J. Clark⁴⁹, R.N. Clarke¹⁶,
 C. Clement^{148a,148b}, Y. Coadou⁸⁸, M. Cobal^{167a,167c}, A. Coccaro⁵², J. Cochran⁶⁷, L. Colasurdo¹⁰⁸,
 B. Cole³⁸, A.P. Colijn¹⁰⁹, J. Collot⁵⁸, T. Colombo¹⁶⁶, P. Conde Muiño^{128a,128b}, E. Coniavitis⁵¹,
 S.H. Connell^{147b}, I.A. Connelly⁸⁷, S. Constantinescu^{28b}, G. Conti³², F. Conventi^{106a,n}, M. Cooke¹⁶,
 A.M. Cooper-Sarkar¹²², F. Cormier¹⁷¹, K.J.R. Cormier¹⁶¹, M. Corradi^{134a,134b}, F. Corriveau^{90,o},
 A. Cortes-Gonzalez³², G. Cortiana¹⁰³, G. Costa^{94a}, M.J. Costa¹⁷⁰, D. Costanzo¹⁴¹, G. Cottin³⁰,
 G. Cowan⁸⁰, B.E. Cox⁸⁷, K. Cranmer¹¹², S.J. Crawley⁵⁶, R.A. Creager¹²⁴, G. Cree³¹,
 S. Crépé-Renaudin⁵⁸, F. Crescioli⁸³, W.A. Cribbs^{148a,148b}, M. Cristinziani²³, V. Croft¹⁰⁸,
 G. Crosetti^{40a,40b}, A. Cueto⁸⁵, T. Cuhadar Donszelmann¹⁴¹, A.R. Cukierman¹⁴⁵, J. Cummings¹⁷⁹,

M. Curatolo⁵⁰, J. Cúth⁸⁶, S. Czekierda⁴², P. Czodrowski³², G. D'amen^{22a,22b}, S. D'Auria⁵⁶,
 L. D'eramo⁸³, M. D'Onofrio⁷⁷, M.J. Da Cunha Sargedas De Sousa^{128a,128b}, C. Da Via⁸⁷,
 W. Dabrowski^{41a}, T. Dado^{146a}, T. Dai⁹², O. Dale¹⁵, F. Dallaire⁹⁷, C. Dallapiccola⁸⁹, M. Dam³⁹,
 J.R. Dandoy¹²⁴, M.F. Daneri²⁹, N.P. Dang¹⁷⁶, A.C. Daniells¹⁹, N.S. Dann⁸⁷, M. Danninger¹⁷¹,
 M. Dano Hoffmann¹³⁸, V. Dao¹⁵⁰, G. Darbo^{53a}, S. Darmora⁸, J. Dassoulas³, A. Dattagupta¹¹⁸,
 T. Daubney⁴⁵, W. Davey²³, C. David⁴⁵, T. Davidek¹³¹, D.R. Davis⁴⁸, P. Davison⁸¹, E. Dawe⁹¹,
 I. Dawson¹⁴¹, K. De⁸, R. de Asmundis^{106a}, A. De Benedetti¹¹⁵, S. De Castro^{22a,22b}, S. De Cecco⁸³,
 N. De Groot¹⁰⁸, P. de Jong¹⁰⁹, H. De la Torre⁹³, F. De Lorenzi⁶⁷, A. De Maria⁵⁷, D. De Pedis^{134a},
 A. De Salvo^{134a}, U. De Sanctis^{135a,135b}, A. De Santo¹⁵¹, K. De Vasconcelos Corga⁸⁸,
 J.B. De Vivie De Regie¹¹⁹, W.J. Dearnaley⁷⁵, R. Debbe²⁷, C. Debenedetti¹³⁹, D.V. Dedovich⁶⁸,
 N. Dehghanian³, I. Deigaard¹⁰⁹, M. Del Gaudio^{40a,40b}, J. Del Peso⁸⁵, D. Delgove¹¹⁹, F. Deliot¹³⁸,
 C.M. Delitzsch⁷, A. Dell'Acqua³², L. Dell'Asta²⁴, M. Dell'Orso^{126a,126b}, M. Della Pietra^{106a,106b},
 D. della Volpe⁵², M. Delmastro⁵, C. Delporte¹¹⁹, P.A. Delsart⁵⁸, D.A. DeMarco¹⁶¹, S. Demers¹⁷⁹,
 M. Demichev⁶⁸, A. Demilly⁸³, S.P. Denisov¹³², D. Denysiuk¹³⁸, D. Derendarz⁴², J.E. Derkaoui^{137d},
 F. Derue⁸³, P. Dervan⁷⁷, K. Desch²³, C. Deterre⁴⁵, K. Dette⁴⁶, M.R. Devesa²⁹, P.O. Deviveiros³²,
 A. Dewhurst¹³³, S. Dhaliwal²⁵, F.A. Di Bello⁵², A. Di Ciaccio^{135a,135b}, L. Di Ciaccio⁵,
 W.K. Di Clemente¹²⁴, C. Di Donato^{106a,106b}, A. Di Girolamo³², B. Di Girolamo³², B. Di Micco^{136a,136b},
 R. Di Nardo³², K.F. Di Petrillo⁵⁹, A. Di Simone⁵¹, R. Di Sipio¹⁶¹, D. Di Valentino³¹, C. Diaconu⁸⁸,
 M. Diamond¹⁶¹, F.A. Dias³⁹, M.A. Diaz^{34a}, E.B. Diehl⁹², J. Dietrich¹⁷, S. Díez Cornell⁴⁵,
 A. Dimitrievska¹⁴, J. Dingfelder²³, P. Dita^{28b}, S. Dita^{28b}, F. Dittus³², F. Djama⁸⁸, T. Djobava^{54b},
 J.I. Djuvtsland^{60a}, M.A.B. do Vale^{26c}, D. Dobos³², M. Dobre^{28b}, C. Doglioni⁸⁴, J. Dolejsi¹³¹,
 Z. Dolezal¹³¹, M. Donadelli^{26d}, S. Donati^{126a,126b}, P. Dondero^{123a,123b}, J. Donini³⁷, J. Dopke¹³³,
 A. Doria^{106a}, M.T. Dova⁷⁴, A.T. Doyle⁵⁶, E. Drechsler⁵⁷, M. Dris¹⁰, Y. Du^{36b}, J. Duarte-Campderros¹⁵⁵,
 A. Dubreuil⁵², E. Duchovni¹⁷⁵, G. Duckeck¹⁰², A. Ducourthial⁸³, O.A. Ducu^{97,p}, D. Duda¹⁰⁹,
 A. Dudarev³², A.Chr. Dudder⁸⁶, E.M. Duffield¹⁶, L. Duflot¹¹⁹, M. Dührssen³², M. Dumancic¹⁷⁵,
 A.E. Dumitriu^{28b}, A.K. Duncan⁵⁶, M. Dunford^{60a}, H. Duran Yildiz^{4a}, M. Düren⁵⁵, A. Durglishvili^{54b},
 D. Duschinger⁴⁷, B. Dutta⁴⁵, D. Duvnjak¹, M. Dyndal⁴⁵, B.S. Dziedzic⁴², C. Eckardt⁴⁵, K.M. Ecker¹⁰³,
 R.C. Edgar⁹², T. Eifert³², G. Eigen¹⁵, K. Einsweiler¹⁶, T. Ekelof¹⁶⁸, M. El Kacimi^{137c}, R. El Kosseifi⁸⁸,
 V. Ellajosyula⁸⁸, M. Ellert¹⁶⁸, S. Elles⁵, F. Ellinghaus¹⁷⁸, A.A. Elliot¹⁷², N. Ellis³², J. Elmsheuser²⁷,
 M. Elsing³², D. Emelyanov¹³³, Y. Enari¹⁵⁷, O.C. Endner⁸⁶, J.S. Ennis¹⁷³, J. Erdmann⁴⁶, A. Ereditato¹⁸,
 M. Ernst²⁷, S. Errede¹⁶⁹, M. Escalier¹¹⁹, C. Escobar¹⁷⁰, B. Esposito⁵⁰, O. Estrada Pastor¹⁷⁰,
 A.I. Etienvre¹³⁸, E. Etzion¹⁵⁵, H. Evans⁶⁴, A. Ezhilov¹²⁵, M. Ezzi^{137e}, F. Fabbri^{22a,22b}, L. Fabbri^{22a,22b},
 V. Fabiani¹⁰⁸, G. Facini⁸¹, R.M. Fakhrutdinov¹³², S. Falciano^{134a}, R.J. Falla⁸¹, J. Faltova³², Y. Fang^{35a},
 M. Fanti^{94a,94b}, A. Farbin⁸, A. Farilla^{136a}, C. Farina¹²⁷, E.M. Farina^{123a,123b}, T. Farooque⁹³, S. Farrell¹⁶,
 S.M. Farrington¹⁷³, P. Farthouat³², F. Fassi^{137e}, P. Fassnacht³², D. Fassouliotis⁹, M. Faucci Giannelli⁴⁹,
 A. Favareto^{53a,53b}, W.J. Fawcett¹²², L. Fayard¹¹⁹, O.L. Fedin^{125,q}, W. Fedorko¹⁷¹, S. Feigl¹²¹,
 L. Feligioni⁸⁸, C. Feng^{36b}, E.J. Feng³², H. Feng⁹², M.J. Fenton⁵⁶, A.B. Fenyük¹³², L. Feremenga⁸,
 P. Fernandez Martinez¹⁷⁰, S. Fernandez Perez¹³, J. Ferrando⁴⁵, A. Ferrari¹⁶⁸, P. Ferrari¹⁰⁹, R. Ferrari^{123a},
 D.E. Ferreira de Lima^{60b}, A. Ferrer¹⁷⁰, D. Ferrere⁵², C. Ferretti⁹², F. Fiedler⁸⁶, A. Filipčič⁷⁸,
 M. Filippuzzi⁴⁵, F. Filthaut¹⁰⁸, M. Fincke-Keeler¹⁷², K.D. Finelli¹⁵², M.C.N. Fiolhais^{128a,128c,r},
 L. Fiorini¹⁷⁰, A. Fischer², C. Fischer¹³, J. Fischer¹⁷⁸, W.C. Fisher⁹³, N. Flaschel⁴⁵, I. Fleck¹⁴³,
 P. Fleischmann⁹², R.R.M. Fletcher¹²⁴, T. Flick¹⁷⁸, B.M. Flierl¹⁰², L.R. Flores Castillo^{62a},
 M.J. Flowerdew¹⁰³, G.T. Forcolin⁸⁷, A. Formica¹³⁸, F.A. Förster¹³, A. Forti⁸⁷, A.G. Foster¹⁹,
 D. Fournier¹¹⁹, H. Fox⁷⁵, S. Fracchia¹⁴¹, P. Francavilla⁸³, M. Franchini^{22a,22b}, S. Franchino^{60a},
 D. Francis³², L. Franconi¹²¹, M. Franklin⁵⁹, M. Frate¹⁶⁶, M. Fraternali^{123a,123b}, D. Freeborn⁸¹,
 S.M. Fressard-Batraneanu³², B. Freund⁹⁷, D. Froidevaux³², J.A. Frost¹²², C. Fukunaga¹⁵⁸,
 T. Fusayasu¹⁰⁴, J. Fuster¹⁷⁰, C. Gabaldon⁵⁸, O. Gabizon¹⁵⁴, A. Gabrielli^{22a,22b}, A. Gabrielli¹⁶,

G.P. Gach^{41a}, S. Gadatsch³², S. Gadomski⁸⁰, G. Gagliardi^{53a,53b}, L.G. Gagnon⁹⁷, C. Galea¹⁰⁸,
 B. Galhardo^{128a,128c}, E.J. Gallas¹²², B.J. Gallop¹³³, P. Gallus¹³⁰, G. Galster³⁹, K.K. Gan¹¹³,
 S. Ganguly³⁷, Y. Gao⁷⁷, Y.S. Gao^{145,g}, F.M. Garay Walls⁴⁹, C. García¹⁷⁰, J.E. García Navarro¹⁷⁰,
 J.A. García Pascual^{35a}, M. Garcia-Sciveres¹⁶, R.W. Gardner³³, N. Garelli¹⁴⁵, V. Garonne¹²¹,
 A. Gascon Bravo⁴⁵, K. Gasnikova⁴⁵, C. Gatti⁵⁰, A. Gaudiello^{53a,53b}, G. Gaudio^{123a}, I.L. Gavrilenco⁹⁸,
 C. Gay¹⁷¹, G. Gaycken²³, E.N. Gazis¹⁰, C.N.P. Gee¹³³, J. Geisen⁵⁷, M. Geisen⁸⁶, M.P. Geisler^{60a},
 K. Gellerstedt^{148a,148b}, C. Gemme^{53a}, M.H. Genest⁵⁸, C. Geng⁹², S. Gentile^{134a,134b}, C. Gentsos¹⁵⁶,
 S. George⁸⁰, D. Gerbaudo¹³, A. Gershon¹⁵⁵, G. Geßner⁴⁶, S. Ghasemi¹⁴³, M. Ghneimat²³,
 B. Giacobbe^{22a}, S. Giagu^{134a,134b}, N. Giangiacomi^{22a,22b}, P. Giannetti^{126a,126b}, S.M. Gibson⁸⁰,
 M. Gignac¹⁷¹, M. Gilchriese¹⁶, D. Gillberg³¹, G. Gilles¹⁷⁸, D.M. Gingrich^{3,d}, N. Giokaris^{9,*},
 M.P. Giordani^{167a,167c}, F.M. Giorgi^{22a}, P.F. Giraud¹³⁸, P. Giromini⁵⁹, G. Giugliarelli^{167a,167c},
 D. Giugni^{94a}, F. Giuli¹²², C. Giuliani¹⁰³, M. Giulini^{60b}, B.K. Gjelsten¹²¹, S. Gkaitatzis¹⁵⁶, I. Gkialas^{9,s},
 E.L. Gkougkousis¹³⁹, P. Gkountoumis¹⁰, L.K. Gladilin¹⁰¹, C. Glasman⁸⁵, J. Glatzer¹³, P.C.F. Glaysher⁴⁵,
 A. Glazov⁴⁵, M. Goblirsch-Kolb²⁵, J. Godlewski⁴², S. Goldfarb⁹¹, T. Golling⁵², D. Golubkov¹³²,
 A. Gomes^{128a,128b,128d}, R. Gonçalo^{128a}, R. Goncalves Gama^{26a}, J. Goncalves Pinto Firmino Da Costa¹³⁸,
 G. Gonella⁵¹, L. Gonella¹⁹, A. Gongadze⁶⁸, S. González de la Hoz¹⁷⁰, S. Gonzalez-Sevilla⁵²,
 L. Goossens³², P.A. Gorbounov⁹⁹, H.A. Gordon²⁷, I. Gorelov¹⁰⁷, B. Gorini³², E. Gorini^{76a,76b},
 A. Gorišek⁷⁸, A.T. Goshaw⁴⁸, C. Gössling⁴⁶, M.I. Gostkin⁶⁸, C.A. Gottardo²³, C.R. Goudet¹¹⁹,
 D. Goujdami^{137c}, A.G. Goussiou¹⁴⁰, N. Govender^{147b,t}, E. Gozani¹⁵⁴, L. Graber⁵⁷,
 I. Grabowska-Bold^{41a}, P.O.J. Gradin¹⁶⁸, J. Gramling¹⁶⁶, E. Gramstad¹²¹, S. Grancagnolo¹⁷,
 V. Gratchev¹²⁵, P.M. Gravila^{28f}, C. Gray⁵⁶, H.M. Gray¹⁶, Z.D. Greenwood^{82,u}, C. Grefe²³,
 K. Gregersen⁸¹, I.M. Gregor⁴⁵, P. Grenier¹⁴⁵, K. Grevtsov⁵, J. Griffiths⁸, A.A. Grillo¹³⁹, K. Grimm⁷⁵,
 S. Grinstein^{13,v}, Ph. Gris³⁷, J.-F. Grivaz¹¹⁹, S. Groh⁸⁶, E. Gross¹⁷⁵, J. Grosse-Knetter⁵⁷, G.C. Grossi⁸²,
 Z.J. Grout⁸¹, A. Grummer¹⁰⁷, L. Guan⁹², W. Guan¹⁷⁶, J. Guenther⁶⁵, F. Guescini^{163a}, D. Guest¹⁶⁶,
 O. Gueta¹⁵⁵, B. Gui¹¹³, E. Guido^{53a,53b}, T. Guillemin⁵, S. Guindon², U. Gul⁵⁶, C. Gumpert³², J. Guo^{36c},
 W. Guo⁹², Y. Guo^{36a,w}, R. Gupta⁴³, S. Gupta¹²², G. Gustavino¹¹⁵, P. Gutierrez¹¹⁵,
 N.G. Gutierrez Ortiz⁸¹, C. Gutschow⁸¹, C. Guyot¹³⁸, M.P. Guzik^{41a}, C. Gwenlan¹²², C.B. Gwilliam⁷⁷,
 A. Haas¹¹², C. Haber¹⁶, H.K. Hadavand⁸, N. Haddad^{137e}, A. Hadef⁸⁸, S. Hageböck²³, M. Hagihara¹⁶⁴,
 H. Hakobyan^{180,*}, M. Haleem⁴⁵, J. Haley¹¹⁶, G. Halladjian⁹³, G.D. Hallewell⁸⁸, K. Hamacher¹⁷⁸,
 P. Hamal¹¹⁷, K. Hamano¹⁷², A. Hamilton^{147a}, G.N. Hamity¹⁴¹, P.G. Hamnett⁴⁵, L. Han^{36a}, S. Han^{35a,35d},
 K. Hanagaki^{69,x}, K. Hanawa¹⁵⁷, M. Hance¹³⁹, B. Haney¹²⁴, P. Hanke^{60a}, J.B. Hansen³⁹, J.D. Hansen³⁹,
 M.C. Hansen²³, P.H. Hansen³⁹, K. Hara¹⁶⁴, A.S. Hard¹⁷⁶, T. Harenberg¹⁷⁸, F. Hariri¹¹⁹, S. Harkusha⁹⁵,
 R.D. Harrington⁴⁹, P.F. Harrison¹⁷³, N.M. Hartmann¹⁰², M. Hasegawa⁷⁰, Y. Hasegawa¹⁴², A. Hasib⁴⁹,
 S. Hassani¹³⁸, S. Haug¹⁸, R. Hauser⁹³, L. Hauswald⁴⁷, L.B. Havener³⁸, M. Havranek¹³⁰,
 C.M. Hawkes¹⁹, R.J. Hawkings³², D. Hayakawa¹⁵⁹, D. Hayden⁹³, C.P. Hays¹²², J.M. Hays⁷⁹,
 H.S. Hayward⁷⁷, S.J. Haywood¹³³, S.J. Head¹⁹, T. Heck⁸⁶, V. Hedberg⁸⁴, L. Heelan⁸, S. Heer²³,
 K.K. Heidegger⁵¹, S. Heim⁴⁵, T. Heim¹⁶, B. Heinemann^{45,y}, J.J. Heinrich¹⁰², L. Heinrich¹¹², C. Heinz⁵⁵,
 J. Hejbal¹²⁹, L. Helary³², A. Held¹⁷¹, S. Hellman^{148a,148b}, C. Helsens³², R.C.W. Henderson⁷⁵,
 Y. Heng¹⁷⁶, S. Henkelmann¹⁷¹, A.M. Henriques Correia³², S. Henrot-Versille¹¹⁹, G.H. Herbert¹⁷,
 H. Herde²⁵, V. Herget¹⁷⁷, Y. Hernández Jiménez^{147c}, H. Herr⁸⁶, G. Herten⁵¹, R. Hertenberger¹⁰²,
 L. Hervas³², T.C. Herwig¹²⁴, G.G. Hesketh⁸¹, N.P. Hessey^{163a}, J.W. Hetherly⁴³, S. Higashino⁶⁹,
 E. Higón-Rodríguez¹⁷⁰, K. Hildebrand³³, E. Hill¹⁷², J.C. Hill³⁰, K.H. Hiller⁴⁵, S.J. Hillier¹⁹, M. Hils⁴⁷,
 I. Hinchliffe¹⁶, M. Hirose⁵¹, D. Hirschbuehl¹⁷⁸, B. Hiti⁷⁸, O. Hladík¹²⁹, X. Hoad⁴⁹, J. Hobbs¹⁵⁰,
 N. Hod^{163a}, M.C. Hodgkinson¹⁴¹, P. Hodgson¹⁴¹, A. Hoecker³², M.R. Hoeferkamp¹⁰⁷, F. Hoenig¹⁰²,
 D. Hohn²³, T.R. Holmes³³, M. Homann⁴⁶, S. Honda¹⁶⁴, T. Honda⁶⁹, T.M. Hong¹²⁷, B.H. Hooberman¹⁶⁹,
 W.H. Hopkins¹¹⁸, Y. Horii¹⁰⁵, A.J. Horton¹⁴⁴, J.-Y. Hostachy⁵⁸, S. Hou¹⁵³, A. Hoummada^{137a},
 J. Howarth⁸⁷, J. Hoya⁷⁴, M. Hrabovsky¹¹⁷, J. Hrdinka³², I. Hristova¹⁷, J. Hrivnac¹¹⁹, T. Hryna'ova⁵,

A. Hrynevich⁹⁶, P.J. Hsu⁶³, S.-C. Hsu¹⁴⁰, Q. Hu^{36a}, S. Hu^{36c}, Y. Huang^{35a}, Z. Hubacek¹³⁰, F. Hubaut⁸⁸,
 F. Huegging²³, T.B. Huffman¹²², E.W. Hughes³⁸, G. Hughes⁷⁵, M. Huhtinen³², P. Huo¹⁵⁰,
 N. Huseynov^{68,b}, J. Huston⁹³, J. Huth⁵⁹, G. Iacobucci⁵², G. Iakovidis²⁷, I. Ibragimov¹⁴³,
 L. Iconomidou-Fayard¹¹⁹, Z. Idrissi^{137e}, P. Iengo³², O. Igonkina^{109,z}, T. Iizawa¹⁷⁴, Y. Ikegami⁶⁹,
 M. Ikeno⁶⁹, Y. Ilchenko^{11,aa}, D. Iliadis¹⁵⁶, N. Ilic¹⁴⁵, G. Introzzi^{123a,123b}, P. Ioannou^{9,*}, M. Iodice^{136a},
 K. Iordanidou³⁸, V. Ippolito⁵⁹, M.F. Isacson¹⁶⁸, N. Ishijima¹²⁰, M. Ishino¹⁵⁷, M. Ishitsuka¹⁵⁹,
 C. Issever¹²², S. Isti^{20a}, F. Ito¹⁶⁴, J.M. Iturbe Ponce^{62a}, R. Iuppa^{162a,162b}, H. Iwasaki⁶⁹, J.M. Izen⁴⁴,
 V. Izzo^{106a}, S. Jabbar³, P. Jackson¹, R.M. Jacobs²³, V. Jain², K.B. Jakobi⁸⁶, K. Jakobs⁵¹, S. Jakobsen⁶⁵,
 T. Jakoubek¹²⁹, D.O. Jamin¹¹⁶, D.K. Jana⁸², R. Jansky⁵², J. Janssen²³, M. Janus⁵⁷, P.A. Janus^{41a},
 G. Jarlskog⁸⁴, N. Javadov^{68,b}, T. Javůrek⁵¹, M. Javurkova⁵¹, F. Jeanneau¹³⁸, L. Jeanty¹⁶, J. Jejelava^{54a,ab},
 A. Jelinskas¹⁷³, P. Jenni^{51,ac}, C. Jeske¹⁷³, S. Jézéquel⁵, H. Ji¹⁷⁶, J. Jia¹⁵⁰, H. Jiang⁶⁷, Y. Jiang^{36a},
 Z. Jiang¹⁴⁵, S. Jiggins⁸¹, J. Jimenez Pena¹⁷⁰, S. Jin^{35a}, A. Jinaru^{28b}, O. Jinnouchi¹⁵⁹, H. Jivan^{147c},
 P. Johansson¹⁴¹, K.A. Johns⁷, C.A. Johnson⁶⁴, W.J. Johnson¹⁴⁰, K. Jon-And^{148a,148b}, R.W.L. Jones⁷⁵,
 S.D. Jones¹⁵¹, S. Jones⁷, T.J. Jones⁷⁷, J. Jongmanns^{60a}, P.M. Jorge^{128a,128b}, J. Jovicevic^{163a}, X. Ju¹⁷⁶,
 A. Juste Rozas^{13,v}, M.K. Köhler¹⁷⁵, A. Kaczmarska⁴², M. Kado¹¹⁹, H. Kagan¹¹³, M. Kagan¹⁴⁵,
 S.J. Kahn⁸⁸, T. Kaji¹⁷⁴, E. Kajomovitz⁴⁸, C.W. Kalderon⁸⁴, A. Kaluza⁸⁶, S. Kama⁴³,
 A. Kamenshchikov¹³², N. Kanaya¹⁵⁷, L. Kanjir⁷⁸, V.A. Kantserov¹⁰⁰, J. Kanzaki⁶⁹, B. Kaplan¹¹²,
 L.S. Kaplan¹⁷⁶, D. Kar^{147c}, K. Karakostas¹⁰, N. Karastathis¹⁰, M.J. Kareem⁵⁷, E. Karentzos¹⁰,
 S.N. Karpov⁶⁸, Z.M. Karpova⁶⁸, K. Karthik¹¹², V. Kartvelishvili⁷⁵, A.N. Karyukhin¹³², K. Kasahara¹⁶⁴,
 L. Kashif¹⁷⁶, R.D. Kass¹¹³, A. Kastanas¹⁴⁹, Y. Kataoka¹⁵⁷, C. Kato¹⁵⁷, A. Katre⁵², J. Katzy⁴⁵,
 K. Kawade⁷⁰, K. Kawagoe⁷³, T. Kawamoto¹⁵⁷, G. Kawamura⁵⁷, E.F. Kay⁷⁷, V.F. Kazanin^{111,c},
 R. Keeler¹⁷², R. Kehoe⁴³, J.S. Keller³¹, E. Kellermann⁸⁴, J.J. Kempster⁸⁰, J Kendrick¹⁹,
 H. Keoshkerian¹⁶¹, O. Kepka¹²⁹, B.P. Kerševan⁷⁸, S. Kersten¹⁷⁸, R.A. Keyes⁹⁰, M. Khader¹⁶⁹,
 F. Khalil-zada¹², A. Khanov¹¹⁶, A.G. Kharlamov^{111,c}, T. Kharlamova^{111,c}, A. Khodinov¹⁶⁰, T.J. Khoo⁵²,
 V. Khovanskiy^{99,*}, E. Khramov⁶⁸, J. Khubua^{54b,ad}, S. Kido⁷⁰, C.R. Kilby⁸⁰, H.Y. Kim⁸, S.H. Kim¹⁶⁴,
 Y.K. Kim³³, N. Kimura¹⁵⁶, O.M. Kind¹⁷, B.T. King⁷⁷, D. Kirchmeier⁴⁷, J. Kirk¹³³, A.E. Kiryunin¹⁰³,
 T. Kishimoto¹⁵⁷, D. Kisielewska^{41a}, V. Kitali⁴⁵, K. Kiuchi¹⁶⁴, O. Kivernyk⁵, E. Kladiva^{146b},
 T. Klapdor-Kleingrothaus⁵¹, M.H. Klein⁹², M. Klein⁷⁷, U. Klein⁷⁷, K. Kleinknecht⁸⁶, P. Klimek¹¹⁰,
 A. Klimentov²⁷, R. Klingenberg⁴⁶, T. Klingl²³, T. Klioutchnikova³², E.-E. Kluge^{60a}, P. Kluit¹⁰⁹,
 S. Kluth¹⁰³, E. Kneringer⁶⁵, E.B.F.G. Knoops⁸⁸, A. Knue¹⁰³, A. Kobayashi¹⁵⁷, D. Kobayashi¹⁵⁹,
 T. Kobayashi¹⁵⁷, M. Kobel⁴⁷, M. Kocian¹⁴⁵, P. Kodys¹³¹, T. Koffas³¹, E. Koffeman¹⁰⁹, N.M. Köhler¹⁰³,
 T. Koi¹⁴⁵, M. Kolb^{60b}, I. Koletsou⁵, A.A. Komar^{98,*}, Y. Komori¹⁵⁷, T. Kondo⁶⁹, N. Kondrashova^{36c},
 K. Köneke⁵¹, A.C. König¹⁰⁸, T. Kono^{69,ae}, R. Konoplich^{112,af}, N. Konstantinidis⁸¹, R. Kopeliansky⁶⁴,
 S. Koperny^{41a}, A.K. Kopp⁵¹, K. Korcyl⁴², K. Kordas¹⁵⁶, A. Korn⁸¹, A.A. Korol^{111,c}, I. Korolkov¹³,
 E.V. Korolkova¹⁴¹, O. Kortner¹⁰³, S. Kortner¹⁰³, T. Kosek¹³¹, V.V. Kostyukhin²³, A. Kotwal⁴⁸,
 A. Koulouris¹⁰, A. Kourkoumeli-Charalampidi^{123a,123b}, C. Kourkoumelis⁹, E. Kourlitis¹⁴¹,
 V. Kouskoura²⁷, A.B. Kowalewska⁴², R. Kowalewski¹⁷², T.Z. Kowalski^{41a}, C. Kozakai¹⁵⁷,
 W. Kozanecki¹³⁸, A.S. Kozhin¹³², V.A. Kramarenko¹⁰¹, G. Kramberger⁷⁸, D. Krasnoperovtsev¹⁰⁰,
 M.W. Krasny⁸³, A. Krasznahorkay³², D. Krauss¹⁰³, J.A. Kremer^{41a}, J. Kretzschmar⁷⁷, K. Kreutzfeldt⁵⁵,
 P. Krieger¹⁶¹, K. Krizka³³, K. Kroeninger⁴⁶, H. Kroha¹⁰³, J. Kroll¹²⁹, J. Kroll¹²⁴, J. Kroseberg²³,
 J. Krstic¹⁴, U. Kruchonak⁶⁸, H. Krüger²³, N. Krumnack⁶⁷, M.C. Kruse⁴⁸, T. Kubota⁹¹, H. Kucuk⁸¹,
 S. Kuday^{4b}, J.T. Kuechler¹⁷⁸, S. Kuehn³², A. Kugel^{60a}, F. Kuger¹⁷⁷, T. Kuhl⁴⁵, V. Kukhtin⁶⁸, R. Kukla⁸⁸,
 Y. Kulchitsky⁹⁵, S. Kuleshov^{34b}, Y.P. Kulinich¹⁶⁹, M. Kuna^{134a,134b}, T. Kunigo⁷¹, A. Kupco¹²⁹,
 T. Kupfer⁴⁶, O. Kuprash¹⁵⁵, H. Kurashige⁷⁰, L.L. Kurchaninov^{163a}, Y.A. Kurochkin⁹⁵, M.G. Kurth^{35a,35d},
 V. Kus¹²⁹, E.S. Kuwertz¹⁷², M. Kuze¹⁵⁹, J. Kvita¹¹⁷, T. Kwan¹⁷², D. Kyriazopoulos¹⁴¹, A. La Rosa¹⁰³,
 J.L. La Rosa Navarro^{26d}, L. La Rotonda^{40a,40b}, F. La Ruffa^{40a,40b}, C. Lacasta¹⁷⁰, F. Lacava^{134a,134b},
 J. Lacey⁴⁵, D.P.J. Lack⁸⁷, H. Lacker¹⁷, D. Lacour⁸³, E. Ladygin⁶⁸, R. Laforge⁵, B. Laforge⁸³,

T. Lagouri¹⁷⁹, S. Lai⁵⁷, S. Lammers⁶⁴, W. Lampl⁷, E. Lançon²⁷, U. Landgraf⁵¹, M.P.J. Landon⁷⁹, M.C. Lanfermann⁵², V.S. Lang^{60a}, J.C. Lange¹³, R.J. Langenberg³², A.J. Lankford¹⁶⁶, F. Lanni²⁷, K. Lantzsch²³, A. Lanza^{123a}, A. Lapertosa^{53a,53b}, S. Laplace⁸³, J.F. Laporte¹³⁸, T. Lari^{94a}, F. Lasagni Manghi^{22a,22b}, M. Lassnig³², P. Laurelli⁵⁰, W. Lavrijsen¹⁶, A.T. Law¹³⁹, P. Laycock⁷⁷, T. Lazovich⁵⁹, M. Lazzaroni^{94a,94b}, B. Le⁹¹, O. Le Dortz⁸³, E. Le Guiriec⁸⁸, E.P. Le Quilleuc¹³⁸, M. LeBlanc¹⁷², T. LeCompte⁶, F. Ledroit-Guillon⁵⁸, C.A. Lee²⁷, G.R. Lee^{133,ag}, S.C. Lee¹⁵³, L. Lee⁵⁹, B. Lefebvre⁹⁰, G. Lefebvre⁸³, M. Lefebvre¹⁷², F. Legger¹⁰², C. Leggett¹⁶, G. Lehmann Miotto³², X. Lei⁷, W.A. Leight⁴⁵, M.A.L. Leite^{26d}, R. Leitner¹³¹, D. Lellouch¹⁷⁵, B. Lemmer⁵⁷, K.J.C. Leney⁸¹, T. Lenz²³, B. Lenzi³², R. Leone⁷, S. Leone^{126a,126b}, C. Leonidopoulos⁴⁹, G. Lerner¹⁵¹, C. Leroy⁹⁷, A.A.J. Lesage¹³⁸, C.G. Lester³⁰, M. Levchenko¹²⁵, J. Levêque⁵, D. Levin⁹², L.J. Levinson¹⁷⁵, M. Levy¹⁹, D. Lewis⁷⁹, B. Li^{36a,w}, Changqiao Li^{36a}, H. Li¹⁵⁰, L. Li^{36c}, Q. Li^{35a,35d}, Q. Li^{36a}, S. Li⁴⁸, X. Li^{36c}, Y. Li¹⁴³, Z. Liang^{35a}, B. Liberti^{135a}, A. Liblong¹⁶¹, K. Lie^{62c}, J. Liebal²³, W. Liebig¹⁵, A. Limosani¹⁵², S.C. Lin¹⁸², T.H. Lin⁸⁶, R.A. Linck⁶⁴, B.E. Lindquist¹⁵⁰, A.E. Lioni⁵², E. Lipeles¹²⁴, A. Lipniacka¹⁵, M. Lisovyi^{60b}, T.M. Liss^{169,ah}, A. Lister¹⁷¹, A.M. Litke¹³⁹, B. Liu^{153,ai}, H. Liu⁹², H. Liu²⁷, J.K.K. Liu¹²², J. Liu^{36b}, J.B. Liu^{36a}, K. Liu⁸⁸, L. Liu¹⁶⁹, M. Liu^{36a}, Y.L. Liu^{36a}, Y. Liu^{36a}, M. Livan^{123a,123b}, A. Lleres⁵⁸, J. Llorente Merino^{35a}, S.L. Lloyd⁷⁹, C.Y. Lo^{62b}, F. Lo Sterzo¹⁵³, E.M. Lobodzinska⁴⁵, P. Loch⁷, F.K. Loebinger⁸⁷, A. Loesle⁵¹, K.M. Loew²⁵, A. Loginov^{179,*}, T. Lohse¹⁷, K. Lohwasser¹⁴¹, M. Lokajicek¹²⁹, B.A. Long²⁴, J.D. Long¹⁶⁹, R.E. Long⁷⁵, L. Longo^{76a,76b}, K.A.Looper¹¹³, J.A. Lopez^{34b}, D. Lopez Mateos⁵⁹, I. Lopez Paz¹³, A. Lopez Solis⁸³, J. Lorenz¹⁰², N. Lorenzo Martinez⁵, M. Losada²¹, P.J. Lösel¹⁰², X. Lou^{35a}, A. Lounis¹¹⁹, J. Love⁶, P.A. Love⁷⁵, H. Lu^{62a}, N. Lu⁹², Y.J. Lu⁶³, H.J. Lubatti¹⁴⁰, C. Luci^{134a,134b}, A. Lucotte⁵⁸, C. Luedtke⁵¹, F. Luehring⁶⁴, W. Lukas⁶⁵, L. Luminari^{134a}, O. Lundberg^{148a,148b}, B. Lund-Jensen¹⁴⁹, M.S. Lutz⁸⁹, P.M. Luzi⁸³, D. Lynn²⁷, R. Lysak¹²⁹, E. Lytken⁸⁴, F. Lyu^{35a}, V. Lyubushkin⁶⁸, H. Ma²⁷, L.L. Ma^{36b}, Y. Ma^{36b}, G. Maccarrone⁵⁰, A. Macchiolo¹⁰³, C.M. Macdonald¹⁴¹, B. Maček⁷⁸, J. Machado Miguens^{124,128b}, D. Madaffari¹⁷⁰, R. Madar³⁷, W.F. Mader⁴⁷, A. Madsen⁴⁵, J. Maeda⁷⁰, S. Maeland¹⁵, T. Maeno²⁷, A.S. Maevskiy¹⁰¹, V. Magerl⁵¹, J. Mahlstedt¹⁰⁹, C. Maiani¹¹⁹, C. Maidantchik^{26a}, A.A. Maier¹⁰³, T. Maier¹⁰², A. Maio^{128a,128b,128d}, O. Majersky^{146a}, S. Majewski¹¹⁸, Y. Makida⁶⁹, N. Makovec¹¹⁹, B. Malaescu⁸³, Pa. Malecki⁴², V.P. Maleev¹²⁵, F. Malek⁵⁸, U. Mallik⁶⁶, D. Malon⁶, C. Malone³⁰, S. Maltezos¹⁰, S. Malyukov³², J. Mamuzic¹⁷⁰, G. Mancini⁵⁰, I. Mandić⁷⁸, J. Maneira^{128a,128b}, L. Manhaes de Andrade Filho^{26b}, J. Manjarres Ramos⁴⁷, K.H. Mankinen⁸⁴, A. Mann¹⁰², A. Manousos³², B. Mansoulié¹³⁸, J.D. Mansour^{35a}, R. Mantifel⁹⁰, M. Mantoani⁵⁷, S. Manzoni^{94a,94b}, L. Mapelli³², G. Marceca²⁹, L. March⁵², L. Marchese¹²², G. Marchiori⁸³, M. Marcisovsky¹²⁹, M. Marjanovic³⁷, D.E. Marley⁹², F. Marroquim^{26a}, S.P. Marsden⁸⁷, Z. Marshall¹⁶, M.U.F Martensson¹⁶⁸, S. Marti-Garcia¹⁷⁰, C.B. Martin¹¹³, T.A. Martin¹⁷³, V.J. Martin⁴⁹, B. Martin dit Latour¹⁵, M. Martinez^{13,v}, V.I. Martinez Outschoorn¹⁶⁹, S. Martin-Haugh¹³³, V.S. Martoiu^{28b}, A.C. Martyniuk⁸¹, A. Marzin³², L. Masetti⁸⁶, T. Mashimo¹⁵⁷, R. Mashinistov⁹⁸, J. Masik⁸⁷, A.L. Maslennikov^{111,c}, L. Massa^{135a,135b}, P. Mastrandrea⁵, A. Mastroberardino^{40a,40b}, T. Masubuchi¹⁵⁷, P. Mättig¹⁷⁸, J. Maurer^{28b}, S.J. Maxfield⁷⁷, D.A. Maximov^{111,c}, R. Mazini¹⁵³, I. Maznas¹⁵⁶, S.M. Mazza^{94a,94b}, N.C. Mc Fadden¹⁰⁷, G. Mc Goldrick¹⁶¹, S.P. Mc Kee⁹², A. McCarn⁹², R.L. McCarthy¹⁵⁰, T.G. McCarthy¹⁰³, L.I. McClymont⁸¹, E.F. McDonald⁹¹, J.A. McFayden⁸¹, G. Mchedlidze⁵⁷, S.J. McMahon¹³³, P.C. McNamara⁹¹, R.A. McPherson^{172,o}, S. Meehan¹⁴⁰, T.J. Megy⁵¹, S. Mehlhase¹⁰², A. Mehta⁷⁷, T. Meideck⁵⁸, K. Meier^{60a}, B. Meirose⁴⁴, D. Melini^{170,aj}, B.R. Mellado Garcia^{147c}, J.D. Mellenthin⁵⁷, M. Melo^{146a}, F. Meloni¹⁸, A. Melzer²³, S.B. Menary⁸⁷, L. Meng⁷⁷, X.T. Meng⁹², A. Mengarelli^{22a,22b}, S. Menke¹⁰³, E. Meoni^{40a,40b}, S. Mergelmeyer¹⁷, P. Mermod⁵², L. Merola^{106a,106b}, C. Meroni^{94a}, F.S. Merritt³³, A. Messina^{134a,134b}, J. Metcalfe⁶, A.S. Mete¹⁶⁶, C. Meyer¹²⁴, J.-P. Meyer¹³⁸, J. Meyer¹⁰⁹, H. Meyer Zu Theenhausen^{60a}, F. Miano¹⁵¹, R.P. Middleton¹³³, S. Miglioranzi^{53a,53b}, L. Mijovic⁴⁹, G. Mikenberg¹⁷⁵, M. Mikestikova¹²⁹, M. Mikuž⁷⁸, M. Milesi⁹¹, A. Milic¹⁶¹,

D.W. Miller³³, C. Mills⁴⁹, A. Milov¹⁷⁵, D.A. Milstead^{148a,148b}, A.A. Minaenko¹³², Y. Minami¹⁵⁷, I.A. Minashvili^{54b}, A.I. Mincer¹¹², B. Mindur^{41a}, M. Mineev⁶⁸, Y. Minegishi¹⁵⁷, Y. Ming¹⁷⁶, L.M. Mir¹³, K.P. Mistry¹²⁴, T. Mitani¹⁷⁴, J. Mitrevski¹⁰², V.A. Mitsou¹⁷⁰, A. Miucci¹⁸, P.S. Miyagawa¹⁴¹, A. Mizukami⁶⁹, J.U. Mjörnmark⁸⁴, T. Mkrtchyan¹⁸⁰, M. Mlynarikova¹³¹, T. Moa^{148a,148b}, K. Mochizuki⁹⁷, P. Mogg⁵¹, S. Mohapatra³⁸, S. Molander^{148a,148b}, R. Moles-Valls²³, R. Monden⁷¹, M.C. Mondragon⁹³, K. Mönig⁴⁵, J. Monk³⁹, E. Monnier⁸⁸, A. Montalbano¹⁵⁰, J. Montejo Berlingen³², F. Monticelli⁷⁴, S. Monzani^{94a,94b}, R.W. Moore³, N. Morange¹¹⁹, D. Moreno²¹, M. Moreno Llácer³², P. Morettini^{53a}, S. Morgenstern³², D. Mori¹⁴⁴, T. Mori¹⁵⁷, M. Morii⁵⁹, M. Morinaga¹⁵⁷, V. Morisbak¹²¹, A.K. Morley³², G. Mornacchi³², J.D. Morris⁷⁹, L. Morvaj¹⁵⁰, P. Moschovakos¹⁰, M. Mosidze^{54b}, H.J. Moss¹⁴¹, J. Moss^{145,ak}, K. Motohashi¹⁵⁹, R. Mount¹⁴⁵, E. Mountricha²⁷, E.J.W. Moyse⁸⁹, S. Muanza⁸⁸, F. Mueller¹⁰³, J. Mueller¹²⁷, R.S.P. Mueller¹⁰², D. Muenstermann⁷⁵, P. Mullen⁵⁶, G.A. Mullier¹⁸, F.J. Munoz Sanchez⁸⁷, W.J. Murray^{173,133}, H. Musheghyan³², M. Muškinja⁷⁸, A.G. Myagkov^{132,al}, M. Myska¹³⁰, B.P. Nachman¹⁶, O. Nackenhorst⁵², K. Nagai¹²², R. Nagai^{69,ae}, K. Nagano⁶⁹, Y. Nagasaka⁶¹, K. Nagata¹⁶⁴, M. Nagel⁵¹, E. Nagy⁸⁸, A.M. Nairz³², Y. Nakahama¹⁰⁵, K. Nakamura⁶⁹, T. Nakamura¹⁵⁷, I. Nakano¹¹⁴, R.F. Naranjo Garcia⁴⁵, R. Narayan¹¹, D.I. Narrias Villar^{60a}, I. Naryshkin¹²⁵, T. Naumann⁴⁵, G. Navarro²¹, R. Nayyar⁷, H.A. Neal⁹², P.Yu. Nechaeva⁹⁸, T.J. Neep¹³⁸, A. Negri^{123a,123b}, M. Negrini^{22a}, S. Nektarijevic¹⁰⁸, C. Nellist¹¹⁹, A. Nelson¹⁶⁶, M.E. Nelson¹²², S. Nemecek¹²⁹, P. Nemethy¹¹², M. Nessi^{32,am}, M.S. Neubauer¹⁶⁹, M. Neumann¹⁷⁸, P.R. Newman¹⁹, T.Y. Ng^{62c}, T. Nguyen Manh⁹⁷, R.B. Nickerson¹²², R. Nicolaïdou¹³⁸, J. Nielsen¹³⁹, V. Nikolaenko^{132,al}, I. Nikolic-Audit⁸³, K. Nikolopoulos¹⁹, J.K. Nilsen¹²¹, P. Nilsson²⁷, Y. Ninomiya¹⁵⁷, A. Nisati^{134a}, N. Nishu^{35c}, R. Nisius¹⁰³, I. Nitsche⁴⁶, T. Nitta¹⁷⁴, T. Nobe¹⁵⁷, Y. Noguchi⁷¹, M. Nomachi¹²⁰, I. Nomidis³¹, M.A. Nomura²⁷, T. Nooney⁷⁹, M. Nordberg³², N. Norjoharuddeen¹²², O. Novgorodova⁴⁷, M. Nozaki⁶⁹, L. Nozka¹¹⁷, K. Ntekas¹⁶⁶, E. Nurse⁸¹, F. Nuti⁹¹, K. O'connor²⁵, D.C. O'Neil¹⁴⁴, A.A. O'Rourke⁴⁵, V. O'Shea⁵⁶, F.G. Oakham^{31,d}, H. Oberlack¹⁰³, T. Obermann²³, J. Ocariz⁸³, A. Ochi⁷⁰, I. Ochoa³⁸, J.P. Ochoa-Ricoux^{34a}, S. Oda⁷³, S. Odaka⁶⁹, A. Oh⁸⁷, S.H. Oh⁴⁸, C.C. Ohm¹⁶, H. Ohman¹⁶⁸, H. Oide^{53a,53b}, H. Okawa¹⁶⁴, Y. Okumura¹⁵⁷, T. Okuyama⁶⁹, A. Olariu^{28b}, L.F. Oleiro Seabra^{128a}, S.A. Olivares Pino^{34a}, D. Oliveira Damazio²⁷, A. Olszewski⁴², J. Olszowska⁴², A. Onofre^{128a,128e}, K. Onogi¹⁰⁵, P.U.E. Onyisi^{11,aa}, H. Oppen¹²¹, M.J. Oreglia³³, Y. Oren¹⁵⁵, D. Orestano^{136a,136b}, N. Orlando^{62b}, R.S. Orr¹⁶¹, B. Osculati^{53a,53b,*}, R. Ospanov^{36a}, G. Otero y Garzon²⁹, H. Otono⁷³, M. Ouchrif^{137d}, F. Ould-Saada¹²¹, A. Ouraou¹³⁸, K.P. Oussoren¹⁰⁹, Q. Ouyang^{35a}, M. Owen⁵⁶, R.E. Owen¹⁹, V.E. Ozcan^{20a}, N. Ozturk⁸, K. Pachal¹⁴⁴, A. Pacheco Pages¹³, L. Pacheco Rodriguez¹³⁸, C. Padilla Aranda¹³, S. Pagan Griso¹⁶, M. Paganini¹⁷⁹, F. Paige²⁷, G. Palacino⁶⁴, S. Palazzo^{40a,40b}, S. Palestini³², M. Palka^{41b}, D. Pallin³⁷, E.St. Panagiotopoulou¹⁰, I. Panagoulias¹⁰, C.E. Pandini^{126a,126b}, J.G. Panduro Vazquez⁸⁰, P. Pani³², S. Panitkin²⁷, D. Pantea^{28b}, L. Paolozzi⁵², Th.D. Papadopoulou¹⁰, K. Papageorgiou^{9,s}, A. Paramonov⁶, D. Paredes Hernandez¹⁷⁹, A.J. Parker⁷⁵, M.A. Parker³⁰, K.A. Parker⁴⁵, F. Parodi^{53a,53b}, J.A. Parsons³⁸, U. Parzefall⁵¹, V.R. Pascuzzi¹⁶¹, J.M. Pasner¹³⁹, E. Pasqualucci^{134a}, S. Passaggio^{53a}, Fr. Pastore⁸⁰, S. Pataraia⁸⁶, J.R. Pater⁸⁷, T. Pauly³², B. Pearson¹⁰³, S. Pedraza Lopez¹⁷⁰, R. Pedro^{128a,128b}, S.V. Peleganchuk^{111,c}, O. Penc¹²⁹, C. Peng^{35a,35d}, H. Peng^{36a}, J. Penwell⁶⁴, B.S. Peralva^{26b}, M.M. Perego¹³⁸, D.V. Perepelitsa²⁷, F. Peri¹⁷, L. Perini^{94a,94b}, H. Pernegger³², S. Perrella^{106a,106b}, R. Peschke⁴⁵, V.D. Peshekhanov^{68,*}, K. Peters⁴⁵, R.F.Y. Peters⁸⁷, B.A. Petersen³², T.C. Petersen³⁹, E. Petit⁵⁸, A. Petridis¹, C. Petridou¹⁵⁶, P. Petroff¹¹⁹, E. Petrolo^{134a}, M. Petrov¹²², F. Petrucci^{136a,136b}, N.E. Pettersson⁸⁹, A. Peyaud¹³⁸, R. Pezoa^{34b}, F.H. Phillips⁹³, P.W. Phillips¹³³, G. Piacquadio¹⁵⁰, E. Pianori¹⁷³, A. Picazio⁸⁹, E. Piccaro⁷⁹, M.A. Pickering¹²², R. Piegaia²⁹, J.E. Pilcher³³, A.D. Pilkington⁸⁷, A.W.J. Pin⁸⁷, M. Pinamonti^{135a,135b}, J.L. Pinfold³, H. Pirumov⁴⁵, M. Pitt¹⁷⁵, L. Plazak^{146a}, M.-A. Pleier²⁷, V. Pleskot⁸⁶, E. Plotnikova⁶⁸, D. Pluth⁶⁷, P. Podberezko¹¹¹, R. Poettgen⁸⁴, R. Poggi^{123a,123b}, L. Poggioli¹¹⁹, I. Pogrebnyak⁹³, D. Pohl²³,

G. Polesello^{123a}, A. Poley⁴⁵, A. Policicchio^{40a,40b}, R. Polifka³², A. Polini^{22a}, C.S. Pollard⁵⁶,
 V. Polychronakos²⁷, K. Pommès³², D. Ponomarenko¹⁰⁰, L. Pontecorvo^{134a}, G.A. Popeneciu^{28d},
 S. Pospisil¹³⁰, K. Potamianos¹⁶, I.N. Potrap⁶⁸, C.J. Potter³⁰, T. Poulsen⁸⁴, J. Poveda³²,
 M.E. Pozo Astigarraga³², P. Pralavorio⁸⁸, A. Pranko¹⁶, S. Prell⁶⁷, D. Price⁸⁷, M. Primavera^{76a},
 S. Prince⁹⁰, N. Proklova¹⁰⁰, K. Prokofiev^{62c}, F. Prokoshin^{34b}, S. Protopopescu²⁷, J. Proudfoot⁶,
 M. Przybycien^{41a}, A. Puri¹⁶⁹, P. Puzo¹¹⁹, J. Qian⁹², G. Qin⁵⁶, Y. Qin⁸⁷, A. Quadt⁵⁷,
 M. Queitsch-Maitland⁴⁵, D. Quilty⁵⁶, S. Raddum¹²¹, V. Radeka²⁷, V. Radescu¹²²,
 S.K. Radhakrishnan¹⁵⁰, P. Radloff¹¹⁸, P. Rados⁹¹, F. Ragusa^{94a,94b}, G. Rahal¹⁸¹, J.A. Raine⁸⁷,
 S. Rajagopalan²⁷, C. Rangel-Smith¹⁶⁸, T. Rashid¹¹⁹, S. Raspovov⁵, M.G. Ratti^{94a,94b}, D.M. Rauch⁴⁵,
 F. Rauscher¹⁰², S. Rave⁸⁶, I. Ravinovich¹⁷⁵, J.H. Rawling⁸⁷, M. Raymond³², A.L. Read¹²¹,
 N.P. Readioff⁵⁸, M. Reale^{76a,76b}, D.M. Rebuzzi^{123a,123b}, A. Redelbach¹⁷⁷, G. Redlinger²⁷, R. Reece¹³⁹,
 R.G. Reed^{147c}, K. Reeves⁴⁴, L. Rehnisch¹⁷, J. Reichert¹²⁴, A. Reiss⁸⁶, C. Rembser³², H. Ren^{35a,35d},
 M. Rescigno^{134a}, S. Resconi^{94a}, E.D. Resseguei¹²⁴, S. Rettie¹⁷¹, E. Reynolds¹⁹, O.L. Rezanova^{111,c},
 P. Reznicek¹³¹, R. Rezvani⁹⁷, R. Richter¹⁰³, S. Richter⁸¹, E. Richter-Was^{41b}, O. Ricken²³, M. Ridel⁸³,
 P. Rieck¹⁰³, C.J. Riegel¹⁷⁸, J. Rieger⁵⁷, O. Rifki¹¹⁵, M. Rijssenbeek¹⁵⁰, A. Rimoldi^{123a,123b},
 M. Rimoldi¹⁸, L. Rinaldi^{22a}, G. Ripellino¹⁴⁹, B. Ristić³², E. Ritsch³², I. Riu¹³, F. Rizatdinova¹¹⁶,
 E. Rizvi⁷⁹, C. Rizzi¹³, R.T. Roberts⁸⁷, S.H. Robertson^{90,o}, A. Robichaud-Veronneau⁹⁰, D. Robinson³⁰,
 J.E.M. Robinson⁴⁵, A. Robson⁵⁶, E. Rocco⁸⁶, C. Roda^{126a,126b}, Y. Rodina^{88,an}, S. Rodriguez Bosca¹⁷⁰,
 A. Rodriguez Perez¹³, D. Rodriguez Rodriguez¹⁷⁰, S. Roe³², C.S. Rogan⁵⁹, O. Røhne¹²¹, J. Roloff⁵⁹,
 A. Romaniouk¹⁰⁰, M. Romano^{22a,22b}, S.M. Romano Saez³⁷, E. Romero Adam¹⁷⁰, N. Rompotis⁷⁷,
 M. Ronzani⁵¹, L. Roos⁸³, S. Rosati^{134a}, K. Rosbach⁵¹, P. Rose¹³⁹, N.-A. Rosien⁵⁷, E. Rossi^{106a,106b},
 L.P. Rossi^{53a}, J.H.N. Rosten³⁰, R. Rosten¹⁴⁰, M. Rotaru^{28b}, J. Rothberg¹⁴⁰, D. Rousseau¹¹⁹,
 A. Rozanov⁸⁸, Y. Rozen¹⁵⁴, X. Ruan^{147c}, F. Rubbo¹⁴⁵, F. Rühr⁵¹, A. Ruiz-Martinez³¹, Z. Rurikova⁵¹,
 N.A. Rusakovich⁶⁸, H.L. Russell⁹⁰, J.P. Rutherford⁷, N. Ruthmann³², Y.F. Ryabov¹²⁵, M. Rybar¹⁶⁹,
 G. Rybkin¹¹⁹, S. Ryu⁶, A. Ryzhov¹³², G.F. Rzehorz⁵⁷, A.F. Saavedra¹⁵², G. Sabato¹⁰⁹, S. Sacerdoti²⁹,
 H.F-W. Sadrozinski¹³⁹, R. Sadykov⁶⁸, F. Safai Tehrani^{134a}, P. Saha¹¹⁰, M. Sahinsoy^{60a}, M. Saimpert⁴⁵,
 M. Saito¹⁵⁷, T. Saito¹⁵⁷, H. Sakamoto¹⁵⁷, Y. Sakurai¹⁷⁴, G. Salamanna^{136a,136b}, J.E. Salazar Loyola^{34b},
 D. Salek¹⁰⁹, P.H. Sales De Bruin¹⁶⁸, D. Salihagic¹⁰³, A. Salnikov¹⁴⁵, J. Salt¹⁷⁰, D. Salvatore^{40a,40b},
 F. Salvatore¹⁵¹, A. Salvucci^{62a,62b,62c}, A. Salzburger³², D. Sammel⁵¹, D. Sampsonidis¹⁵⁶,
 D. Sampsonidou¹⁵⁶, J. Sánchez¹⁷⁰, V. Sanchez Martinez¹⁷⁰, A. Sanchez Pineda^{167a,167c}, H. Sandaker¹²¹,
 R.L. Sandbach⁷⁹, C.O. Sander⁴⁵, M. Sandhoff¹⁷⁸, C. Sandoval²¹, D.P.C. Sankey¹³³, M. Sannino^{53a,53b},
 Y. Sano¹⁰⁵, A. Sansoni⁵⁰, C. Santoni³⁷, H. Santos^{128a}, I. Santoyo Castillo¹⁵¹, A. Sapronov⁶⁸,
 J.G. Saraiva^{128a,128d}, B. Sarrazin²³, O. Sasaki⁶⁹, K. Sato¹⁶⁴, E. Sauvan⁵, G. Savage⁸⁰, P. Savard^{161,d},
 N. Savic¹⁰³, C. Sawyer¹³³, L. Sawyer^{82,u}, J. Saxon³³, C. Sbarra^{22a}, A. Sbrizzi^{22a,22b}, T. Scanlon⁸¹,
 D.A. Scannicchio¹⁶⁶, M. Scarcella¹⁵², J. Schaarschmidt¹⁴⁰, P. Schacht¹⁰³, B.M. Schachtner¹⁰²,
 D. Schaefer³², L. Schaefer¹²⁴, R. Schaefer⁴⁵, J. Schaeffer⁸⁶, S. Schaepe²³, S. Schaetzl^{60b}, U. Schäfer⁸⁶,
 A.C. Schaffter¹¹⁹, D. Schaile¹⁰², R.D. Schamberger¹⁵⁰, V.A. Schegelsky¹²⁵, D. Scheirich¹³¹,
 M. Schernau¹⁶⁶, C. Schiavi^{53a,53b}, S. Schier¹³⁹, L.K. Schildgen²³, C. Schillo⁵¹, M. Schioppa^{40a,40b},
 S. Schlenker³², K.R. Schmidt-Sommerfeld¹⁰³, K. Schmieden³², C. Schmitt⁸⁶, S. Schmitt⁴⁵, S. Schmitz⁸⁶,
 U. Schnoor⁵¹, L. Schoeffel¹³⁸, A. Schoening^{60b}, B.D. Schoenrock⁹³, E. Schopf²³, M. Schott⁸⁶,
 J.F.P. Schouwenberg¹⁰⁸, J. Schovancova³², S. Schramm⁵², N. Schuh⁸⁶, A. Schulte⁸⁶, M.J. Schultens²³,
 H.-C. Schultz-Coulon^{60a}, H. Schulz¹⁷, M. Schumacher⁵¹, B.A. Schumm¹³⁹, Ph. Schune¹³⁸,
 A. Schwartzman¹⁴⁵, T.A. Schwarz⁹², H. Schweiger⁸⁷, Ph. Schwemling¹³⁸, R. Schwienhorst⁹³,
 J. Schwindling¹³⁸, A. Sciandra²³, G. Sciolla²⁵, M. Scornajenghi^{40a,40b}, F. Scuri^{126a,126b}, F. Scutti⁹¹,
 J. Searcy⁹², P. Seema²³, S.C. Seidel¹⁰⁷, A. Seiden¹³⁹, J.M. Seixas^{26a}, G. Sekhniaidze^{106a}, K. Sekhon⁹²,
 S.J. Sekula⁴³, N. Semprini-Cesari^{22a,22b}, S. Senkin³⁷, C. Serfon¹²¹, L. Serin¹¹⁹, L. Serkin^{167a,167b},
 M. Sessa^{136a,136b}, R. Seuster¹⁷², H. Severini¹¹⁵, T. Sfiligoj⁷⁸, F. Sforza³², A. Sfyrla⁵², E. Shabalina⁵⁷,

N.W. Shaikh^{148a,148b}, L.Y. Shan^{35a}, R. Shang¹⁶⁹, J.T. Shank²⁴, M. Shapiro¹⁶, P.B. Shatalov⁹⁹,
 K. Shaw^{167a,167b}, S.M. Shaw⁸⁷, A. Shcherbakova^{148a,148b}, C.Y. Shehu¹⁵¹, Y. Shen¹¹⁵, N. Sherafati³¹,
 P. Sherwood⁸¹, L. Shi^{153,ao}, S. Shimizu⁷⁰, C.O. Shimmin¹⁷⁹, M. Shimojima¹⁰⁴, I.P.J. Shipsey¹²²,
 S. Shirabe⁷³, M. Shiyakova^{68,ap}, J. Shlomi¹⁷⁵, A. Shmeleva⁹⁸, D. Shoaleh Saadi⁹⁷, M.J. Shochet³³,
 S. Shojaei^{94a}, D.R. Shope¹¹⁵, S. Shrestha¹¹³, E. Shulga¹⁰⁰, M.A. Shupe⁷, P. Sicho¹²⁹, A.M. Sickles¹⁶⁹,
 P.E. Sidebo¹⁴⁹, E. Sideras Haddad^{147c}, O. Sidiropoulou¹⁷⁷, A. Sidoti^{22a,22b}, F. Siegert⁴⁷, Dj. Sijacki¹⁴,
 J. Silva^{128a,128d}, S.B. Silverstein^{148a}, V. Simak¹³⁰, L. Simic¹⁴, S. Simion¹¹⁹, E. Simioni⁸⁶, B. Simmons⁸¹,
 M. Simon⁸⁶, P. Sinervo¹⁶¹, N.B. Sinev¹¹⁸, M. Sioli^{22a,22b}, G. Siragusa¹⁷⁷, I. Siral⁹², S.Yu. Sivoklokov¹⁰¹,
 J. Sjölin^{148a,148b}, M.B. Skinner⁷⁵, P. Skubic¹¹⁵, M. Slater¹⁹, T. Slavicek¹³⁰, M. Slawinska⁴², K. Sliwa¹⁶⁵,
 R. Slovak¹³¹, V. Smakhtin¹⁷⁵, B.H. Smart⁵, J. Smiesko^{146a}, N. Smirnov¹⁰⁰, S.Yu. Smirnov¹⁰⁰,
 Y. Smirnov¹⁰⁰, L.N. Smirnova^{101,aq}, O. Smirnova⁸⁴, J.W. Smith⁵⁷, M.N.K. Smith³⁸, R.W. Smith³⁸,
 M. Smizanska⁷⁵, K. Smolek¹³⁰, A.A. Snesarev⁹⁸, I.M. Snyder¹¹⁸, S. Snyder²⁷, R. Sobie^{172,o},
 F. Socher⁴⁷, A. Soffer¹⁵⁵, A. Søgaard⁴⁹, D.A. Soh¹⁵³, G. Sokhrannyi⁷⁸, C.A. Solans Sanchez³²,
 M. Solar¹³⁰, E.Yu. Soldatov¹⁰⁰, U. Soldevila¹⁷⁰, A.A. Solodkov¹³², A. Soloshenko⁶⁸,
 O.V. Solovyanov¹³², V. Solovyev¹²⁵, P. Sommer⁵¹, H. Son¹⁶⁵, A. Sopczak¹³⁰, D. Sosa^{60b},
 C.L. Sotropoulou^{126a,126b}, R. Soualah^{167a,167c}, A.M. Soukharev^{111,c}, D. South⁴⁵, B.C. Sowden⁸⁰,
 S. Spagnolo^{76a,76b}, M. Spalla^{126a,126b}, M. Spangenberg¹⁷³, F. Spanò⁸⁰, D. Sperlich¹⁷, F. Spettel¹⁰³,
 T.M. Spieker^{60a}, R. Spighi^{22a}, G. Spigo³², L.A. Spiller⁹¹, M. Spousta¹³¹, R.D. St. Denis^{56,*},
 A. Stabile^{94a}, R. Stamen^{60a}, S. Stamm¹⁷, E. Stanecka⁴², R.W. Stanek⁶, C. Stanescu^{136a},
 M.M. Stanitzki⁴⁵, B.S. Staph¹⁰⁹, S. Starnes¹²¹, E.A. Starchenko¹³², G.H. Stark³³, J. Stark⁵⁸, S.H. Stark³⁹,
 P. Staroba¹²⁹, P. Starovoitov^{60a}, S. Stärz³², R. Staszewski⁴², P. Steinberg²⁷, B. Stelzer¹⁴⁴, H.J. Stelzer³²,
 O. Stelzer-Chilton^{163a}, H. Stenzel⁵⁵, G.A. Stewart⁵⁶, M.C. Stockton¹¹⁸, M. Stoebe⁹⁰, G. Stoica^{28b},
 P. Stolte⁵⁷, S. Stonjek¹⁰³, A.R. Stradling⁸, A. Straessner⁴⁷, M.E. Stramaglia¹⁸, J. Strandberg¹⁴⁹,
 S. Strandberg^{148a,148b}, M. Strauss¹¹⁵, P. Strizenec^{146b}, R. Ströhmer¹⁷⁷, D.M. Strom¹¹⁸, R. Stroynowski⁴³,
 A. Strubig⁴⁹, S.A. Stucci²⁷, B. Stugu¹⁵, N.A. Styles⁴⁵, D. Su¹⁴⁵, J. Su¹²⁷, S. Suchek^{60a}, Y. Sugaya¹²⁰,
 M. Suk¹³⁰, V.V. Sulin⁹⁸, DMS Sultan^{162a,162b}, S. Sultansoy^{4c}, T. Sumida⁷¹, S. Sun⁵⁹, X. Sun³,
 K. Suruliz¹⁵¹, C.J.E. Suster¹⁵², M.R. Sutton¹⁵¹, S. Suzuki⁶⁹, M. Svatos¹²⁹, M. Swiatlowski³³,
 S.P. Swift², I. Sykora^{146a}, T. Sykora¹³¹, D. Ta⁵¹, K. Tackmann⁴⁵, J. Taenzer¹⁵⁵, A. Taffard¹⁶⁶,
 R. Tafirout^{163a}, E. Tahirovic⁷⁹, N. Taiblum¹⁵⁵, H. Takai²⁷, R. Takashima⁷², E.H. Takasugi¹⁰³,
 T. Takeshita¹⁴², Y. Takubo⁶⁹, M. Talby⁸⁸, A.A. Talyshев^{111,c}, J. Tanaka¹⁵⁷, M. Tanaka¹⁵⁹, R. Tanaka¹¹⁹,
 S. Tanaka⁶⁹, R. Tanioka⁷⁰, B.B. Tannenwald¹¹³, S. Tapia Araya^{34b}, S. Tapprogge⁸⁶, S. Tarem¹⁵⁴,
 G.F. Tartarelli^{94a}, P. Tas¹³¹, M. Tasevsky¹²⁹, T. Tashiro⁷¹, E. Tassi^{40a,40b}, A. Tavares Delgado^{128a,128b},
 Y. Tayalati^{137e}, A.C. Taylor¹⁰⁷, G.N. Taylor⁹¹, P.T.E. Taylor⁹¹, W. Taylor^{163b}, P. Teixeira-Dias⁸⁰,
 D. Temple¹⁴⁴, H. Ten Kate³², P.K. Teng¹⁵³, J.J. Teoh¹²⁰, F. Tepel¹⁷⁸, S. Terada⁶⁹, K. Terashi¹⁵⁷,
 J. Terron⁸⁵, S. Terzo¹³, M. Testa⁵⁰, R.J. Teuscher^{161,o}, T. Theveneaux-Pelzer⁸⁸, F. Thiele³⁹,
 J.P. Thomas¹⁹, J. Thomas-Wilsker⁸⁰, P.D. Thompson¹⁹, A.S. Thompson⁵⁶, L.A. Thomsen¹⁷⁹,
 E. Thomson¹²⁴, M.J. Tibbetts¹⁶, R.E. Ticse Torres⁸⁸, V.O. Tikhomirov^{98,ar}, Yu.A. Tikhonov^{111,c},
 S. Timoshenko¹⁰⁰, P. Tipton¹⁷⁹, S. Tisserant⁸⁸, K. Todome¹⁵⁹, S. Todorova-Nova⁵, S. Todt⁴⁷, J. Tojo⁷³,
 S. Tokár^{146a}, K. Tokushuku⁶⁹, E. Tolley¹¹³, L. Tomlinson⁸⁷, M. Tomoto¹⁰⁵, L. Tompkins^{145,as},
 K. Toms¹⁰⁷, B. Tong⁵⁹, P. Tornambe⁵¹, E. Torrence¹¹⁸, H. Torres¹⁴⁴, E. Torró Pastor¹⁴⁰, J. Toth^{88,at},
 F. Touchard⁸⁸, D.R. Tovey¹⁴¹, C.J. Treado¹¹², T. Trefzger¹⁷⁷, F. Tresoldi¹⁵¹, A. Tricoli²⁷,
 I.M. Trigger^{163a}, S. Trincatz-Duvoid⁸³, M.F. Tripiana¹³, W. Trischuk¹⁶¹, B. Trocmé⁵⁸, A. Trofymov⁴⁵,
 C. Troncon^{94a}, M. Trottier-McDonald¹⁶, M. Trovatelli¹⁷², L. Truong^{147b}, M. Trzebinski⁴², A. Trzupek⁴²,
 K.W. Tsang^{62a}, J.C-L. Tseng¹²², P.V. Tsiareshka⁹⁵, G. Tsipolitis¹⁰, N. Tsirintanis⁹, S. Tsiskaridze¹³,
 V. Tsiskaridze⁵¹, E.G. Tskhadadze^{54a}, K.M. Tsui^{62a}, I.I. Tsukerman⁹⁹, V. Tsulaia¹⁶, S. Tsuno⁶⁹,
 D. Tsybychev¹⁵⁰, Y. Tu^{62b}, A. Tudorache^{28b}, V. Tudorache^{28b}, T.T. Tulbure^{28a}, A.N. Tuna⁵⁹,
 S.A. Tupputi^{22a,22b}, S. Turchikhin⁶⁸, D. Turgeman¹⁷⁵, I. Turk Cakir^{4b,au}, R. Turra^{94a}, P.M. Tuts³⁸,

G. Ucchielli^{22a,22b}, I. Ueda⁶⁹, M. Ughetto^{148a,148b}, F. Ukegawa¹⁶⁴, G. Unal³², A. Undrus²⁷, G. Unel¹⁶⁶,
 F.C. Ungaro⁹¹, Y. Unno⁶⁹, C. Unverdorben¹⁰², J. Urban^{146b}, P. Urquijo⁹¹, P. Urrejola⁸⁶, G. Usai⁸,
 J. Usui⁶⁹, L. Vacavant⁸⁸, V. Vacek¹³⁰, B. Vachon⁹⁰, K.O.H. Vadla¹²¹, A. Vaidya⁸¹, C. Valderanis¹⁰²,
 E. Valdes Santurio^{148a,148b}, M. Valente⁵², S. Valentineti^{22a,22b}, A. Valero¹⁷⁰, L. Valéry¹³, S. Valkar¹³¹,
 A. Vallier⁵, J.A. Valls Ferrer¹⁷⁰, W. Van Den Wollenberg¹⁰⁹, H. van der Graaf¹⁰⁹, P. van Gemmeren⁶,
 J. Van Nieuwkoop¹⁴⁴, I. van Vulpen¹⁰⁹, M.C. van Woerden¹⁰⁹, M. Vanadia^{135a,135b}, W. Vandelli³²,
 A. Vaniachine¹⁶⁰, P. Vankov¹⁰⁹, G. Vardanyan¹⁸⁰, R. Vari^{134a}, E.W. Varnes⁷, C. Varni^{53a,53b}, T. Varol⁴³,
 D. Varouchas¹¹⁹, A. Vartapetian⁸, K.E. Varvell¹⁵², J.G. Vasquez¹⁷⁹, G.A. Vasquez^{34b}, F. Vazeille³⁷,
 T. Vazquez Schroeder⁹⁰, J. Veatch⁵⁷, V. Veeraraghavan⁷, L.M. Veloce¹⁶¹, F. Veloso^{128a,128c},
 S. Veneziano^{134a}, A. Ventura^{76a,76b}, M. Venturi¹⁷², N. Venturi³², A. Venturini²⁵, V. Vercesi^{123a},
 M. Verducci^{136a,136b}, W. Verkerke¹⁰⁹, A.T. Vermeulen¹⁰⁹, J.C. Vermeulen¹⁰⁹, M.C. Vetterli^{144,d},
 N. Viaux Maira^{34b}, O. Viazlo⁸⁴, I. Vichou^{169,*}, T. Vickey¹⁴¹, O.E. Vickey Boeriu¹⁴¹,
 G.H.A. Viehhauser¹²², S. Viel¹⁶, L. Vigani¹²², M. Villa^{22a,22b}, M. Villaplana Perez^{94a,94b}, E. Vilucchi⁵⁰,
 M.G. Vincter³¹, V.B. Vinogradov⁶⁸, A. Vishwakarma⁴⁵, C. Vittori^{22a,22b}, I. Vivarelli¹⁵¹, S. Vlachos¹⁰,
 M. Vogel¹⁷⁸, P. Vokac¹³⁰, G. Volpi^{126a,126b}, H. von der Schmitt¹⁰³, E. von Toerne²³, V. Vorobel¹³¹,
 K. Vorobev¹⁰⁰, M. Vos¹⁷⁰, R. Voss³², J.H. Vossebeld⁷⁷, N. Vranjes¹⁴, M. Vranjes Milosavljevic¹⁴,
 V. Vrba¹³⁰, M. Vreeswijk¹⁰⁹, R. Vuillermet³², I. Vukotic³³, P. Wagner²³, W. Wagner¹⁷⁸,
 J. Wagner-Kuhr¹⁰², H. Wahlberg⁷⁴, S. Wahrmund⁴⁷, J. Wakabayashi¹⁰⁵, J. Walder⁷⁵, R. Walker¹⁰²,
 W. Walkowiak¹⁴³, V. Wallangen^{148a,148b}, C. Wang^{35b}, C. Wang^{36b,aw}, F. Wang¹⁷⁶, H. Wang¹⁶, H. Wang³,
 J. Wang⁴⁵, J. Wang¹⁵², Q. Wang¹¹⁵, R. Wang⁶, S.M. Wang¹⁵³, T. Wang³⁸, W. Wang^{153,aw}, W. Wang^{36a,ax},
 Z. Wang^{36c}, C. Wanotayaroj¹¹⁸, A. Warburton⁹⁰, C.P. Ward³⁰, D.R. Wardrobe⁸¹, A. Washbrook⁴⁹,
 P.M. Watkins¹⁹, A.T. Watson¹⁹, M.F. Watson¹⁹, G. Watts¹⁴⁰, S. Watts⁸⁷, B.M. Waugh⁸¹, A.F. Webb¹¹,
 S. Webb⁸⁶, M.S. Weber¹⁸, S.W. Weber¹⁷⁷, S.A. Weber³¹, J.S. Webster⁶, A.R. Weidberg¹²², B. Weinert⁶⁴,
 J. Weingarten⁵⁷, M. Weirich⁸⁶, C. Weiser⁵¹, H. Weits¹⁰⁹, P.S. Wells³², T. Wenaus²⁷, T. Wengler³²,
 S. Wenig³², N. Wermes²³, M.D. Werner⁶⁷, P. Werner³², M. Wessels^{60a}, T.D. Weston¹⁸, K. Whalen¹¹⁸,
 N.L. Whallon¹⁴⁰, A.M. Wharton⁷⁵, A.S. White⁹², A. White⁸, M.J. White¹, R. White^{34b}, D. Whiteson¹⁶⁶,
 B.W. Whitmore⁷⁵, F.J. Wickens¹³³, W. Wiedenmann¹⁷⁶, M. Wielers¹³³, C. Wiglesworth³⁹,
 L.A.M. Wiik-Fuchs⁵¹, A. Wildauer¹⁰³, F. Wilk⁸⁷, H.G. Wilkens³², H.H. Williams¹²⁴, S. Williams¹⁰⁹,
 C. Willis⁹³, S. Willocq⁸⁹, J.A. Wilson¹⁹, I. Wingerter-Seez⁵, E. Winkels¹⁵¹, F. Winklmeier¹¹⁸,
 O.J. Winston¹⁵¹, B.T. Winter²³, M. Wittgen¹⁴⁵, M. Wobisch^{82,u}, T.M.H. Wolf¹⁰⁹, R. Wolff⁸⁸,
 M.W. Wolter⁴², H. Wolters^{128a,128c}, V.W.S. Wong¹⁷¹, S.D. Worm¹⁹, B.K. Wosiek⁴², J. Wotschack³²,
 K.W. Wozniak⁴², M. Wu³³, S.L. Wu¹⁷⁶, X. Wu⁵², Y. Wu⁹², T.R. Wyatt⁸⁷, B.M. Wynne⁴⁹, S. Xella³⁹,
 Z. Xi⁹², L. Xia^{35c}, D. Xu^{35a}, L. Xu²⁷, T. Xu¹³⁸, B. Yabsley¹⁵², S. Yacoob^{147a}, D. Yamaguchi¹⁵⁹,
 Y. Yamaguchi¹²⁰, A. Yamamoto⁶⁹, S. Yamamoto¹⁵⁷, T. Yamanaka¹⁵⁷, M. Yamatani¹⁵⁷, K. Yamauchi¹⁰⁵,
 Y. Yamazaki⁷⁰, Z. Yan²⁴, H. Yang^{36c}, H. Yang¹⁶, Y. Yang¹⁵³, Z. Yang¹⁵, W-M. Yao¹⁶, Y.C. Yap⁸³,
 Y. Yasu⁶⁹, E. Yatsenko⁵, K.H. Yau Wong²³, J. Ye⁴³, S. Ye²⁷, I. Yeletskikh⁶⁸, E. Yigitbasi²⁴,
 E. Yildirim⁸⁶, K. Yorita¹⁷⁴, K. Yoshihara¹²⁴, C. Young¹⁴⁵, C.J.S. Young³², J. Yu⁸, J. Yu⁶⁷, S.P.Y. Yuen²³,
 I. Yusuff^{30,ay}, B. Zabinski⁴², G. Zacharis¹⁰, R. Zaidan¹³, A.M. Zaitsev^{132,al}, N. Zakharchuk⁴⁵,
 J. Zalieckas¹⁵, A. Zaman¹⁵⁰, S. Zambito⁵⁹, D. Zanzi⁹¹, C. Zeitnitz¹⁷⁸, G. Zemaityte¹²², A. Zemla^{41a},
 J.C. Zeng¹⁶⁹, Q. Zeng¹⁴⁵, O. Zenin¹³², T. Ženiš^{146a}, D. Zerwas¹¹⁹, D. Zhang⁹², F. Zhang¹⁷⁶,
 G. Zhang^{36a,ax}, H. Zhang^{35b}, J. Zhang⁶, L. Zhang⁵¹, L. Zhang^{36a}, M. Zhang¹⁶⁹, P. Zhang^{35b}, R. Zhang²³,
 R. Zhang^{36a,av}, X. Zhang^{36b}, Y. Zhang^{35a,35d}, Z. Zhang¹¹⁹, X. Zhao⁴³, Y. Zhao^{36b,az}, Z. Zhao^{36a},
 A. Zhemchugov⁶⁸, B. Zhou⁹², C. Zhou¹⁷⁶, L. Zhou⁴³, M. Zhou^{35a,35d}, M. Zhou¹⁵⁰, N. Zhou^{35c},
 C.G. Zhu^{36b}, H. Zhu^{35a}, J. Zhu⁹², Y. Zhu^{36a}, X. Zhuang^{35a}, K. Zhukov⁹⁸, A. Zibell¹⁷⁷, D. Ziemska⁶⁴,
 N.I. Zimine⁶⁸, C. Zimmermann⁸⁶, S. Zimmermann⁵¹, Z. Zinonos¹⁰³, M. Zinser⁸⁶, M. Ziolkowski¹⁴³,
 L. Živković¹⁴, G. Zobernig¹⁷⁶, A. Zoccoli^{22a,22b}, R. Zou³³, M. zur Nedden¹⁷, L. Zwalinski³².

- ¹ Department of Physics, University of Adelaide, Adelaide, Australia
² Physics Department, SUNY Albany, Albany NY, United States of America
³ Department of Physics, University of Alberta, Edmonton AB, Canada
⁴ ^(a) Department of Physics, Ankara University, Ankara; ^(b) Istanbul Aydin University, Istanbul; ^(c) Division of Physics, TOBB University of Economics and Technology, Ankara, Turkey
⁵ LAPP, CNRS/IN2P3 and Université Savoie Mont Blanc, Annecy-le-Vieux, France
⁶ High Energy Physics Division, Argonne National Laboratory, Argonne IL, United States of America
⁷ Department of Physics, University of Arizona, Tucson AZ, United States of America
⁸ Department of Physics, The University of Texas at Arlington, Arlington TX, United States of America
⁹ Physics Department, National and Kapodistrian University of Athens, Athens, Greece
¹⁰ Physics Department, National Technical University of Athens, Zografou, Greece
¹¹ Department of Physics, The University of Texas at Austin, Austin TX, United States of America
¹² Institute of Physics, Azerbaijan Academy of Sciences, Baku, Azerbaijan
¹³ Institut de Física d'Altes Energies (IFAE), The Barcelona Institute of Science and Technology, Barcelona, Spain
¹⁴ Institute of Physics, University of Belgrade, Belgrade, Serbia
¹⁵ Department for Physics and Technology, University of Bergen, Bergen, Norway
¹⁶ Physics Division, Lawrence Berkeley National Laboratory and University of California, Berkeley CA, United States of America
¹⁷ Department of Physics, Humboldt University, Berlin, Germany
¹⁸ Albert Einstein Center for Fundamental Physics and Laboratory for High Energy Physics, University of Bern, Bern, Switzerland
¹⁹ School of Physics and Astronomy, University of Birmingham, Birmingham, United Kingdom
²⁰ ^(a) Department of Physics, Bogazici University, Istanbul; ^(b) Department of Physics Engineering, Gaziantep University, Gaziantep; ^(d) Istanbul Bilgi University, Faculty of Engineering and Natural Sciences, Istanbul; ^(e) Bahcesehir University, Faculty of Engineering and Natural Sciences, Istanbul, Turkey
²¹ Centro de Investigaciones, Universidad Antonio Narino, Bogota, Colombia
²² ^(a) INFN Sezione di Bologna; ^(b) Dipartimento di Fisica e Astronomia, Università di Bologna, Bologna, Italy
²³ Physikalisches Institut, University of Bonn, Bonn, Germany
²⁴ Department of Physics, Boston University, Boston MA, United States of America
²⁵ Department of Physics, Brandeis University, Waltham MA, United States of America
²⁶ ^(a) Universidade Federal do Rio De Janeiro COPPE/EE/IF, Rio de Janeiro; ^(b) Electrical Circuits Department, Federal University of Juiz de Fora (UFJF), Juiz de Fora; ^(c) Federal University of Sao Joao del Rei (UFSJ), Sao Joao del Rei; ^(d) Instituto de Fisica, Universidade de Sao Paulo, Sao Paulo, Brazil
²⁷ Physics Department, Brookhaven National Laboratory, Upton NY, United States of America
²⁸ ^(a) Transilvania University of Brasov, Brasov; ^(b) Horia Hulubei National Institute of Physics and Nuclear Engineering, Bucharest; ^(c) Department of Physics, Alexandru Ioan Cuza University of Iasi, Iasi; ^(d) National Institute for Research and Development of Isotopic and Molecular Technologies, Physics Department, Cluj Napoca; ^(e) University Politehnica Bucharest, Bucharest; ^(f) West University in Timisoara, Timisoara, Romania
²⁹ Departamento de Física, Universidad de Buenos Aires, Buenos Aires, Argentina
³⁰ Cavendish Laboratory, University of Cambridge, Cambridge, United Kingdom
³¹ Department of Physics, Carleton University, Ottawa ON, Canada
³² CERN, Geneva, Switzerland
³³ Enrico Fermi Institute, University of Chicago, Chicago IL, United States of America

- ³⁴ ^(a) Departamento de Física, Pontificia Universidad Católica de Chile, Santiago; ^(b) Departamento de Física, Universidad Técnica Federico Santa María, Valparaíso, Chile
- ³⁵ ^(a) Institute of High Energy Physics, Chinese Academy of Sciences, Beijing; ^(b) Department of Physics, Nanjing University, Jiangsu; ^(c) Physics Department, Tsinghua University, Beijing 100084; ^(d) University of Chinese Academy of Science (UCAS), Beijing, China
- ³⁶ ^(a) Department of Modern Physics and State Key Laboratory of Particle Detection and Electronics, University of Science and Technology of China, Anhui; ^(b) School of Physics, Shandong University, Shandong; ^(c) Department of Physics and Astronomy, Key Laboratory for Particle Physics, Astrophysics and Cosmology, Ministry of Education; Shanghai Key Laboratory for Particle Physics and Cosmology, Shanghai Jiao Tong University, Shanghai(also at PKU-CHEP), China
- ³⁷ Université Clermont Auvergne, CNRS/IN2P3, LPC, Clermont-Ferrand, France
- ³⁸ Nevis Laboratory, Columbia University, Irvington NY, United States of America
- ³⁹ Niels Bohr Institute, University of Copenhagen, Kobenhavn, Denmark
- ⁴⁰ ^(a) INFN Gruppo Collegato di Cosenza, Laboratori Nazionali di Frascati; ^(b) Dipartimento di Fisica, Università della Calabria, Rende, Italy
- ⁴¹ ^(a) AGH University of Science and Technology, Faculty of Physics and Applied Computer Science, Krakow; ^(b) Marian Smoluchowski Institute of Physics, Jagiellonian University, Krakow, Poland
- ⁴² Institute of Nuclear Physics Polish Academy of Sciences, Krakow, Poland
- ⁴³ Physics Department, Southern Methodist University, Dallas TX, United States of America
- ⁴⁴ Physics Department, University of Texas at Dallas, Richardson TX, United States of America
- ⁴⁵ DESY, Hamburg and Zeuthen, Germany
- ⁴⁶ Lehrstuhl für Experimentelle Physik IV, Technische Universität Dortmund, Dortmund, Germany
- ⁴⁷ Institut für Kern- und Teilchenphysik, Technische Universität Dresden, Dresden, Germany
- ⁴⁸ Department of Physics, Duke University, Durham NC, United States of America
- ⁴⁹ SUPA - School of Physics and Astronomy, University of Edinburgh, Edinburgh, United Kingdom
- ⁵⁰ INFN e Laboratori Nazionali di Frascati, Frascati, Italy
- ⁵¹ Fakultät für Mathematik und Physik, Albert-Ludwigs-Universität, Freiburg, Germany
- ⁵² Departement de Physique Nucleaire et Corpusculaire, Université de Genève, Geneva, Switzerland
- ⁵³ ^(a) INFN Sezione di Genova; ^(b) Dipartimento di Fisica, Università di Genova, Genova, Italy
- ⁵⁴ ^(a) E. Andronikashvili Institute of Physics, Iv. Javakhishvili Tbilisi State University, Tbilisi; ^(b) High Energy Physics Institute, Tbilisi State University, Tbilisi, Georgia
- ⁵⁵ II Physikalischs Institut, Justus-Liebig-Universität Giessen, Giessen, Germany
- ⁵⁶ SUPA - School of Physics and Astronomy, University of Glasgow, Glasgow, United Kingdom
- ⁵⁷ II Physikalischs Institut, Georg-August-Universität, Göttingen, Germany
- ⁵⁸ Laboratoire de Physique Subatomique et de Cosmologie, Université Grenoble-Alpes, CNRS/IN2P3, Grenoble, France
- ⁵⁹ Laboratory for Particle Physics and Cosmology, Harvard University, Cambridge MA, United States of America
- ⁶⁰ ^(a) Kirchhoff-Institut für Physik, Ruprecht-Karls-Universität Heidelberg, Heidelberg; ^(b) Physikalischs Institut, Ruprecht-Karls-Universität Heidelberg, Heidelberg, Germany
- ⁶¹ Faculty of Applied Information Science, Hiroshima Institute of Technology, Hiroshima, Japan
- ⁶² ^(a) Department of Physics, The Chinese University of Hong Kong, Shatin, N.T., Hong Kong; ^(b) Department of Physics, The University of Hong Kong, Hong Kong; ^(c) Department of Physics and Institute for Advanced Study, The Hong Kong University of Science and Technology, Clear Water Bay, Kowloon, Hong Kong, China
- ⁶³ Department of Physics, National Tsing Hua University, Taiwan, Taiwan
- ⁶⁴ Department of Physics, Indiana University, Bloomington IN, United States of America

- ⁶⁵ Institut für Astro- und Teilchenphysik, Leopold-Franzens-Universität, Innsbruck, Austria
⁶⁶ University of Iowa, Iowa City IA, United States of America
⁶⁷ Department of Physics and Astronomy, Iowa State University, Ames IA, United States of America
⁶⁸ Joint Institute for Nuclear Research, JINR Dubna, Dubna, Russia
⁶⁹ KEK, High Energy Accelerator Research Organization, Tsukuba, Japan
⁷⁰ Graduate School of Science, Kobe University, Kobe, Japan
⁷¹ Faculty of Science, Kyoto University, Kyoto, Japan
⁷² Kyoto University of Education, Kyoto, Japan
⁷³ Research Center for Advanced Particle Physics and Department of Physics, Kyushu University, Fukuoka, Japan
⁷⁴ Instituto de Física La Plata, Universidad Nacional de La Plata and CONICET, La Plata, Argentina
⁷⁵ Physics Department, Lancaster University, Lancaster, United Kingdom
⁷⁶ ^(a) INFN Sezione di Lecce; ^(b) Dipartimento di Matematica e Fisica, Università del Salento, Lecce, Italy
⁷⁷ Oliver Lodge Laboratory, University of Liverpool, Liverpool, United Kingdom
⁷⁸ Department of Experimental Particle Physics, Jožef Stefan Institute and Department of Physics, University of Ljubljana, Ljubljana, Slovenia
⁷⁹ School of Physics and Astronomy, Queen Mary University of London, London, United Kingdom
⁸⁰ Department of Physics, Royal Holloway University of London, Surrey, United Kingdom
⁸¹ Department of Physics and Astronomy, University College London, London, United Kingdom
⁸² Louisiana Tech University, Ruston LA, United States of America
⁸³ Laboratoire de Physique Nucléaire et de Hautes Energies, UPMC and Université Paris-Diderot and CNRS/IN2P3, Paris, France
⁸⁴ Fysiska institutionen, Lunds universitet, Lund, Sweden
⁸⁵ Departamento de Fisica Teorica C-15, Universidad Autonoma de Madrid, Madrid, Spain
⁸⁶ Institut für Physik, Universität Mainz, Mainz, Germany
⁸⁷ School of Physics and Astronomy, University of Manchester, Manchester, United Kingdom
⁸⁸ CPPM, Aix-Marseille Université and CNRS/IN2P3, Marseille, France
⁸⁹ Department of Physics, University of Massachusetts, Amherst MA, United States of America
⁹⁰ Department of Physics, McGill University, Montreal QC, Canada
⁹¹ School of Physics, University of Melbourne, Victoria, Australia
⁹² Department of Physics, The University of Michigan, Ann Arbor MI, United States of America
⁹³ Department of Physics and Astronomy, Michigan State University, East Lansing MI, United States of America
⁹⁴ ^(a) INFN Sezione di Milano; ^(b) Dipartimento di Fisica, Università di Milano, Milano, Italy
⁹⁵ B.I. Stepanov Institute of Physics, National Academy of Sciences of Belarus, Minsk, Republic of Belarus
⁹⁶ Research Institute for Nuclear Problems of Byelorussian State University, Minsk, Republic of Belarus
⁹⁷ Group of Particle Physics, University of Montreal, Montreal QC, Canada
⁹⁸ P.N. Lebedev Physical Institute of the Russian Academy of Sciences, Moscow, Russia
⁹⁹ Institute for Theoretical and Experimental Physics (ITEP), Moscow, Russia
¹⁰⁰ National Research Nuclear University MEPhI, Moscow, Russia
¹⁰¹ D.V. Skobeltsyn Institute of Nuclear Physics, M.V. Lomonosov Moscow State University, Moscow, Russia
¹⁰² Fakultät für Physik, Ludwig-Maximilians-Universität München, München, Germany
¹⁰³ Max-Planck-Institut für Physik (Werner-Heisenberg-Institut), München, Germany
¹⁰⁴ Nagasaki Institute of Applied Science, Nagasaki, Japan

- ¹⁰⁵ Graduate School of Science and Kobayashi-Maskawa Institute, Nagoya University, Nagoya, Japan
¹⁰⁶ ^(a) INFN Sezione di Napoli; ^(b) Dipartimento di Fisica, Università di Napoli, Napoli, Italy
¹⁰⁷ Department of Physics and Astronomy, University of New Mexico, Albuquerque NM, United States of America
¹⁰⁸ Institute for Mathematics, Astrophysics and Particle Physics, Radboud University Nijmegen/Nikhef, Nijmegen, Netherlands
¹⁰⁹ Nikhef National Institute for Subatomic Physics and University of Amsterdam, Amsterdam, Netherlands
¹¹⁰ Department of Physics, Northern Illinois University, DeKalb IL, United States of America
¹¹¹ Budker Institute of Nuclear Physics, SB RAS, Novosibirsk, Russia
¹¹² Department of Physics, New York University, New York NY, United States of America
¹¹³ Ohio State University, Columbus OH, United States of America
¹¹⁴ Faculty of Science, Okayama University, Okayama, Japan
¹¹⁵ Homer L. Dodge Department of Physics and Astronomy, University of Oklahoma, Norman OK, United States of America
¹¹⁶ Department of Physics, Oklahoma State University, Stillwater OK, United States of America
¹¹⁷ Palacký University, RCPTM, Olomouc, Czech Republic
¹¹⁸ Center for High Energy Physics, University of Oregon, Eugene OR, United States of America
¹¹⁹ LAL, Univ. Paris-Sud, CNRS/IN2P3, Université Paris-Saclay, Orsay, France
¹²⁰ Graduate School of Science, Osaka University, Osaka, Japan
¹²¹ Department of Physics, University of Oslo, Oslo, Norway
¹²² Department of Physics, Oxford University, Oxford, United Kingdom
¹²³ ^(a) INFN Sezione di Pavia; ^(b) Dipartimento di Fisica, Università di Pavia, Pavia, Italy
¹²⁴ Department of Physics, University of Pennsylvania, Philadelphia PA, United States of America
¹²⁵ National Research Centre "Kurchatov Institute" B.P.Konstantinov Petersburg Nuclear Physics Institute, St. Petersburg, Russia
¹²⁶ ^(a) INFN Sezione di Pisa; ^(b) Dipartimento di Fisica E. Fermi, Università di Pisa, Pisa, Italy
¹²⁷ Department of Physics and Astronomy, University of Pittsburgh, Pittsburgh PA, United States of America
¹²⁸ ^(a) Laboratório de Instrumentação e Física Experimental de Partículas - LIP, Lisboa; ^(b) Faculdade de Ciências, Universidade de Lisboa, Lisboa; ^(c) Department of Physics, University of Coimbra, Coimbra; ^(d) Centro de Física Nuclear da Universidade de Lisboa, Lisboa; ^(e) Departamento de Física, Universidade do Minho, Braga; ^(f) Departamento de Física Teórica y del Cosmos, Universidad de Granada, Granada; ^(g) Dep Física and CEFITEC of Faculdade de Ciencias e Tecnologia, Universidade Nova de Lisboa, Caparica, Portugal
¹²⁹ Institute of Physics, Academy of Sciences of the Czech Republic, Praha, Czech Republic
¹³⁰ Czech Technical University in Prague, Praha, Czech Republic
¹³¹ Charles University, Faculty of Mathematics and Physics, Prague, Czech Republic
¹³² State Research Center Institute for High Energy Physics (Protvino), NRC KI, Russia
¹³³ Particle Physics Department, Rutherford Appleton Laboratory, Didcot, United Kingdom
¹³⁴ ^(a) INFN Sezione di Roma; ^(b) Dipartimento di Fisica, Sapienza Università di Roma, Roma, Italy
¹³⁵ ^(a) INFN Sezione di Roma Tor Vergata; ^(b) Dipartimento di Fisica, Università di Roma Tor Vergata, Roma, Italy
¹³⁶ ^(a) INFN Sezione di Roma Tre; ^(b) Dipartimento di Matematica e Fisica, Università Roma Tre, Roma, Italy
¹³⁷ ^(a) Faculté des Sciences Ain Chock, Réseau Universitaire de Physique des Hautes Energies - Université Hassan II, Casablanca; ^(b) Centre National de l'Energie des Sciences Techniques Nucléaires,

Rabat; ^(c) Faculté des Sciences Semlalia, Université Cadi Ayyad, LPHEA-Marrakech; ^(d) Faculté des Sciences, Université Mohamed Premier and LPTPM, Oujda; ^(e) Faculté des sciences, Université Mohammed V, Rabat, Morocco

¹³⁸ DSM/IRFU (Institut de Recherches sur les Lois Fondamentales de l'Univers), CEA Saclay (Commissariat à l'Energie Atomique et aux Energies Alternatives), Gif-sur-Yvette, France

¹³⁹ Santa Cruz Institute for Particle Physics, University of California Santa Cruz, Santa Cruz CA, United States of America

¹⁴⁰ Department of Physics, University of Washington, Seattle WA, United States of America

¹⁴¹ Department of Physics and Astronomy, University of Sheffield, Sheffield, United Kingdom

¹⁴² Department of Physics, Shinshu University, Nagano, Japan

¹⁴³ Department Physik, Universität Siegen, Siegen, Germany

¹⁴⁴ Department of Physics, Simon Fraser University, Burnaby BC, Canada

¹⁴⁵ SLAC National Accelerator Laboratory, Stanford CA, United States of America

¹⁴⁶ ^(a) Faculty of Mathematics, Physics & Informatics, Comenius University, Bratislava; ^(b) Department of Subnuclear Physics, Institute of Experimental Physics of the Slovak Academy of Sciences, Kosice, Slovak Republic

¹⁴⁷ ^(a) Department of Physics, University of Cape Town, Cape Town; ^(b) Department of Physics, University of Johannesburg, Johannesburg; ^(c) School of Physics, University of the Witwatersrand, Johannesburg, South Africa

¹⁴⁸ ^(a) Department of Physics, Stockholm University; ^(b) The Oskar Klein Centre, Stockholm, Sweden

¹⁴⁹ Physics Department, Royal Institute of Technology, Stockholm, Sweden

¹⁵⁰ Departments of Physics & Astronomy and Chemistry, Stony Brook University, Stony Brook NY, United States of America

¹⁵¹ Department of Physics and Astronomy, University of Sussex, Brighton, United Kingdom

¹⁵² School of Physics, University of Sydney, Sydney, Australia

¹⁵³ Institute of Physics, Academia Sinica, Taipei, Taiwan

¹⁵⁴ Department of Physics, Technion: Israel Institute of Technology, Haifa, Israel

¹⁵⁵ Raymond and Beverly Sackler School of Physics and Astronomy, Tel Aviv University, Tel Aviv, Israel

¹⁵⁶ Department of Physics, Aristotle University of Thessaloniki, Thessaloniki, Greece

¹⁵⁷ International Center for Elementary Particle Physics and Department of Physics, The University of Tokyo, Tokyo, Japan

¹⁵⁸ Graduate School of Science and Technology, Tokyo Metropolitan University, Tokyo, Japan

¹⁵⁹ Department of Physics, Tokyo Institute of Technology, Tokyo, Japan

¹⁶⁰ Tomsk State University, Tomsk, Russia

¹⁶¹ Department of Physics, University of Toronto, Toronto ON, Canada

¹⁶² ^(a) INFN-TIFPA; ^(b) University of Trento, Trento, Italy

¹⁶³ ^(a) TRIUMF, Vancouver BC; ^(b) Department of Physics and Astronomy, York University, Toronto ON, Canada

¹⁶⁴ Faculty of Pure and Applied Sciences, and Center for Integrated Research in Fundamental Science and Engineering, University of Tsukuba, Tsukuba, Japan

¹⁶⁵ Department of Physics and Astronomy, Tufts University, Medford MA, United States of America

¹⁶⁶ Department of Physics and Astronomy, University of California Irvine, Irvine CA, United States of America

¹⁶⁷ ^(a) INFN Gruppo Collegato di Udine, Sezione di Trieste, Udine; ^(b) ICTP, Trieste; ^(c) Dipartimento di Chimica, Fisica e Ambiente, Università di Udine, Udine, Italy

¹⁶⁸ Department of Physics and Astronomy, University of Uppsala, Uppsala, Sweden

- ¹⁶⁹ Department of Physics, University of Illinois, Urbana IL, United States of America
¹⁷⁰ Instituto de Fisica Corpuscular (IFIC), Centro Mixto Universidad de Valencia - CSIC, Spain
¹⁷¹ Department of Physics, University of British Columbia, Vancouver BC, Canada
¹⁷² Department of Physics and Astronomy, University of Victoria, Victoria BC, Canada
¹⁷³ Department of Physics, University of Warwick, Coventry, United Kingdom
¹⁷⁴ Waseda University, Tokyo, Japan
¹⁷⁵ Department of Particle Physics, The Weizmann Institute of Science, Rehovot, Israel
¹⁷⁶ Department of Physics, University of Wisconsin, Madison WI, United States of America
¹⁷⁷ Fakultät für Physik und Astronomie, Julius-Maximilians-Universität, Würzburg, Germany
¹⁷⁸ Fakultät für Mathematik und Naturwissenschaften, Fachgruppe Physik, Bergische Universität Wuppertal, Wuppertal, Germany
¹⁷⁹ Department of Physics, Yale University, New Haven CT, United States of America
¹⁸⁰ Yerevan Physics Institute, Yerevan, Armenia
¹⁸¹ Centre de Calcul de l’Institut National de Physique Nucléaire et de Physique des Particules (IN2P3), Villeurbanne, France
¹⁸² Academia Sinica Grid Computing, Institute of Physics, Academia Sinica, Taipei, Taiwan
^a Also at Department of Physics, King’s College London, London, United Kingdom
^b Also at Institute of Physics, Azerbaijan Academy of Sciences, Baku, Azerbaijan
^c Also at Novosibirsk State University, Novosibirsk, Russia
^d Also at TRIUMF, Vancouver BC, Canada
^e Also at Department of Physics & Astronomy, University of Louisville, Louisville, KY, United States of America
^f Also at Physics Department, An-Najah National University, Nablus, Palestine
^g Also at Department of Physics, California State University, Fresno CA, United States of America
^h Also at Department of Physics, University of Fribourg, Fribourg, Switzerland
ⁱ Also at II Physikalisches Institut, Georg-August-Universität, Göttingen, Germany
^j Also at Departament de Fisica de la Universitat Autonoma de Barcelona, Barcelona, Spain
^k Also at Departamento de Fisica e Astronomia, Faculdade de Ciencias, Universidade do Porto, Portugal
^l Also at Tomsk State University, Tomsk, and Moscow Institute of Physics and Technology State University, Dolgoprudny, Russia
^m Also at The Collaborative Innovation Center of Quantum Matter (CICQM), Beijing, China
ⁿ Also at Universita di Napoli Parthenope, Napoli, Italy
^o Also at Institute of Particle Physics (IPP), Canada
^p Also at Horia Hulubei National Institute of Physics and Nuclear Engineering, Bucharest, Romania
^q Also at Department of Physics, St. Petersburg State Polytechnical University, St. Petersburg, Russia
^r Also at Borough of Manhattan Community College, City University of New York, New York City, United States of America
^s Also at Department of Financial and Management Engineering, University of the Aegean, Chios, Greece
^t Also at Centre for High Performance Computing, CSIR Campus, Rosebank, Cape Town, South Africa
^u Also at Louisiana Tech University, Ruston LA, United States of America
^v Also at Institucio Catalana de Recerca i Estudis Avancats, ICREA, Barcelona, Spain
^w Also at Department of Physics, The University of Michigan, Ann Arbor MI, United States of America
^x Also at Graduate School of Science, Osaka University, Osaka, Japan
^y Also at Fakultät für Mathematik und Physik, Albert-Ludwigs-Universität, Freiburg, Germany
^z Also at Institute for Mathematics, Astrophysics and Particle Physics, Radboud University Nijmegen/Nikhef, Nijmegen, Netherlands

- aa* Also at Department of Physics, The University of Texas at Austin, Austin TX, United States of America
ab Also at Institute of Theoretical Physics, Ilia State University, Tbilisi, Georgia
ac Also at CERN, Geneva, Switzerland
ad Also at Georgian Technical University (GTU), Tbilisi, Georgia
ae Also at Ochadai Academic Production, Ochanomizu University, Tokyo, Japan
af Also at Manhattan College, New York NY, United States of America
ag Also at Departamento de Física, Pontificia Universidad Católica de Chile, Santiago, Chile
ah Also at The City College of New York, New York NY, United States of America
ai Also at School of Physics, Shandong University, Shandong, China
aj Also at Departamento de Física Teórica y del Cosmos, Universidad de Granada, Granada, Portugal
ak Also at Department of Physics, California State University, Sacramento CA, United States of America
al Also at Moscow Institute of Physics and Technology State University, Dolgoprudny, Russia
am Also at Departement de Physique Nucléaire et Corpusculaire, Université de Genève, Geneva, Switzerland
an Also at Institut de Física d'Altes Energies (IFAE), The Barcelona Institute of Science and Technology, Barcelona, Spain
ao Also at School of Physics, Sun Yat-sen University, Guangzhou, China
ap Also at Institute for Nuclear Research and Nuclear Energy (INRNE) of the Bulgarian Academy of Sciences, Sofia, Bulgaria
aq Also at Faculty of Physics, M.V.Lomonosov Moscow State University, Moscow, Russia
ar Also at National Research Nuclear University MEPhI, Moscow, Russia
as Also at Department of Physics, Stanford University, Stanford CA, United States of America
at Also at Institute for Particle and Nuclear Physics, Wigner Research Centre for Physics, Budapest, Hungary
au Also at Giresun University, Faculty of Engineering, Turkey
av Also at CPPM, Aix-Marseille Université and CNRS/IN2P3, Marseille, France
aw Also at Department of Physics, Nanjing University, Jiangsu, China
ax Also at Institute of Physics, Academia Sinica, Taipei, Taiwan
ay Also at University of Malaya, Department of Physics, Kuala Lumpur, Malaysia
az Also at LAL, Univ. Paris-Sud, CNRS/IN2P3, Université Paris-Saclay, Orsay, France
** Deceased*